Carbon Nanotube Cold Cathodes for Applications under Vacuum to Partial Pressure in Helium and Dryair

by

Ramesh Bokka

A thesis submitted to the Graduate Faculty of
Auburn University
in partial fulfillment of the
requirements for the Degree of
Master of Science

Auburn, Alabama
August 06, 2011

Key words: Carbon nanotubes, Field emission, Sputtering
Growth time, Lifetime

Approved by

Hulya Kirkici, Chair, Professor of Electrical and Computer Engineering
Lloyd Stephen Riggs, Professor of Electrical and Computer Engineering
Michael Hamilton, Assistant Professor of Electrical and Computer Engineering

Abstract

Carbon nanotubes are known for their excellent field emission characteristics. This property of carbon nanotubes makes them a good choice for the cold cathode material for many high power applications. In this work carbon nanotubes are studied in order to develop cold cathode material with efficient field emission characteristics. These coatings of nanotubes then will be used for the triggering mechanism of pseudospark switch.

In this research work randomly aligned Multi-Walled carbon nanotubes (MWNTs) are fabricated using chemical vapor deposition method (CVD). The MWNTs are fabricated under different growth conditions by varying sputtering times of the catalyst and growth times of CNTs. The change in the densities of MWNTs with different growth conditions is discussed and results are presented. These nanotubes are then tested for their field emission characteristics at different pressures ranging from $5x10^{-7}$ Torr to $20x10^{-3}$ Torr. The experiments were carried out in different background gases of Helium and dryair. Effects of different gases at different pressures on the field emission properties of carbon nanotubes are studied and results are presented. The lifetime and current stability tests were also performed at $5x10^{-7}$ Torr and $20x10^{-3}$ Torr and relevant plots are presented. The use of these CNTs as trigger electrode for pseudospark switch is part of another study and only an introduction to pseudospark switches given here.

Acknowledgments

First and foremost, I would like to express sincere gratitude to my advisor Dr. Hulya Kirkici for the continuous support of my study and research, for her patience, motivation and enthusiasm. Her guidance helped me throughout the research and writing of this thesis. I could not have imagined having a better advisor and mentor for me at Auburn University.

Besides my advisor, I would like to thank the rest of my thesis committee: Dr. Lloyd Riggs and Dr. Michael Hamilton, for their help in reviewing my thesis, insightful comments and suggestions.

My sincere thanks also go to the technical staff Linda Barresi and Calvin Cutshaw and others who helped me during my research. I thank my fellow lab mates Haitao Zhao, Shaomao Li, Mark Lipham, Zhenhong Li, Fang Li and Huirong Li for providing a stimulating and fun environment during my research. Especially I want to thank Haitao Zhao for his help, discussions and suggestions throughout my research.

Lastly, and most importantly I wish to thank my family and friends for their love, support and encouragement.

Table of Contents

List of Tables

List of Figures

CHAPTER 1

INTRODUCTION

Carbon nanotubes are one of the pure forms of the carbon and have been of greatest interest since their discovery in 1991 by Iijma [1]. The name for the nanotube is derived from their size as the diameter of nanotube is in the order of nanometers and their lengths could be of several micrometers length. In an ideal nanotube hexagonal network of carbon atoms are wrapped into a seamless hollow cylinder and capped or not by fullerenes-like structures. A nanotube is also known as a buckytubes (shown in the Figure 1.1) and is a member of the fullerene structural family. Carbon nanotubes have emerged as unique nano structures with remarkable electrical, mechanical and chemical properties. There has been significant progress in carbon nanotubes synthesis, as well as the investigations on their electronic, mechanical, optical and chemical characteristics.

The uniqueness of carbon nanotubes lies mainly in two factors. One is helicity and the other is topology. Helicity is defined by the diameter and symmetry of the nanotube. This is responsible for the unique electronic character of the nanotube by introducing significant changes in the electron density of states [3]. The topology on the other hand is closed geometry of individual layers in each tube and has profound effect on the physical properties of nanotubes. Carbon nanotubes occur widely in different forms depending structures, graphitizations and appearances. Single-walled and multi-walled are the most common nanotube structures. A single-walled carbon nanotube (SWNT) is formed by rolling up a graphene sheet, which is

assumed to be a single layer from a 3D graphite crystal, into a cylinder capping each end of the cylinder with half of fullerene molecule. Similar structure is used to explain multi-walled carbon nanotubes (MWNT) with more than one cylindrical layer appear in this case.

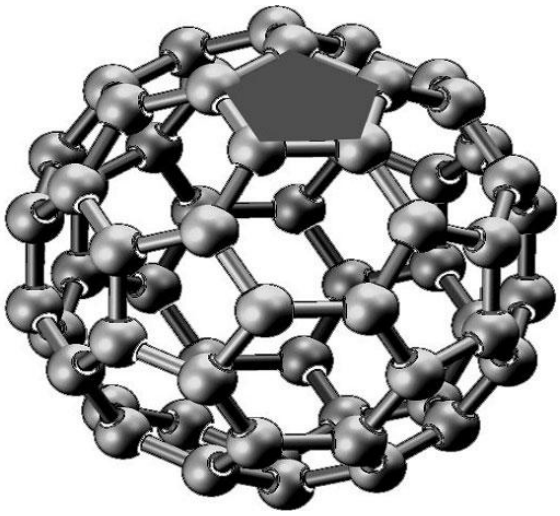

Figure 1.1: Schematic structure of the Buck-minster Fullerene (C60) [2]

The structure of CNTs is essentially graphitic, in terms of bonding of carbon nanotubes (sp^2) and hybridization of orbital. This has the structure with an inside hollow tubular surrounded by the basal plane(s) (002) of graphite (Figure 1.3). The structure is curved symmetrically in cylindrical geometry and remains parallel to the tube axis. The low free energy of the basal plane in graphite is responsible for the tubular structure of the CNTs. The free energy required for nanotubes growth is minimized when the outer surface is a curved basal plane, rather than precipitated a highly strained prismatic plane [5].

The circular curvature of the nano tubes causes quantum confinement and the σ-π rehybridization where three σ bonds are slightly out of plane and π orbital is more delocalized

outside of the tube for the compensation. This is the reason for the high mechanical strength, and unique electrical and chemical properties of the nanotubes [5].

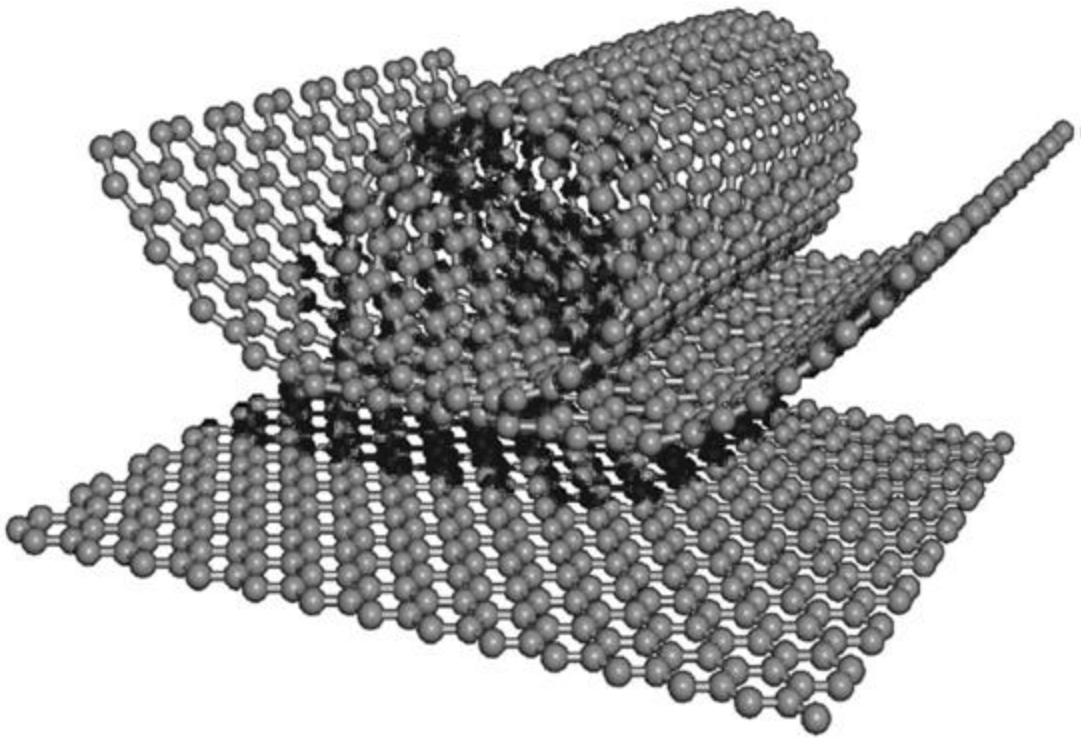

Figure 1.2: Schematic of an individual layer of honeycomb-like carbon called graphene, showing the layers rolled into CNT [4]

There are several mechanisms that are in practice for the fabrication of CNTs. However the growth mechanism is still far from well known, due to the diverse fabrications methods to produce wide range categories of CNTs [10]. Mostly the growth mechanisms are uncontrollable and quick and it is difficult to be observed in situ. The growth mechanism of CNTs is usually driven by a catalyst such as iron, molybdenum etc that pyrolizes hydrocarbon gas mixtures [12]. Acetylene and methane are few common gases used in the growth mechanism [5].

Different methods for growing CNTs at present are thermal chemical vapor deposition [6], plasma-enhanced chemical vapor deposition (PECVD) [5], carbon arc discharge method [7], laser ablation [8] and DC-arc plasma jet [9].

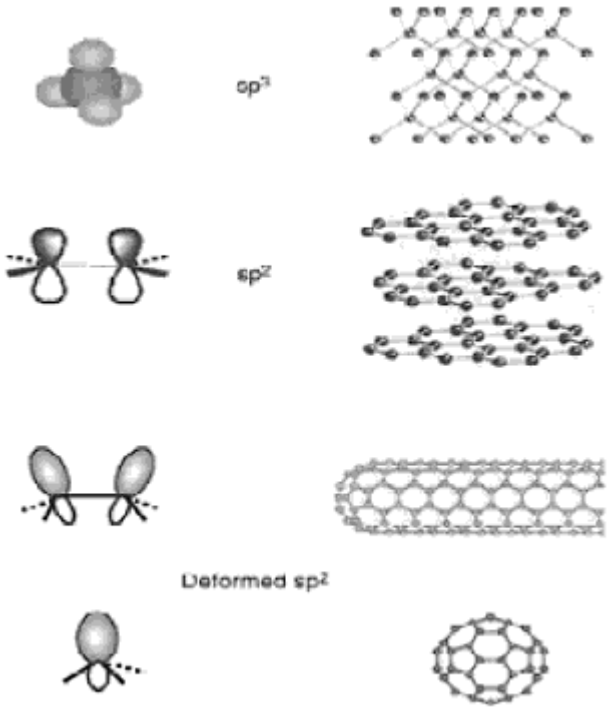

Figure 1.3: Bonding structures of diamond, graphite, nanotubes, and fullerenes: when a graphite sheet is rolled over to form a nanotube, the sp^2 hybrid orbital is deformed for rehybridization of sp^2 toward sp^3 orbital or σ-π bond mixing. This rehybridization structural feature, together with π electron confinement, gives nanotubes unique, extraordinary electronic, mechanical, chemical, thermal, magnetic, and optical properties [5].

1.1 Pseudospark Switch [10]

In many pulsed power and high power applications the switches need to be capable of handling high power levels about 10^{12} W range with low jitter time in the orders of 10^{-9} s. The usual conventional switches such as voltage switch gears are no longer adequate to meet these requirements. Based on various applications, high energy systems may require different kind of

switches such as capacitive and inductive energy storage switches. The closing switches uses capacitive and opening switches uses inductive energy storage mechanisms.

The pseudospark switch also known as cold-cathode thyratron, is one of the plasma device to control high voltage (several kV to mV) and high current pulse discharges. It is a gas filled tube which operates at low pressures and capable of high speed switching [10]. It is characterized by a very rapid breakdown phase with high hold-off voltages of several tens of kV and peak currents 10kA with pulse repetition up to several kHz. The discharge can be operated at 100% current reversal without turning into a constricted arc [11].

The construction of pseudospark switch is much simpler than thyratron tube and suffers less electrode wear than high pressure switches. The basic schematic of the pseudospark switch is shown in the Figure 1.4. The basic discharge system consists of two conductive metal cups which acts as two electrodes of the switch separated by an insulator. Both electrodes have a small hole at the centre and an electrode backspace formed by metal cage. The whole device is cylindrical and symmetric about its vertical axis [10]. The empty areas within the device contain gas at low pressure, typically between 75 and 750 mTorr. The dimensions of the hole and the spacing between electrodes range between 2-5 mm.

A triggering mechanism is needed to be added to this structure to make it a useful switch. Several triggering methods have been reported in the literature. One of the triggering methods is to add a third electrode, which acts as source of seed electrons, inside one of the cups [11]. The other method is optical triggering, where light pulse is used to illuminate inside the cup structures to generate seed electrons [12]. These methods initiate plasma, allowing the transition of the gas from insulating state to conducting state.

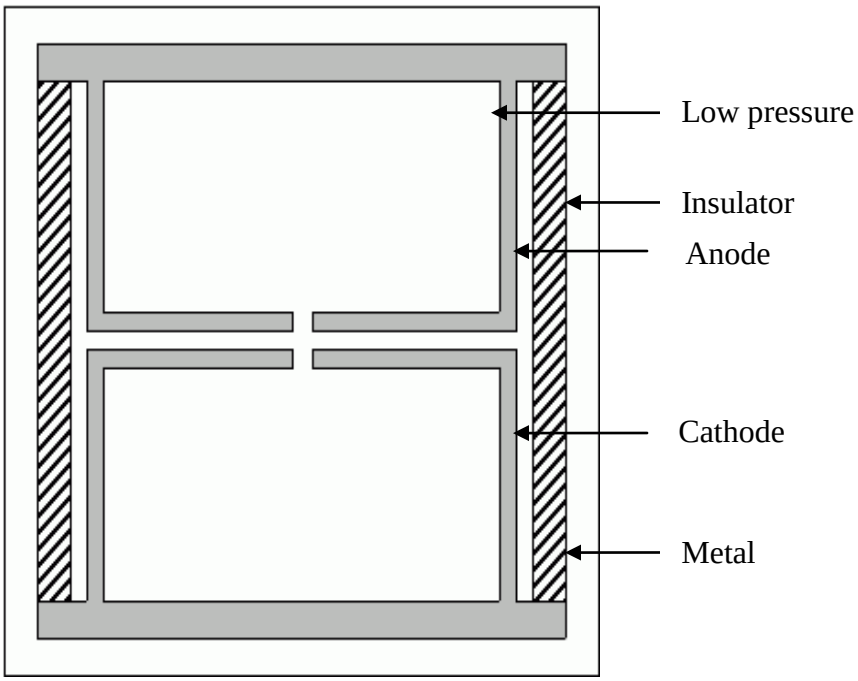

Figure 1.4: Cross sectional view of single channel pseudospark switch [13].

1.1.1 Carbon Nanotubes as Cold Cathode Material

Carbon nanotubes are among the best choice used for the triggering mechanism in many high power switches. Carbon nanotubes exhibit excellent field emission characteristics with low turn-on voltage and high current density. They can emit electrons at relatively low electric fields, with capability of handling high emission current densities. The large aspect ratio and small radius of tip curvature, each CNT coupled with the highly conductive graphitic walls ensures the efficient electron emission from the nanotubes. The large effective surface area, tubular structure, light weight, chemical stability, high electrical and thermal conductivity make these materials attractive for many applications such as energy storage in super capacitors, batteries, materials for field emission display (FED), and as cold cathode material in many high voltage applications. One of the cold-cathode applications is the use of the CNTs in pseudospark switches for the triggering mechanism.

Generally the CNTs show excellent field emission characteristics in the high vacuum conditions. The turn-on electric fields are very low with high current densities in high vacuum where as these parameters seem to be deteriorated with increase in the operating pressure levels. Different gas gases in which CNTs tested also affects the turn-on electric field and maximum current densities of nanotubes. The lifetime, emission degradation and its long term emission stability is also important when considering for the applications such as flat panel displays, pseudospark switches.

The purity of CNTs is always a concern with most of the reactions is quick and least controlled and lot of impurity clusters such as polydedral graphite nano-particles in the cluster of carbon nano tubes appeared among the carbon nanotubes after their growth. The effect of these clusters on the field emission properties also studied and results are presented.

The emphasis is on the field emission characteristics of CNT cathodes with different gas gases at different pressure ranges, their stability over long run in both high vacuum ($5x10^{-7}$ Torr) and high pressure conditions ($20x10^{-3}$ Torr). The field emission curves also compared with respect to their growth times and sputtering times and their effect on the field emission characteristics are studied and analyzed. The effect on the field emission properties with the presence of impurities such as polydedral graphite nano-particles in the cluster of carbon nano tubes are also analyzed and presented.

CHAPTER 2

LITERATURE REVIEW

2.1 Types, Structure and Material Properties of CNTs

2.1.1 Structural Concepts of CNTs

Carbon nanotube is unique nano structured material made of carbon atoms with inter-atomic bond length of 1.42Å between each adjacent C-C bonding. The orientation of the six-membered carbon bonds (hexagonal) in honeycomb periodic lattice pattern along the axis of the tube forms the basic structure of nanotube. Atomic number of carbon is six and the six electrons occupy $1s^2$, $2s^2$, and $2p^2$ atomic orbitals. The electrons of $1s^2$ are strongly bound to the nucleus where as the $2s^2$, and $2p^2$ atomic orbitals energies are relatively close and results in the configuration consisting of 2s, $2p_x$, $2p_y$, $2p_z$ orbitals [4]. The wave functions of these orbitals readily mix with each other and optimize the bonding energy with neighbors. Intermixing of these atomic orbitals gives rise to new hybrid molecular orbits sp^3, sp^2 and sp^1 and hybridization determines the type of bonding between the carbon and neighbors. The sp^2 hybridization corresponds to the planar structures of graphite and graphene where carbon atoms bind to 3 neighbors. Carbon is the only element in the periodic table that has isomers from 0 dimensions (0D) to 3 dimensions (3D), as shown in Table 2.1 [14].

Carbon nanotubes are classified into different categories based on their structure, length, thickness, construction type of helicity, and number of layers. Although all these different types of tubes are formed from the similar graphite sheet, their electrical and physical characteristics

change depending on structural variations. Nanotubes can be either electrically conductive or semi-conductive, depending on their helicity.

Table 2.1: Isomers of carbon [14].

Dimension	**0-D**	**1-D**	**2-D**	**3-D**
Isomer	C_{60} fullerene	Nanotube	Graphite	Diamond
State		Carbine	Fiber	Amorphous
Hybridization	sp^2	sp^2 (sp)	sp^2	sp^3
Density(g/ cm^3)	1.72	1.2-2.0	2.26	3.515
Bond length(Å)	1.40 (C=C), 1.46(C-C)	1.44 (C=C)	1.42(C=C) 1.44(C=C)	1.54 (C=C)
Electronic properties	Semiconductor E_g =1.9eV	Metal or Semiconductor	Semimetal	Insulating E_g =5.47eV

Even though there are many different forms of CNTs available, they are basically categorized into three types by their structures:

- Single-wall CNTs (SWCNT)
- Multi-wall CNTs (MWCNT)
- Double-wall CNTs (DWCNT)

Among these three the SWCNTs and MWCNTs are most commonly produced and used in various applications.

2.1.1.1 Single-Wall CNTs

A tube made of Single graphite layer rolled up into hollow cylinder with axial symmetry, exhibiting chirality is called SWCNT. The structure of SWCNT is differentiated into two regions with different physical and chemical properties. One is the sidewall and the second is the end cap of the tube. The symmetry and the electronic structures of nanotubes changes with the change in the directions, diameter and rolling of graphene sheet. The Figure 2.1 shows a SWCNT where a graphene with hexagonal structures is rolled into different directions and diameters. This is better explained with the chiral vector which are a pair of indices (n, m), used to explain the wrapping of the graphene sheet. The integers n and m denote the number of unit vectors along the directions in the honeycomb crystal lattice of the graphene [5].

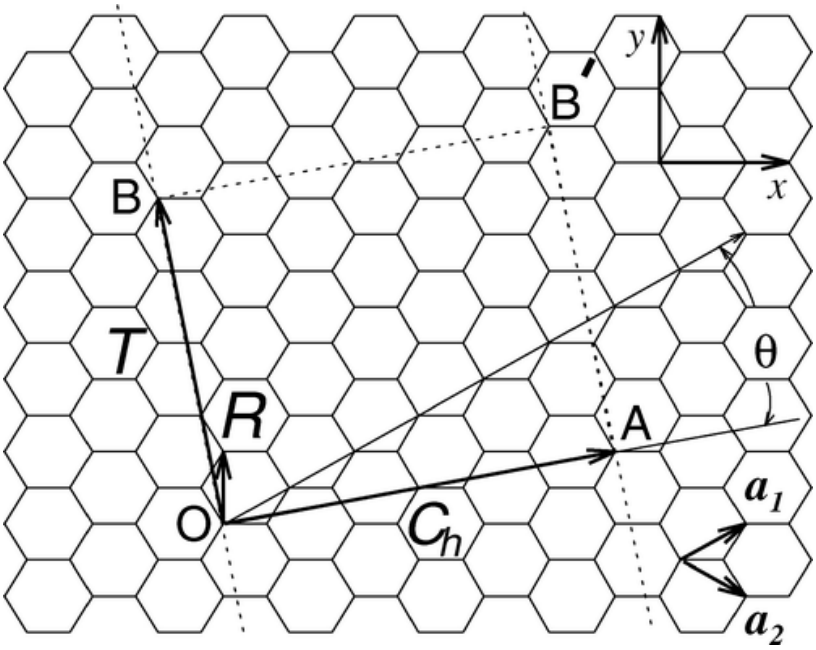

Figure 2.1: Unrolled hexagonal lattice of a carbon nanotube as a graphene sheet [15].

The SWCNT structure is classified into three different types based on the values chiral vector i.e., unit vectors n and m. if the value of m=0, i.e., (n, 0) it is zigzag, for n=m or m=n (m, m) or (n, n) it is called “armchair” and for other cases they are called as chiral.

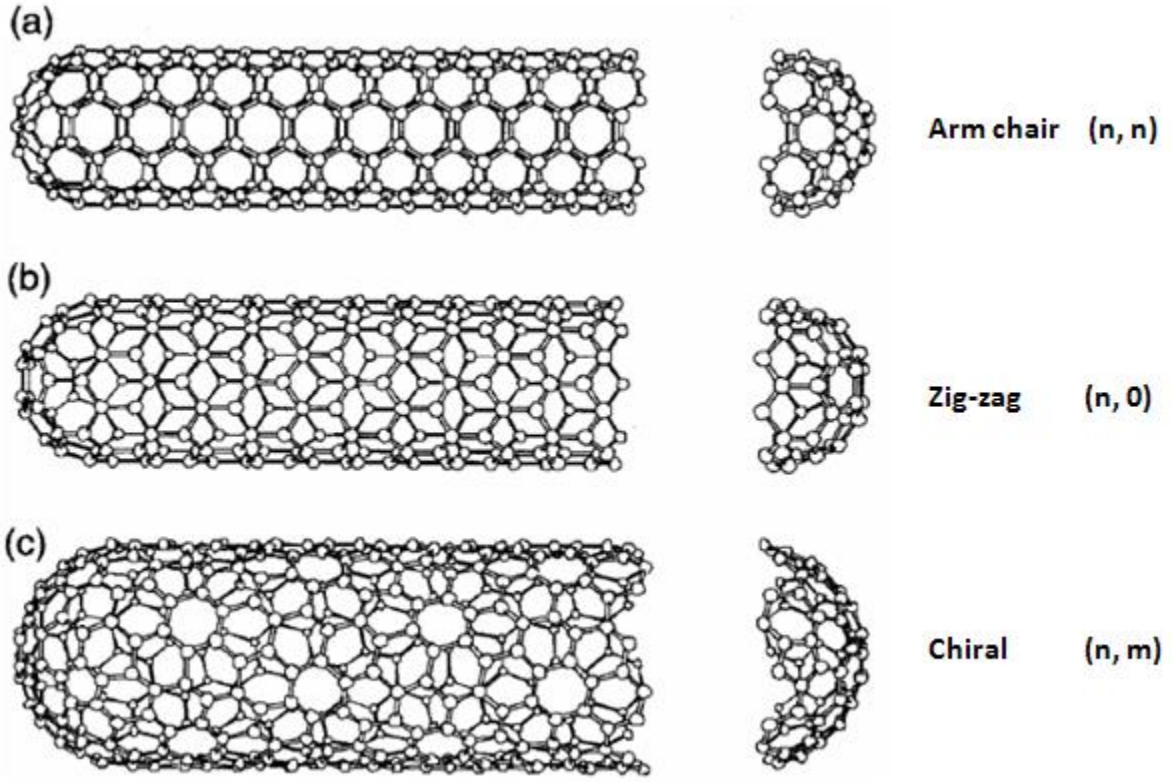

Figure 2.2: Classification of CNT based on chiral vector: (a) armchair, (b) zigzag, and (c) chiral nanotubes [16]

For a CNT, the length of base vectors is a = 2.49 Å, and then the length of chiral vector is given by the equation

$$C_h = a\sqrt{n^2 + m^2 + nm}$$

And the diameter of the SWCNT is given by the equation.

$$d_t = a\sqrt{n^2 + m^2 + nm} / \pi r^2$$

The chiral angle can be obtained by the equation

$$\theta = \cos^{-1} \frac{2n+m}{2\sqrt{n^2+m^2+nm}}$$

Thus with the chiral vector (n, m) the structure of a SWCNT can be explained along with the above geometric parameters such as length of chiral vector, diameter and the chiral angle.

2.1.1.2 Multi-Wall CNTs

Multi-walled carbon nanotubes (MWCNTs) consist of multiple layers of graphite superimposed and rolled on themselves to form a tubular shape with interlayer spacing approximately of 3.4Å. The inner diameter of MWCNT usually ranges within several nanometers and the outer diameter may range from 1 to 50nm.

The structure of MWCNT is described with two models namely Russian doll and Parchment. In Russian doll the sheets of graphite are arranged in concentric cylinders, e.g., a (0, 8) SWCNT within a larger (0, 10) SWCNT where as in Parchment model a single sheet of graphite is rolled in around itself, resembling a scroll of parchment or a rolled up newspaper.

The CNTs are grown on a silicon wafer after cleaning the wafer with HF solution and deionized water. Since the surface of polysilicon is microscopically rough, it is sometimes difficult to grow high density or well aligned CNTs coating on it, if transition metal catalyst thin film is deposited directly onto the surface [86]. The adhesion of nanotubes to polysilicon is also

poor. So, sometimes the adhesion promotion layer such as Ti and the silicon buffer layer are used to grow high density of CNTs on the polysilicon surface. The adhesion of CNTs to the substrates is tested by Ultrasonication by dipping the specimen into an ultrasonic acetone bath. The adhesion of the CNTs is greatly improved using electron-beam evaporated Ti/Si/Fe catalyst system [92]. Only small parts of nanotubes are suspended in acetone for these samples, while most of tubes staying on the original substrate after several minutes of Ultrasonication. The specimen of CNTs grown with Fe sputtering catalyst lost all its nanotubes when it is suspended in acetone after only a few seconds of ultrasonic agitation [91].

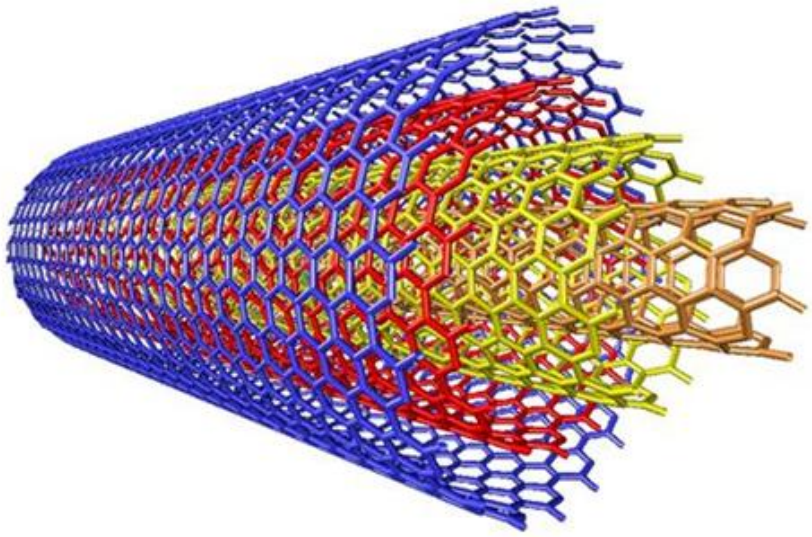

Figure 2.3: Multi walled carbon nanotubes [17].

2.1.1.3 Double-Wall CNTs

A Double-wall carbon nanotubes (DWCNTs), consists of two concentric cylindrical graphene layers as shown in the Figure 2.4. In these structures, two SWCNTs are concentrically

nested with typical inter-wall separations of approximately 0.37± 0.04 nm. They are structurally intermediate between SWCNT and MWCNT [66].

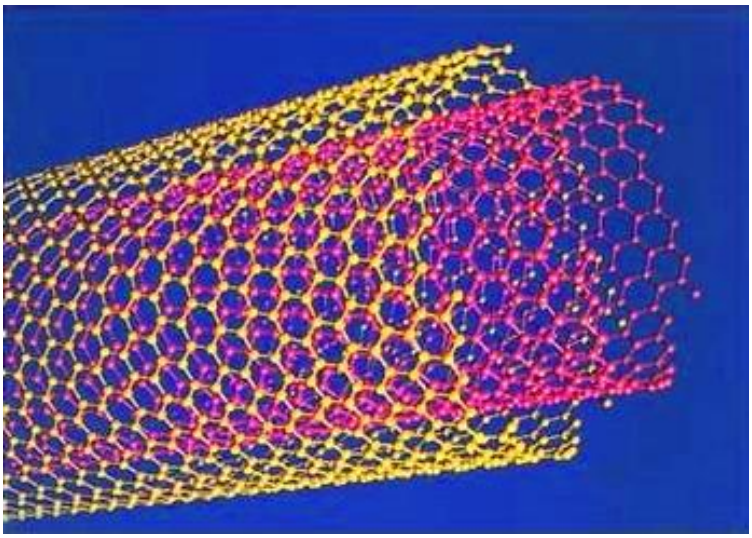

Figure 2.4: Double walled carbon nano tubes (DWCNTs) [17]

2.1.2 Electrical Properties of CNTs

Carbon nanotubes exhibit unique electrical properties which vary widely from semi-conductive nature to the metallic depending on the configuration and molecular structure that result in a different band structure and thus different band gap. Chiralities and morphologies are the main factors which decide the electrical properties of CNTs.

A SWNT may be either metallic or semi-conductive depending on the chirality i.e., the angle with which the graphene sheet is folded. It is metallic when the structure is armchair and semi-conductive with zigzag type and the chiral-type tube (m, n) with 2m+n=3N (N; positive integer).

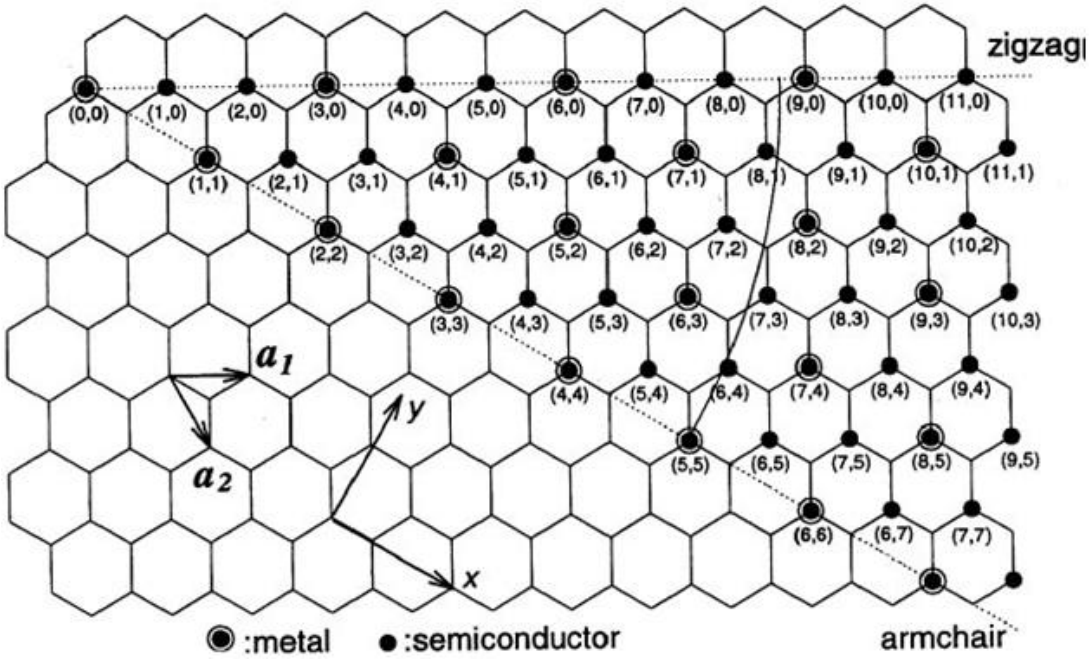

Figure 2.5: Schematic showing the folding procedure for creating nanotube cylinders from planar graphene sheets. All possible structures of SWNTs can be formed from chiral vectors lying in the range given by this figure. (n, m) [15]

The band structures of MWNTs are more complicated compared to SWNTs because of their interlayer coupling. However, theoretical discussion by Saito et. al. [14] emphasized that the interlayer had little effect on the electrical properties of individual tubes [21]. Thus a two coaxial armchair nanotubes yield double-walled tube which is metallic in nature. Even with the introduction of interlayer interaction the coaxial metallic-semiconducting and semiconducting-metallic tubes will retain their respective characters.

CNTs are electronically characterized by using different technologies like Raman spectroscopy, Scanning tunneling microscopy (STM), Electron energy loss spectroscopy (EELS), Electron spin resonance (ESR) and spectroscopy [22]. Even though several theoretical predictions regarding the electronic structures of CNTs have been validated experimentally, still there are few theories yet to be proved experimentally. For example the band structure calculations that linked to the helicity and size were proved to be true by using STM/STS [19].

However the theory regarding the additional electronic states due to interlayer correlation explained by Satio et. al. [14] is in contradiction to the states noticed by the STS in MWNT.

A four probe measurement arrangement method proposed by Ebbesen at al [20] to measure the resistivities of the nanotubes is one of the best studies which describe the electrical properties of MWNTs. In this method four tungsten wires shown in Figure 2.6 are arranged in such a way that all probes are connected to the MWNT which is settled onto an oxidized silicon surface. They measured the resistivities of eight different nanotubes which ranged from 1.2×10^{-4} Ω-cm to 5.1×10^{-6} Ω-cm [20]. The samples of MWNTs are known to be structurally heterogeneous and these results clearly suggest that the electronic properties of CNTs can vary greatly according to their structure. Resistivities of SWNTs are also measured by using four-probe arrangement by Smalley et. al. [22] which range from 0.34 μΩ-m to 1.0 μΩ-m.

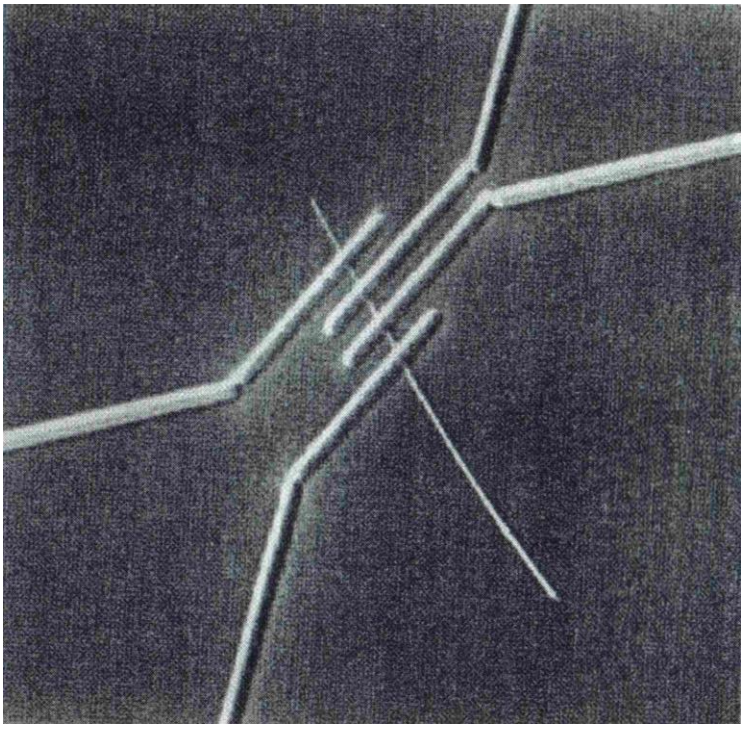

Figure 2.6: Four probe measurement geometry for individual CNTs [20].

The unique electronic properties of carbon nanotubes are predicted to be essentially caused by the confinement of electrons normal to the nanotube axis. So the propagation of electrons occurs along the nanotube axis through well separated, discrete electron states. The consequence of this quantum confinement is ballistic conduction of carbon nanotubes at room temperature. Ballistic transport occurs when electrons encounter no resistance in the conductor. Walt de Heer et. al. [24] first observed this by an arrangement in which nanotube bundle is dipped into a heatable reservoir containing mercury. They found the conductance increased in series jumps, consistent with conductance quantization but did not change smoothly with position as in the case of a classical conductor. The nanotubes were found to be undamaged at relatively high voltages for extended times [8]. If the nanotubes acted as classical resistors, the power dissipation at this high voltage would produce enormously high temperature (up to 20,000K) in the tubes. The survival of nanotubes therefore provided evidence for ballistic transport of electrons through the nanotubes.

2.1.3 Chemical Properties of CNTs

Carbon nanotubes are supposed to be one of the unique material exhibiting very unique properties. The small diameter and large surface area combined with its nanostructures size make it more attractive in many chemical and biological applications. For these applications lot of research have been carried out to determine the chemical properties of the carbon nanotubes such wetting, opening, absorption, filling, charge transfer, doping, and intercalation.

Carbon nanotubes are highly graphitized carbonaceous materials and exhibits low chemical reactivity. Oxidation of carbon nanotubes is one of the important chemical reactions; they undergo at high temperatures more than 750ºC. The oxidation takes place from the tips of CNTs

and inward layer by layer [16 25] which results open and thinner tubes after oxidation. The open nanotubes can also be achieved by oxidizing the CNTs with strong acids in liquid phase. Huira et. al. [26] reported that different oxides groups such as carbonyl (-CO), and hydroxylic (-COH), carboxylic (-COOH) covers the surface of the nanotube after oxidation which in turn improve the chemical reactivity of CNTs and modify their wetting properties.

Carbon nanotubes with defects are more sensitive to the chemical reduction and were observed to be gradually degraded when mixed with the alkali metals. The nanotubes broke up into small graphite pieces intercalated into each other. This mechanism is explained as the alkali metals are more likely reacts with the defects and penetrate through graphitic shell layers, with such as 5, 7 pairs on the nanotubes [16 27]. The surface chemisorptions of gas species by carbon nanotubes were also investigated by Huira et. al. [26]. The effect of surface absorption on the electrical resistance of SWNTs by oxygen molecules were reported in the by Collins et. al. [29]. The SWNTs were exposed to vacuum conditions followed by oxygen gas and observed that the measured resistance of SWNTs had an apparent and repeatable variation. Similar variations in electrical resistances were observed with bulk SWNTs with NO2 and NH3 molecules by Kong et. al. [28].

2.1.4 Mechanical Properties of CNTs

Carbon nanotubes are the materials with highest mechanical strength and are considered as the stiffest material in terms of the tensile strength and elastic modulus. The covalent C-C bonds with sp2 hybridization in nanotubes make it as the strongest structures in the nature [5]. The Young's modulus for ideal SWNT in terms of stiffness has been theoretically calculated as high as 5 TPa [30]. The average value of Young's modulus for nanotubes is supposed to be around 1.8 TPa which is very high compare to the maximum value of the Young's modulus of steel

0.186 TPa. The Young's modulus, tensile strength and densities of SWNTs and MWNTs compared with the other materials shown in the Table 2.2.

The defect free nanotubes are much stronger than the graphite because of the axial component of σ bonding. This component is greatly increased with rolling of graphite sheet into a seamless cylinder structure. The Young's modulus of MWNTs is more compared to SWNTs typically in the range of 1.1 to 1.3 TPa [19]. This is because of MWNTs consists of multiple layers of SWNT and the highest Young's modulus of SWNT is considered along with the coaxial intertube coupling of van der Walls force.

Table 2.2: Young's modulus, tensile strength, and density of carbon nanotubes compared with other materials [8].

Material	Young's modulus(GPa	Tensile Strength(GPa)	Density(g/cm3)
MWNT	1200	150	2.6
Single-wall nanotube	1054	150	1.3
SWNT bundle	563	150	1.3
Graphite (in plane)	350	2.5	2.6
Steel	208	0.4	7.8
Epoxy	3.5	0.005	1.25
Wood	16	0.008	0.6

Nano tubes also highly flexible and extremely elastic in nature. According to Despres et. al. [31] the nanotubes are buckle up together when they are bent and straightened out without any damage after releasing the bending force. From the past observations [32] the stiffest materials fail with a strain of approximately 1% considering the defects and dislocations, but CNTs can

withstand 15% tensile strain before any fractures to it [33]. Similar results were observed with deformation, stress and tensile stress of carbon nanotubes which explains their incredible strength and durability.

2.1.5 Magnetic and Other Properties of CNTs

Even though the electrical and mechanical properties of CNTs are of more interest, there are other unique properties exhibited, that make them useful in wide range of applications. According to Davids et. al. [34] the carbon nanotubes exhibit a paramagnetic- to diamagnetic-ordering transition with increase in the radius of CNTs above a critical value 6.4 Å [34]. Magnetic properties such as susceptibility and anisotropic g-factor are expected to be similar to those of graphite even though there is possibility of some unusual properties always exist with nanotubes. The average spin susceptibility and g-value are observed to be is 7×10^{-9} Am^2/kg and 2.012 respectively [35]. These are slightly lower than the graphite which has susceptibility and g-value 2×10^{-8} Am^2/kg and 2.018 respectively. Electron spin response (ESR) is the technique used to measure the magnetic properties [35]. But the interesting part was the electrical response observed when the nanotubes are subjected to external magnetic field.

The effects of electronic states near the Fermi level was observed by Ajiki et. al. [36]. They found an interesting relation between the magnetic moment and magnetic flux of nanotubes by applying magnetic field both parallel and perpendicular to the nanotube axis [36, 37]. The magnetic moment was found to be oscillating as a function of magnetic flux for magnetic field oriented parallel to the nanotube axis. The magnetic moment and magnetic flux was found to be in the same direction when subjected to small flux in case of metallic nanotubes. But for semiconducting nanotubes their direction was opposite. Metal-insulator transition and band gap change for semiconducting tubes cited as the reason by Lu et. al. [38] under magnetic field

parallel to the tube axis. The magnetic character of CNTs is explained by the oscillatory change in the band gap. From Aharonov-Bohm effect, the application of external magnetic field can tune the metallic and semiconducting nature of carbon nanotubes. The resistance change in MWNTs by the application of magnetic field parallel to the tube axis confirms their oscillatory behavior [39].

Thermally, nanotubes are good conductors along the axis of the tube and this property is also described as "Ballistic conduction", but they behave as good insulators laterally to the axis of tube [40]. The thermal conductivity of a SWNT at room temperature is measured as 3500 $W \cdot m^{-1} \cdot K^{-1}$ along the axis where as the thermal conductivity across the axis at the same condition is 1.52 $W \cdot m^{-1} \cdot K^{-1}$. A well known good thermal conductor copper has the conductivity 385 $W \cdot m^{-1} \cdot K^{-1}$ [41].

2.2 Synthesis of CNTs and Purification Methods

2.2.1 CNTs Growth by Arc Discharge Method [15]

Arc discharge method is one of the most common, perhaps the easiest way used to grow carbon nanotubes. Carbon nanotubes are believed to be observed for the first time in the product of electric arc-discharge system [1]. Earlier the arc-discharge method is used to produce structures such as C60 fullerenes, carbon whiskers [42, 43]. A schematic diagram of DC arc-discharge method used for synthesizing CNTs is shown in the Figure 2.2 [15]. This method is optimized for the production of both SWNTs as well as MWNTs depending on the technique used [44].

Two carbon rods act as cathode and anode of the system are placed against each other separated by distance approximately 1mm- 4mm in water cooled vacuum chamber [16]. The chamber is

filled with inert gases such as helium and argon and maintained at pressures between 50 and 700 mbar. A DC current of 80-100 A is passed through the high purity graphite electrodes in helium atmosphere. This generates arc-discharge between the two electrodes. This arc forms high temperature plasma at about 3700ºC [44]. During this arc-discharge, a deposit of randomly oriented MWNTs with some by-products such as polyhedral particles and other graphitic particles form on the cathode. The deposit grows at a rate of 1 to 2 mm/min. During the discharge the other carbon electrode observed to be consumed or evaporated. In order to stabilize the discharge, this electrode is adjusted in such a way that the distance between the electrodes remains constant.

Although the critical parameters that decide the structure of nanotubes are type and pressure of the gas surrounding the arc, the uniformity of the plasma arc and the temperature of the deposit formed on the electrode are also very important for the yield and quality of the nano tubes [45].

The change in the diameter distributions of nanotubes depends on the mixture of the helium and argon gases during the arc process [5] shown in Table 2.3. Different diffusions coefficients and thermal conductivities of mixture of these gases affect the diffusion speed, cooling of carbon and catalyst molecules, resulting in the change in diameters of nanotubes.

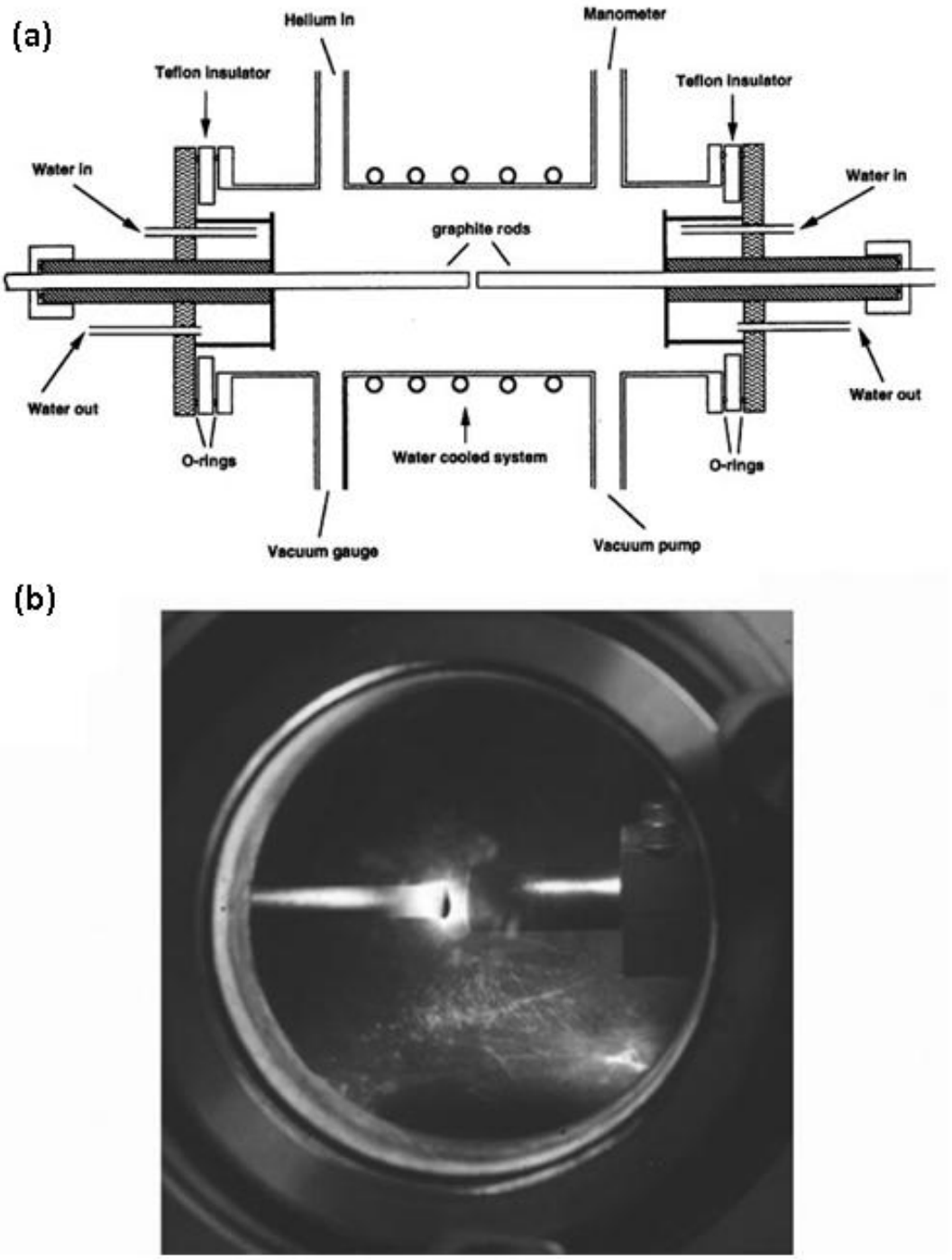

Figure 2.7: (*a*) Schematics of the arc-discharge apparatus employed for fullerene and nanotube production; (*b*) image of the arc experiment between two graphite rods (courtesy P. Redlich). The extreme temperature reached during the experiment is located between the rods (~3000–4000 K) [15].

Table 2.3: The change in diameters with the change in the input parameters for MWNTs during arc synthesis with 6-mm diameter anode rods [5].

N	He	I	Feed rate	Gap(mm)	Deposit diameter(mm)	Growth rate(mg/min)	MWNT amount(%)	MWNT diameter(nm)
1	100	80	4	3.9	7.8	115	5	8-20
2	200	65	4	2.2	6.5	170	10	8-22
3	700	55	4	0.5	7.4	260	20	8-23
4	500	65	8	0.4	8.0	350	20	5-29
5	500	65	2.5	3.5	7.6	90	30	5-46
6	1500	65	1.4	4.2	5.5	20	35	4-60
7	2000	65	1.4	3.3	5.5	22	30	4-60
8	500	160	0.65	0.8	11.6	160	30	5-50
9	500	132	1.0	1.7	1.09	195	30	5-50

Despite of good quality of MWNTs obtained through this method higher yield is always a concern. Helium is considered to be the best of all inert gases, probably because of its low ionization energy. Therefore good control over helium and dc current with constant feed rate and arc current should be maintained for the high yield.

The same method can also be used for the synthesis of SWNTs. Several metals and combinations of metals [5, 48-51] are used for the synthesis of SWNTs using arc discharge method. Commonly used catalysts combinations for the SWNTs synthesis are Ni-Y and Co-Ni. A list of catalysts used in the arc-discharge method at a pressure of 550 Torr He are listed in the Table 2.4 [53].

Table 2.4: Different metals and metal compounds combination that are used as catalyst for the synthesis of SWNTs. (Modified from ref. [53]).

Metal/compounds	Location of SWNT	Density of SWNT
Fe	Soot	Low
Ni	Soot	Low
Co	Soot Weblike	High High
Fe/Ni	Soot Weblike	Very high Very high
Fe/Co	Soot Weblike	High Very high
Ni/Co	Soot Weblike	Very high Very high
Ni/Cu	Soot	Low
Ni/Ti	Soot	Very low
Cu/Co	Soot	Low
Mg/Ni	Soot	Low
Y_2O_3/Co	Soot	Low Radial
YC-2	Soot	High Radial

The SWNTs synthesized are formed as bundles which are tightly bound together in a honeycomb lattice. The lengths of nanotubes are few tens of micrometers long with diameters ranging 1.2- to 1.5 nm. It was also reported in the literature that the nanotubes diameter also depend on the temperature under which they are grown. With the temperatures ranging between 800 and 1200ºC the diameters of nanotubes were 1 to 5nm [54].

2.2.2 Laser Ablation Method for the Synthesis of CNTs [57]

Another way of producing CNTs is by using laser ablation method. Ablation is the removal of surface layer of any solid material through evaporation, chipping or other erosive

process. In this method a laser is used to vaporize the graphite target in an oven at temperature 1200 °C. The laser could be either continuous or pulsed laser. The pulsed laser demands higher light intensity such as 100kW/cm^2 where as continuous laser requires 12kW/cm^2 [55].

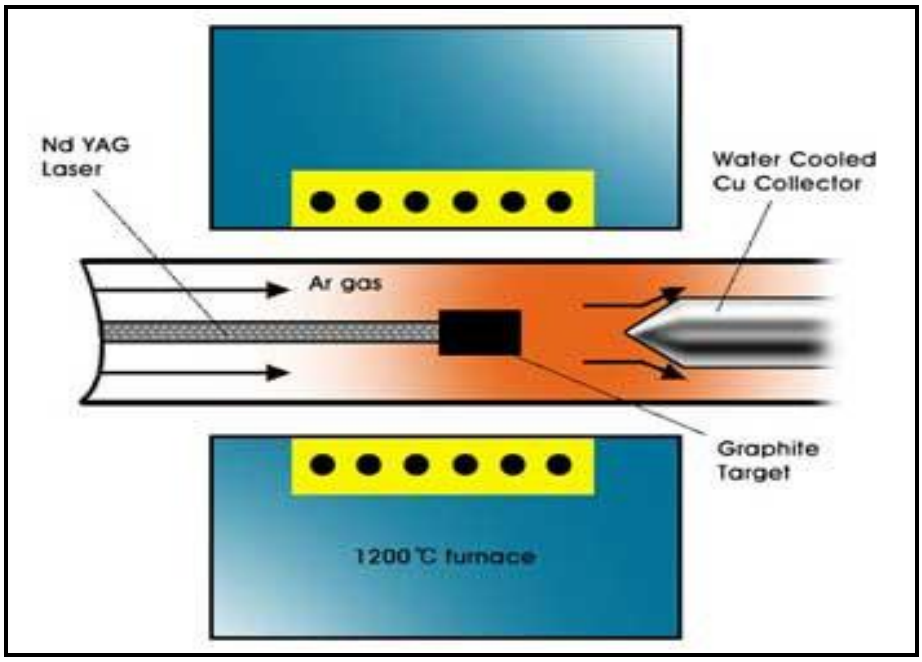

Figure 2.8: Schematic of Laser ablation method [57].

The Laser ablation setup consists of quartz tube furnace with a graphite target in the center as shown in the Figure 2.6. The furnace is maintained at a temperature of 1200°C. The furnace is filled with helium and argon at a pressure of 500 Torr [57]. The intended laser beam is focused on the graphite target. Upon the incident of the laser beam uniformly, the target graphite is vaporized and sublimed. This hot vapor expands at elevated temperatures and cools down. With the cooling of this vaporized species small carbon molecules and atoms quickly condense to form larger cluster and fullerenes. The catalysts used in this process also begin to condense at this point but relatively slow and attach to the earlier carbon clusters and prevent them from

closing into a cage structures. The initial clusters of carbon are responsible for the growth of SWNTs and are bundled together by van der Waals forces [57].

The resultant condensates are contaminated with lot of carbon nano particles and carbon nanotubes. Both MWNTs and SWNTs can be synthesized using the laser ablation method. For MWNTs a pure graphite electrode is used where as in the case of SWNTs a mixture of graphite with Ni, Co, Fe and Y etc are used [57].

The laser ablation method produces SWNTs of diameters ranging from 1 to 2 nm. The pulsed laser technique with catalyst mixture Ni-Co at 1470 °C produces SWNTs with diameters 1.3 to 1.4 nm where as a continuous laser at 1200 °C and Ni-Y catalyst mixture with ratios 2:0.5 gives an average diameter of 1.4 nm [57].

2.2.3 Chemical Vapor Deposition Method

Chemical vapor deposition (CVD) is the widely used method to synthesize SWNTs and MWNTs. More precise and controllable growth of nanotubes on patterned substrates can be achieved at reasonable rates. The CVD method of nanotube preparation essentially involves two steps. One is preparation of the catalyst and the other is actual growth of carbon nanotubes. The preparation of the catalyst involves sputtering of a transition metal such as Ni, Fe and Co on to the substrate material [5]. Then this substrate is subjected to either thermal annealing or chemical etching to induce catalyst particle nucleation. Clusters of transition metal formed on the substrate as a result of annealing. Nanotubes are achieved by the changing the carbon source molecules into gas phase using different energy sources such as plasma or resistively heated coil. This energy is used to break the source carbon molecules into reactive carbon atoms and nanotubes are formed on the transition metals if the proper parameters are maintained.

The two important methods of CVD are thermal chemical vapor deposition and Plasma-enhanced chemical vapor deposition (PECVD). Thermal CVD uses a conventional heat sources such as resistive, inductive filaments, or infrared (IR) lamp to heat the furnace to the required temperature. PECVD uses plasma as the source to create glow discharge which contains radicals, electrons, and ions.

In thermal CVD the substrate is initially sputtered with Fe, Ni, Co or an alloy of the three catalytic metals in a sputtering chamber. Then the substrate is etched in a diluted HF solution with distilled water. The specimen is then placed on a quartz boat into the CVD reaction furnace. After additional etching of the catalytic metal film at temperatures 750 to 1050 °C using NH3 gas nanometer sized catalytic metal particles are formed. The CNTs are grown on these fine catalytic metal particles. Controlling the nucleation site of transition metals deposited on silicon substrate by dipping in HF solution and/or NH3 pretreatment is crucial step of the growth of vertically aligned CNTs prior to the pyrolysis of C2H2 gas. Figure 2.8 shows a schematic diagram of thermal CVD apparatus in the synthesis of carbon nanotubes. Both SWNTs and MWNTs are synthesized using this method. The appropriate choosing of metal catalyst we use in the process decides whether the tubes are multi-walled or single-walled. Acetylene is used as a source of carbon atoms for the synthesis of MWNTs with temperatures typically between 600 to 800°C [57].

To grow SWNTs, carbon monoxide or methane are used at temperature 900 to 1200°C [57]. The temperatures used are high in this case due to the fact that they have higher energy of formation. The gases chosen have increased stability at this high temperatures compared to the acetylene.

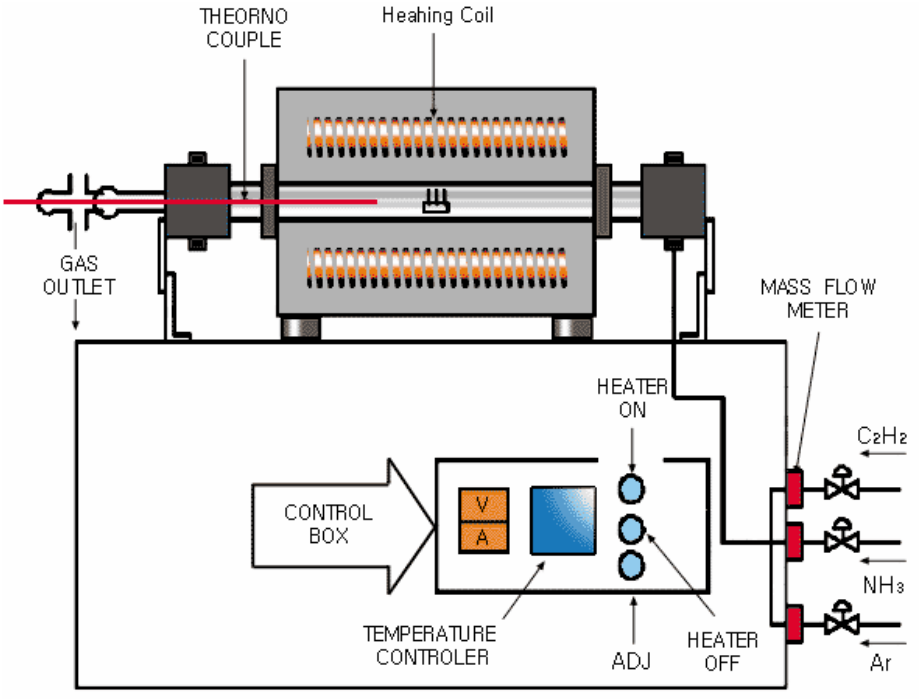

Figure 2.9: Schematic of Thermal CVD method for the synthesis of CNTs [57].

Plasma enhanced CVD (PECVD) is the other method to synthesize nanotubes [5]. In this method nanotubes are synthesized by the glow discharge in a chamber or furnace by applying a high frequency high voltage to both the electrodes. Fig 2.10 shows the schematic diagram of a PECVD apparatus [5]. The chamber consists of parallel plate electrode structure with substrate placed on the grounded electrode. The distance between two electrodes is adjusted in order to sustain the discharge by using Pd=constant equation, where P is the pressure and d is the distance between electrodes. A separate heat source is used for the electrode holding the substrate in order to maintain the temperature of the wafer at the desired level and to enhance the nucleation density.

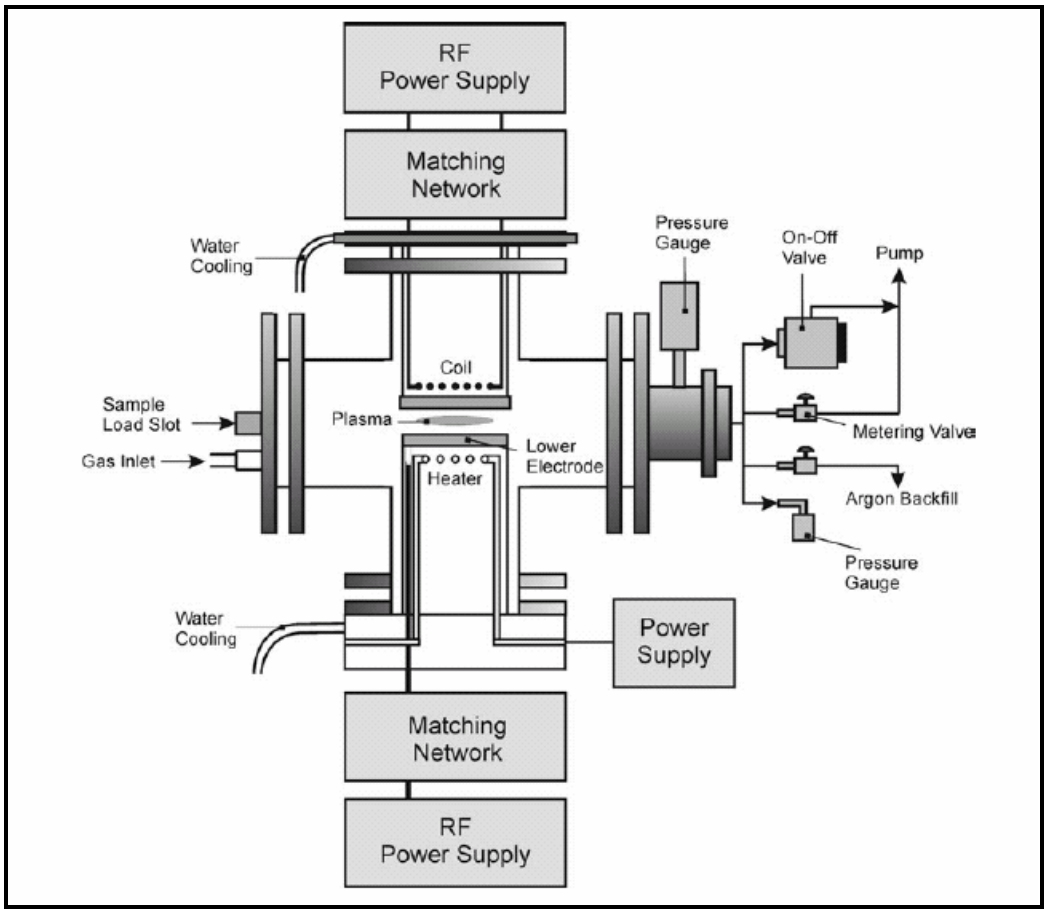

Figure 2.10: Schematic of PECVD method to synthesize CNTs [5].

As in the case of thermal CVD the substrate is sputtered with catalytic metals such as Fe, Co and Ni. The substrates can be Si, SiO2 or any other glass to grow nanotubes on it. Sources such as DC, RF (13.56 MHz) or Microwave (2.45 GHz) are used to generate the plasma [5]. The reaction gas is supplied from the opposite plate of the substrate holding electrode in order to form a uniform layer of CNT film. The typical operating pressures for the nanotube deposition are 1 to 20 mTorr. The feed gas such as C2H2, CH4, C2H4, C2H6, CO is supplied to the PECVD chamber during the discharge. The breakdown of this feed gas occurs with a negative bias voltage (>300V) applied on the cathode [19]. This result in the glow discharge composing of ions (positive and negative), electrons, atoms and radicals. Carbon nanotubes are grown on the

fine nanoscopic metal particles which are already sputtered on the substrate. Hydro-carbon gases that are used for the discharge are diluted with gases such as argon, hydrogen or ammonia to prevent any ionization due to plasma. This ionization can create reactive radicals and pure hydrocarbon in plasma reactors, which may result in substantial amorphous carbon deposition. The local electric field formed between the plasma and the substrate holder allows carbon nanotubes to grow extremely vertical with high density.

The low operating temperatures during the growth mechanism of nanotubes compared to the other methods makes PECVD attractive for the integrating carbon nanotubes into the applications of semiconductors device fabrication. Good individual free-standing vertically aligned CNTs can be produced by this method; whereas marginal aligned nanotubes resulted from crowding effect and supporting each other by van der Waals attraction are observed in the case of thermal CVD. The catalyst used has the strong effect on the nanotubes morphology, growth rate and diameter.

2.2.4 Purification of CNTs

Carbon nanotubes produced by the methods discussed above contains impurities. These impurities affect the intrinsic characteristics and desired properties of CNTs. Impurities such as catalytic metal particles, graphite impurities and large amounts of polyhedral nano particles are also seen with the CNTs. Most methods used for the fabrication of CNTs yields a significant amount of by-products such as amorphous carbon that deposits on the nanotube walls, carbon nano-spheres, other carbon allotropes such as fullerenes and atomic carbons.

Oxidative treatment is one of the most widely used method for the purification of the CNTs. Chemical oxidation of the material in oxygen-containing gas or acid is a good way to remove carbonaceous impurities and to clear the metal surface [40]. The basal planes of graphite which

are carbon nanotubes walls are subjected to oxidation only if defects are present. The main disadvantage of this method is, it also oxidize the CNTs which is not desired. Ebbesen et. al. [40] tested the oxidative treatment method on the MWNTs prepared by arc discharge method to remove the polyhedral graphite-like particles [64]. From the results it is appeared that more than 95% of the starting material is damaged and the remaining nanotubes became more reactive at their ends due to the presence of dangling bonds (open ends). High temperature annealing (2800°C) was necessary to eliminate dangling bonds. For SWNTs refluxing the raw material in acid followed by centrifugation or cross-flow filtration is used to remove catalyst particles and amorphous carbon [65, 66].

Micro filtration is the next method of purification which is based on the size of the particles to be separated and involves physical separation of impurities [57]. Small amounts of nano-particles are trapped along with the SWNTs while most of the particles (fullerenes, catalyst metal and carbon nano-particles) are filtered out. Figure 2.7 shows the schematic diagram of the micro filtration cell [57].

The SWNTs with impurities are first soaked in the CS2 (Carbon Disulphide) solution. The impurities such as fullerenes, catalyst metal and carbon nano-particles which are solvated in the CS2 solution are passed through the filter. The insolubles of CS2 solution which are SWNTs are then trapped in a filter as shown in the Figure 2.11. A colloidal suspension of CNTs by chromatography method is also used for the purification. Bonard et. al. [67] developed method of where properties of colloidal suspensions are used for the purification of the MWNTs [68]. Residues with CNTs content over 90% in weight were obtained as compared to 40% for the starting material.

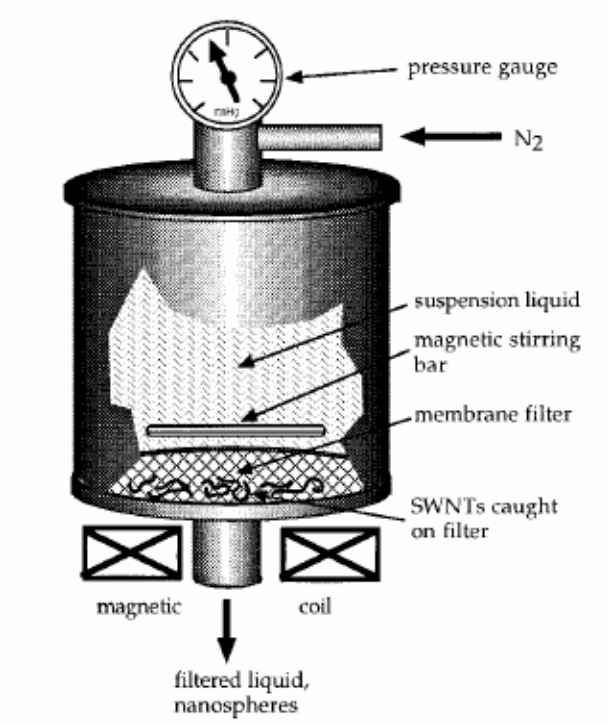

Figure 2.11: Schematic for the micro-filtration method [57]

In addition to the above purification techniques, methods such as Annealing, Ultrasonication, Functionalisation, Acid treatment and magnetic purification are also used for the purification of CNTs. It is important to emphasize that the above methods may alter the structural surface of the CNTs, leading to drastic change in the electronic, mechanical, and chemical properties.

2.2.5 Growth Mechanism of CNTs

Various theories have been proposed to explain the growth mechanism of CNTs. Here two methods namely tip-growth and base-growth are discussed, with existence of metal catalyst in the pyrolysis process during the fabrication of CNTs. According to the Baker and coworkers [70], the hydrocarbon is decomposed into C_n and H on to the top surface of the metal catalyst. CNTs are supposed to be grown when these carbon fragments diffuse into the metal particle and precipitate at the other end of the particle. The catalyst particle remains on the tip of the tube

during the growth process until the leading catalytic particle is neutralized or the reaction is stopped with the hydrocarbon gas, due to the encapsulation of metal catalyst by a layer of carbon [70]. But according to Baird et. al. [71] and Oberlin et. al. [72] the postulations the carbon fragments diffuse via the surface instead of the body of catalyst metal particles and precipitates at the other end.

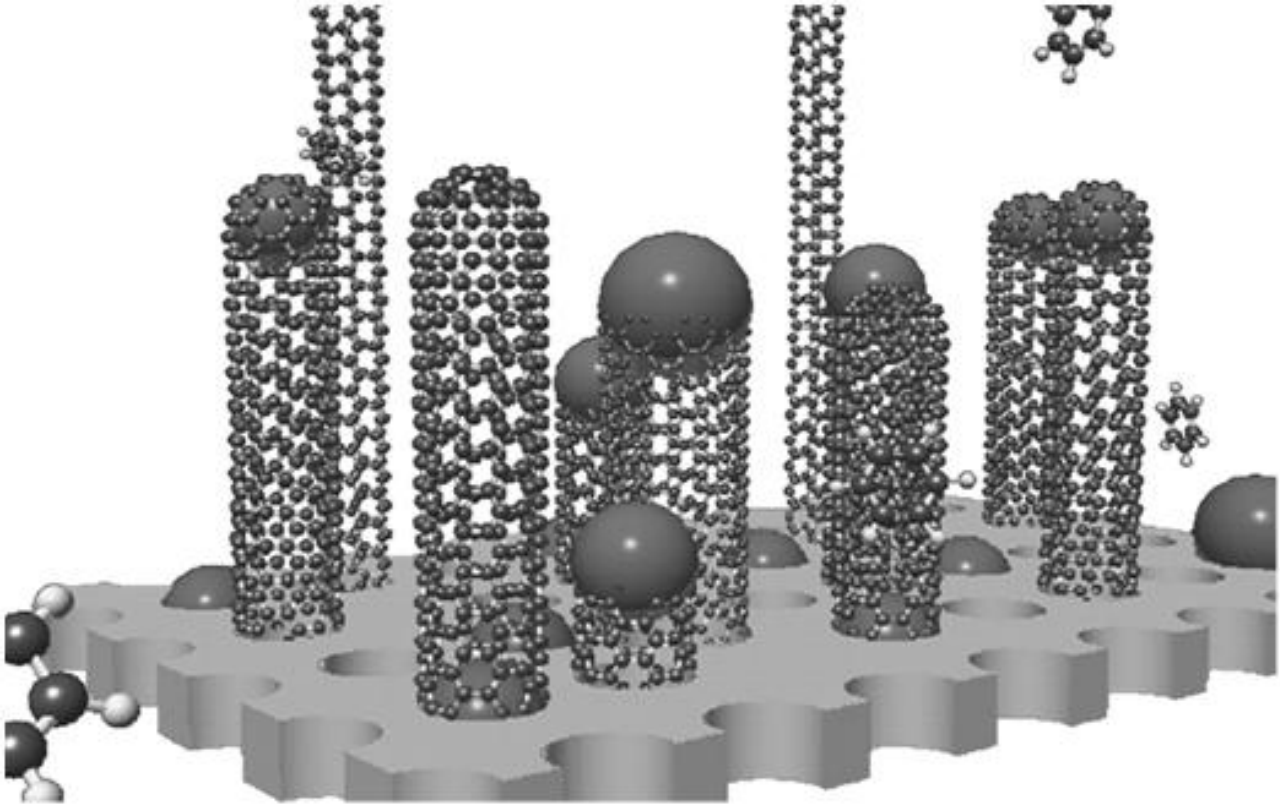

Figure 2.12: A graphical description of the tip-growth and root-growth nanotube models, in which the catalytic particles are located at the tip and at the root, respectively. Carbon species are illustrated as benzene molecules, and the base is the simplified model of the zeolite (Hayashi et. al. 2003) [4]

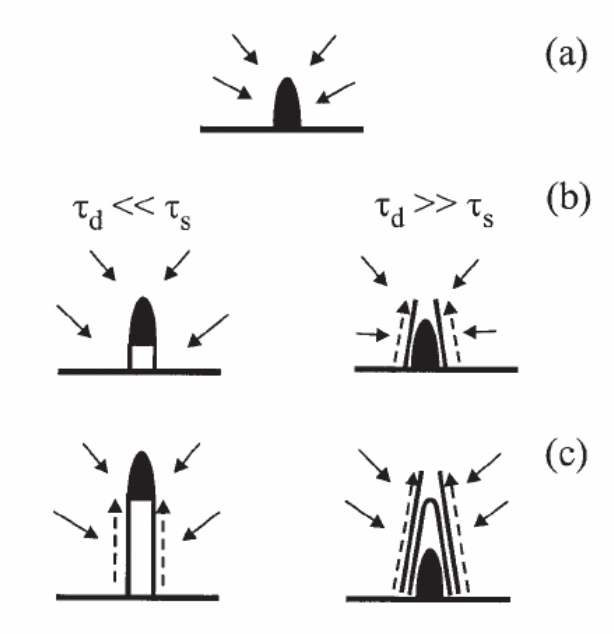

Figure 2.13: Schematic of CNTs growth mechanism tip-growth and base-growth model. On the left, the nanoparticle is detached from the substrate on the tip of nanotube, catalyzing growth and preventing nanotubes closure. On the right hand side, the nanoparticle remains on the substrate, severing as an initial template for nanotubes nucleation. Figure (a) shows the saturation of nanoparticle with carbon (b) nanotubes nucleation stage and (c) post-nucleation growth [75].

The other theory explains CNTs growth mechanism with diffusion of carbon species through the surface of metal catalyst. The catalytic metal particle always supposed to be remained at the bottom of the filament or tube during the growth process [70, 73]. The rapid diffusion of carbon species through the catalyst results in the growth of the filament. In this model the nanotubes grow from their bases unlike the first model where the tubes are grown from their tips. The bottom growth of CNTs was confirmed in many reports including Zhu and coworkers [74]. They observed the left over cone shaped Co particles on the silicon substrate after complete removal of nanotubes from the surface.

Louchev proposed a model that combines both tip-growth and base-growth models together which is illustrated in the Figure 2.13 [75]. For CNTs nucleation and growth, the diffusion

process of carbon species through the catalytic metal particles is important. Two characteristic times were defined to explain the growth mechanism of CNTs.

(i) The characteristic diffusion time of carbon through the catalytic metal nano-particle to the nanotube growing point is given by

$$\tau_d = R_p^{\,2}/D_b$$

Here R_p is the radius of catalytic metal particle and D_b is the diffusion coefficient.

(ii) The surface saturation time of order

$$\tau_s = C^2 D_b / Q^2$$

Here C is the saturation concentration of carbon and Q is impinging carbon flux.

Increase in the carbon content to the saturation concentration level is known as surface saturation which is responsible for triggering the carbon precipitation directly on the outer surface of the metal nano-particles. If $\tau_d << \tau_s$ the tip growth mechanism dominates [86]. In this case the carbon diffuses through the metal particle much faster than the time of particles surface reaches the saturation point. Therefore the carbon is precipitated at the bottom of the catalytic particle, lifting the particle during the growth process resulting in the tip-growth process. $\tau_d >> \tau_s$ implies the surface saturation time for carbon through the surface of metal is faster than the diffusion through the body, results in the precipitation of carbon on the catalytic particle surface, providing a nucleation template for the CNTs. The metal remains at the bottom and the nanotube grows out of the metal particle which is regarded as base-growth model [86].

In addition to the nucleation and carbon diffusion parameters during the pyrolytic process the growth of CNTs also depends on particle adherence, dimensions of metal particles, processing temperature, hydrocarbon and other gases involved.

2.3 Field Emission of Electrons from Solid Surface

2.3.1 Field Emission from Metal and Semiconductor Surface

Electron field emission is the extraction of electrons from a solid by tunneling through the surface potential barrier when a strong electric field is applied. Wave-mechanical methods were applied to the basic theoretical considerations of electron emission from metals under the influence of an external electrical field by Fowler and Nordheim [76]. There were few basic assumptions made for this model. (1) A simple one-band electron distribution using Fermi-Dirac statistics; (2) A smooth, plane metal surface where irregularities of atomic dimensions are neglected; (3) A classical image force; (4) And a uniform distribution of work function. Based on the above assumptions, the field emission current density J is given as

$$J=A\,(F^2/\Phi)\,exp(-B\Phi^{3/2}/F)$$

Where J is current density in A/cm^2, A= 1.56x10^{-6}, B=6.83x10^{-9}, F is applied electric field in V/cm and Φ is the work function of the solid in eV [86].

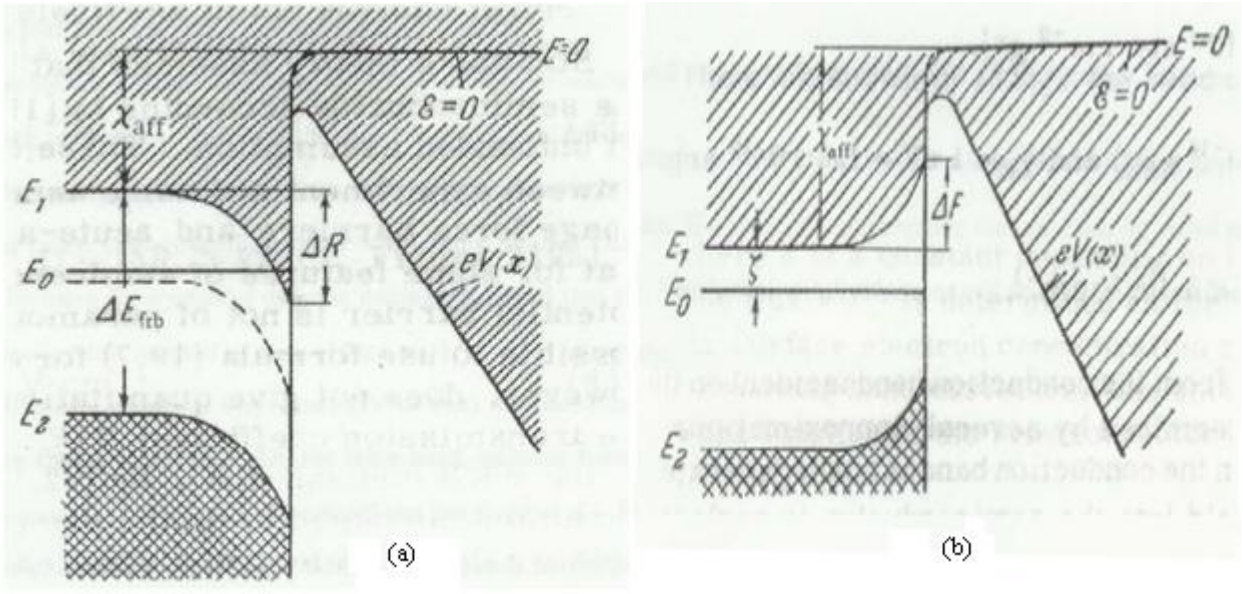

Figure 2.14: (a) Band diagrams with bending near the semiconductor surface by strong electric field. (b) Internal barrier generated by internal retarding field [77].

When a potential difference of V is applied across two planar parallel electrodes with separation distance d, the electric field is given as $E=V/d$. Instead of flat surface, if there is sharp needle on the emitting surface, the local electric field on the tip of the needle is much stronger by a factor of β. Here β is known as enhancement factor, determined by the geometric shape of the emitter and the electric field at the emitter surface given as

$$F= \beta E= \beta V/d$$

where E is the macroscopic field between anode and cathode.

Electrons tunneling through the surface barrier become significant when the local microscopic electric field is high enough that the thickness of the potential barrier is comparable to the electron wavelength in the solid. Using the above two equations the electron emission current as a function of local electric field is given by

$$I \propto (\beta^2 E^2/ \Phi) \exp(-B\Phi^{3/2}/\beta E)$$

The above relationship is also known as Fowler-Nordheim equation [78]. Theoretically speaking this model is valid only for flat metal surface at 0K. However the model is valid in most other cases too and is widely used because the deviation is negligible [78].

The small variations of the shape surrounding the emitter which determine the field enhancement factor β has great impact on the emission current density because of exponential relationship between current and field enhancement factor. Similarly any change in the surface chemical state will also have strong impact on the emission current density as it influences the work function. Field enhancement factor and work function can be estimated by Fowler-Nordheim model. This can be done by Fowler-Nordheim plot by plotting $\ln(I/E^2)$ versus $1/E$ using the following equation.

$$\mathrm{Ln}(I/E^2) \propto \mathrm{s}\ 1/E$$

A straight line can be obtained with the slope s depending on β and Φ, which is given by

$$s = -B\,\Phi^{3/2}/\beta$$

Work function for the CNTs is usually in the range 4.5 to 5eV [8]. Shiraishi et. al. [79] measured work function of SWNTs and MWNTs using photoelectron emission (PEE) technique as 5.05 and 4.95eV respectively [79].

2.3.2 Field Emission from CNTs

CNTs are considered as fairly good electron emitters with conductivity, among other carbon compounds such as diamond and diamond-like carbon (DLC). A summary of electron emission behaviors measured for different materials are listed in the Table 2.5. The field emission characteristics of CNTs so far are excellent with macroscopic electric field 1 V/μm and turn-on electric field around 3-5 V/μm. Though there is no perfect definition for the turn-on electric (E_{to}) and threshold electric field (E_{thr}) field. They are generally defined as macroscopic electric field needed to extract emission current density of 10uA/cm^2 and 10mA/cm^2 respectively in the case of flat panel display applications.

The emission currents reported to be fairly stable over long runs of operation without any degradation [80, 81]. The field emission current of a single nanotube is observed to be constrained because of its very small dimensions. Using array of aligned nanotubes or nanotube film could be improvement for the above case. The interesting point to be observed here is, the high density of nanotubes at the emitting surface does not give high emission site density during the field emission. This can be understood as too many tubes result in screening out the electric field [82]. Vertically aligned nanotubes are considered as the ideal emitting structures with spacing among each tube roughly equal to their height. However even in a dense carbon nanotube film where all the tubes are closely packed and vertically aligned, the density of emitting tips (e.g., on the order of 10^5 cm^{-2}) is

only small fraction of complete density (~10^8 cm^{-2}) [82]. It implies that only the tubes with sharp tips and those tubes protruding out of the surface emit efficiently. On the other hand an interesting phenomenon was observed in the case of randomly oriented CNTs by W. Zhu et. al. [80]. A phosphorous screen is placed on the emitter to find the emission sites of a SWNT film which were grown on Si substrate using laser ablation method. When the applied electric field was low, well-defined rings were observed on the screen and with increase in the field a two-fold symmetric pattern is observed. This may be because when low electric field is applied, the field emission is dominated by the tubes that are perpendicular to the surface. With larger electric fields the loops of nanotubes may also contributed to the emission. Finally the phosphorous becomes overloaded with further increase in the electric field which eventually increases the emission site density and the current. Hence it is not possible to determine the emission pattern with higher electric fields. There is also possibility that the loose ends of nanotubes align themselves to outer electric field and the electrons are emitted from those ends which protrude out from the surface [86].

Table 2.5: Emission threshold electric fields for various emitter materials [80].

Material	**Threshold field (V/μm)**
Mo Tips	50-100
Si Tips	50-100
p-type semiconducting diamond	160
Undoped, defective CVD diamond	30-120
Amorphic diamond	20-40
Cesium-coated diamond	20-30
Graphite powders (<1 μm size)	17
Nanostructured diamond particles	
As Coated	Arcing-no emission
Heat-treated in hydrogen gas	Arcing-no emission
Heat-treated in hydrogen plasma	3-5
Carbon nanotubes (both MWNTs, SWNTs)	1-5

Walter de Heer and colleagues conducted series of field emission experiments on single nanotubes as well as SWNT and MWNT films. Assuming $\Phi=5\ eV$ typical field enhancement factors calculated form F-N slope ranged from 30000 to 50000 for single MWNT and from 1000 to 3000 for MWNT films. The values for E_{to} and E_{thr} were found to be 2.6 V/μm and 4.6 V/μm respectively. Similarly for SWNTs films β ranged from 2500 to 10000 with E_{to}= 1.5-4.5 V/μm and E_{thr}= 3.9-7.8 V/μm [67, 68].

The field enhancement factors were significantly larger for SWNTs than the MWNTs, probably due to the smaller tip radius and smaller curvature radius of SWNTs. Stability of the currents emitted and the degradation tests for both SWNTs and MWNTs were also examined. Gradual degradation in the emission current was observed with time. This could be because of gradual destruction of the tubes, primarily through bombardment by gas phase electron ionization or by ion desorption from the anode, both induced by the emitted electrons. The degradation in the case of SWNTs is more compared to the MWNTs. Experiments show that the operating pressure in the testing chamber plays major role in the degradation of CNTs. This is because the excess residual gas molecules in the chamber are ionized during the aging process resulting in the destruction of the tips of nanotubes. Therefore higher vacuum conditions results in better and stable current emissions compared to the results in poor vacuum conditions.

Y. Saito et. al. [14] studied the field emission characteristics of individual SWNT micro bundles and MWNTs with open caps, where they have used these tubes as the sources in field emission microscope. One of the important methods to test various emission mechanisms for the emitted electrons is Electron Energy Distribution (EED). It distinguishes the states where exactly electrons come from. Experiment results show that electrons are emitted from a narrow band state of 0.2 eV half-width for MWNTs films. The position of the band with respect to the Fermi level varied from one tube to the other. Even the Field emission microscopy of MWNT films also revealed that,

electrons are emitted from electronic states localized at the tip, but not delocalized conduction band electrons as in metals. The measurements from scanning tunneling spectroscopy and the theoretical calculations confirmed that the local density of states at the tip present sharp band states which may be located on either side of the Fermi-level depending on the geometry [14].

Recently many applications based on the electron field emission of CNTs have been demonstrated. CNTs for the flat panel displays were proposed as the alternative for the many other field emission displays in 1995 [82]. A fully sealed 4.5 inch three color field emission display was demonstrated by Samsung [83]. Other applications such as Microwave tubes, X-ray tubes, general cold-cathode lighting sources, lightning arrestors, and electron microscope sources have been demonstrated [86].

2.3.3 I-V Instabilities and Arcing Protection

The stability and reproducibility of Field emission characteristics of field emission cathodes is the major problem when they are used in low power applications. Ion sputtering due to poor vacuum, arcing, resistive heating of emission site and surface migration are the major factors contributing to the degradation and premature failure of the field emission cathodes [86]. Ionization of gas molecules and/or desorbed contaminants probably the reason for arcing failure, is the primary barrier for the field emission utilization in high current applications such as klystrons, twystrons and travelling wave amplifiers. Efforts have been carried out to stabilize the I-V characteristics and lifetime issues of the field emission system using methods like passive resistor stabilization, active transistor cathode current limiting and closed loop stabilization [17]. Integrated passive resistors that provide current limiting are used in applications such as flat panel displays for resolving lifetime and stability issues. However this approach may not be suitable for the operation at high frequencies and current density.

2.4 Applications of CNTs

Carbon nanotubes nano size structures, high mechanical strength and remarkable physical properties make them unique material. With their special electrical, chemical, magnetic and mechanical properties they are considered to be the most attractive material for variety of potential applications. Recent research and studies on CNTs increasing the scope of its applications over wide range and many prototype electronic devices have been developed using CNTs [5].

2.4.1 Electronic Applications

High electrical conductivity and the sharp tips of CNTs (with sharper tips the concentration of electric field will be high) leads to the field emission. The emission of electrons at very low applied voltage is due to the fact that the tips of CNTs are very sharp. They also can carry high current densities for long duration. The immediate application of these characteristics is in flat-panel displays. The low turn electric field, high current density and steady long-lived behaviour of CNTs are preferred instead of traditional cathode ray tube display systems [5]. Other applications using the field emission characteristics include electron microscope, lightning arrestors and cold-cathode lighting sources.

The application of CNTs in nanotechnology has been effective for building electronic circuits. As the dimensions of electronic circuits are shrinking to nano-scale the interconnections between the active devices and other switches becomes more important. The geometrical structures, electrical conductivity, and ability to derive precisely, make CNTs best choice for connections in electronics. Both conductive and semi-conductive nature of CNTs combined with flexibility in nano-scale design enable wide variety of device configurations. A transistor with semiconducting single nanotube connected to metal nano electrodes was fabricated by Sanders

et. al. [84]. This transistor operates at room temperature and the performance in terms of switching speeds, owing to low capacitance is excellent. It was said that MWNTs can also be used as n- and p- type material for the novel p-n junctions and transistors fabrication where N-doped CNTs behave as n-type and P-doped tubes behaves as p-type conductors [85]. Research has been conducted on metal-metal, metal-semiconductor and semiconductor-semiconductor nanotube junctions to find their electronic behaviour by Yao and his colleagues [100]. They found that the metal-semiconductor junction behaves like rectifying diode with nonlinear transport characteristics.

2.4.2 Mechanical Applications

One of the potential applications of CNTs is as reinforcement for metals, ceramics, or polymers. The reinforced material could be used for the ablative coatings for rocket nose cones, nozzles for rocket engines and brake shoes for aircraft [86].

The high mechanical strength and elasticity of CNTs makes this an excellent material for the production of high resolution, long life microscope tips and nano tools such as nano tweezers Figure 2.15 with electronic interactions between carbon tube cylinders to operate [87].

The nanotubes can also be fabricated as one-dimensional nanowires. With relatively straight and narrow channels in the centre, it was speculated that there is possibility to stack atoms of foreign molecules in these cavities. The capillary forces in nanotubes should be strong enough to hold gases and fluids inside the cavities. Low melting compounds such as (Pb-C-O), V_2O_5 [48, 89] are used to fill the channel cavities of MWNTs. With thermal treatment of silver nitrate at 400 ºC decomposes it into pure silver and a silver nanorod is generated in the cavity of CNT.

These led to the use of CNTs as moulds to fabricate nanowires and one-dimensional composites with interesting electrical and mechanical properties. Electromechanical actuator which could be used in artificial muscles [90] is one novel application which is based on sheets of SWNTs.

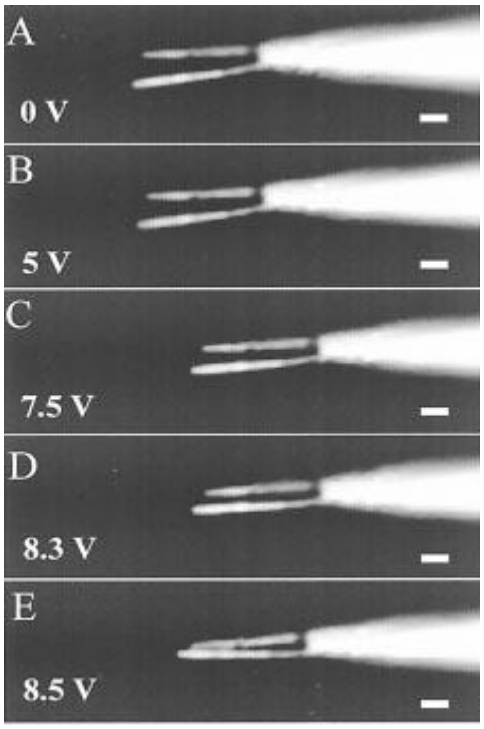

Figure 2.15: Nanotweezers with increasing gap with increase in applied voltage [87].

In addition there are other potential applications for CNTs such as nano-porous fillers [104], catalyst supports [103], energy storage [101, 102], strain sensors [104] and various biomedical applications [105]. In future there are possibilities of many unanticipated applications that could come into practice by this remarkable material.

CHAPTER 3

FABRICATION OF CARBON NANOTUBES

3.1 Introduction

Since the discovery of carbon nanotubes various methods have been investigated and reported for their fabrication. In recent times, researches are focused on the controlled synthesis of various types of CNTs by chemical vapour deposition method. Mostly, highly aligned and uniform length CNTs found to be promising for the applications in field electron emitters for many other electronic devices. However, in practice the effective use of CNTs in various applications as cold cathode emitter is limited. The reason for this is the synthesis of CNTs on various substrates such as silicon, silicon oxide, polysilicon metal and other non-planar surfaces is difficult and not as repeatable. It is very hard to control the morphology of CNTs that are directly synthesized on materials with microscopically rough surfaces. In order to grow CNTs on metal surfaces, the diffusion of metal catalyst into the metal substrate at high temperatures is the major problem. It is also difficult to control selective deposition of CNTs with desired orientation and length using non-planar surface substrates with holes and trenches.

As mentioned earlier the thermal CVD method has its advantageous over microwave, plasma enhanced CVD, and other CNT fabrication techniques. Even though it is difficult to control the alignment and density of CNTs using this method, the simple equipment setup and excellent uniformity over large substrate makes it much more desirable. This method is also less expensive

and more productive compared to the other methods. However there are few by-products such as amorphous carbon, fullerenes, and some polyhedral compounds are observed in the CNTs grown by thermal CVD. The CNTs grown by this method are usually randomly oriented, but evenly growth of aligned nanotubes is also possible. The repeatability of the process is poor. The adhesion of directly grown CNTs to the substrate is poor because of weak van der Waals force. This could be a problem during the practical applications of the tubes. For instant, during the field emission characteristic testing of CNTs coated on a silicon sample, some nanotubes were pulled out of the original substrate by strong electric force when high electric field is applied. The tubes are deposited onto the clean counter electrode and started to emit electrons [86].

3.2 Growth Process

In this work, thermal CVD is used to fabricate CNTs. Silicon wafers are used as the substrates for the growth of nanotubes. These wafers are first cleaned by the standard cleaning procedures adopted by the semiconductor industry. This includes cleaning wafer with diluted HF solution and DI water. The cleaned wafers then are loaded into the sputtering chamber. The wafer is baked for 5 minutes at the temperature 100ºC to ensure there is no moisture on the surface before sputtering. Iron is used as the catalyst to deposit onto the surface of wafer using DC sputtering using cast iron target. The pressure in the chamber is maintained at $5x10^{-6}$ Torr. The typical sputtering times used ranges from 5 min to 20 min. Figure 3.1 show an SEM image of sputtered silicon substrate with iron as catalyst and DC sputtering time of 5 min.

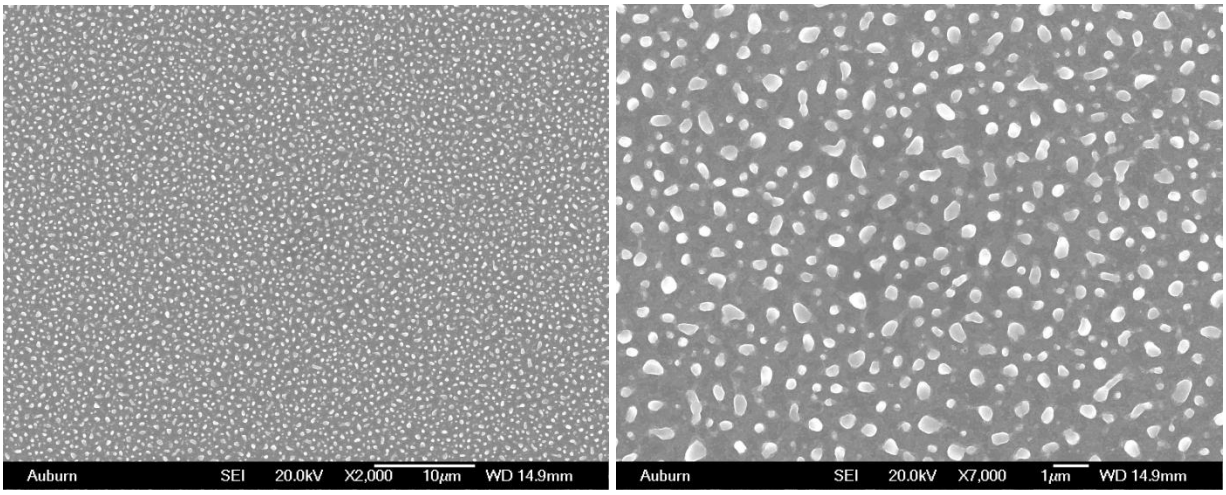

Figure 3.1: Silicon wafer sputtered with Fe. Images with resolutions 2000x and 7000x

After sputtering process the silicon wafer substrate is then loaded into quartz-tube furnace the thermal CVD reactor shown in the Figure 3.2 to grow CNTs. A resistive heater is used to heat the quartz substrate and the substrate holder inside the furnace [86]. A thermocouple is connected to the substrate holder to measure the temperature. Flow meter connected between the chamber and the gas cylinders is used to measure the flow into the CVD chamber. The pressure in the chamber is controlled by a valve, which is connected between mechanical pump and the pressure gauge. Mixture of Acetylene and Argon with 20 and 75sccm respectively were used as the feed gases for the growth of CNTs. The growth of CNTs is carried at a temperature of 700 to 750ºC and at a pressure of 70 Torr.

The growth time was typically in the range of 10-240 minutes depending on the desired densities of carbon nano tubes. In order to find the effects of growth time on the field emission characteristics, and the life time, and current stability, different growth periods were considered. It is observed that the CNTs grown with growth times 10 and 20 min had less density. The

density of CNTs is observed to be increased with increase in growth time. Typically the CNTs samples fabricated with growth time 40 min and above had higher density of CNTs with very long tubes. These samples have relatively low turn-on and high current densities compared to the samples with less growth periods. It is observed that, the sputtering time also affected the growth of CNTs. Though the difference in the density of CNTs is not obvious from the SEM images of samples with same growth time but 5 min and 10 min sputtering times; small difference is observed in the turn-on electric field and current densities. High density of impurity clusters observed along with the CNTs for those samples with sputtering time of 20 min and above. The turn-on voltage for 20 min sputtering samples was high compared to that of 5 min and 10 min sputtering.

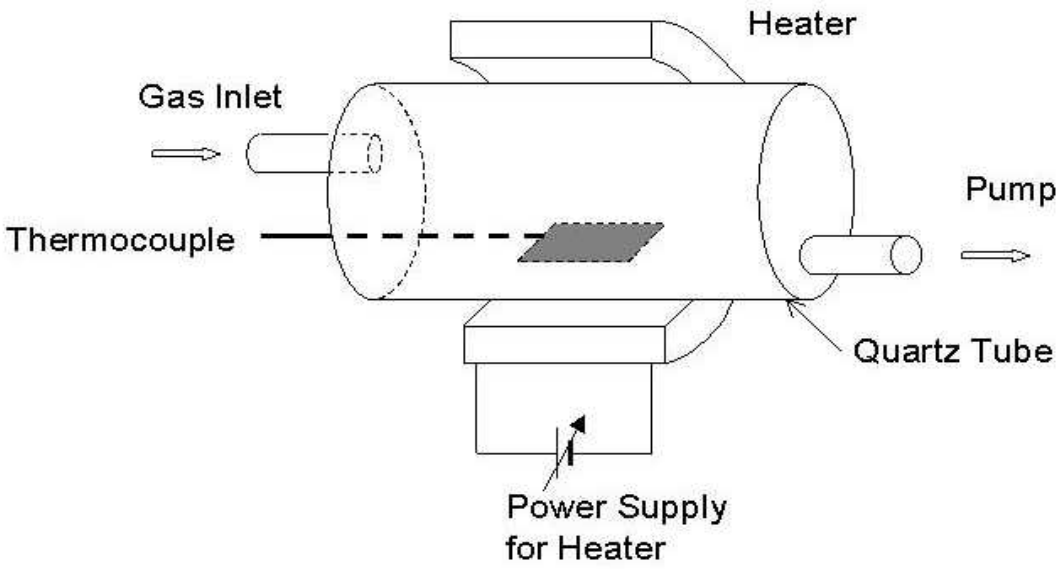

Figure 3.2: Schematic of Thermal CVD growth of CNTs [91].

In this research work the CNTs are fabricated with growth times of 10, 20, 40, 80, 120 and 240 min. A set of CNT samples of above growth time period were fabricated with sputtering time of 5 min and other set with 10 min. The catalyst used for the sputtering was iron. Samples with sputtering time of 20 min are also used to compare for changes in the growth or alignment of the CNTs. Figures 3.3, Figure 3.4 and Figure 3.5 shows the SEM images of different samples of CNTs grown under different conditions. The notation 5-10 means sample with 5 min sputtering and 10 min growth period. The same notation is used for all the samples throughout this book.

3.2.1 SEM Images

Following are the SEM images of the samples with 5 min, 10 min sputtering and 20 min sputtering. The samples with different growth time for both cases are presented with resolutions 9000X and 30000X. The following images show that the samples with both 5 min and 10 min sputtering time are cluster free CNTs. But the CNTs with sputtering period 20 min consist of lot of impurity clusters in them. The carbon clusters probably could be the result of higher decomposition rate of hydrocarbons than that of CNTs growth rate [7]. The 10 minutes sputtering of silicon substrate with Fe after 5 minutes baking, and then CVD growth of CNTs has produced very good quality randomly aligned Multi Walled Carbon-nano tubes (MWCNTs)(See Figure 3.4). These tubes are free from any kind of impurity clusters. The decrease in the sputtering time from 20 min greatly reduced the impurity clusters and almost there were no clusters in the tubes with 5 min, and 10 min sputtering. The length and density of nanotubes is increased with increasing the growth period in all cases.

3.2.1.1 Images of CNTs with 5 min Sputtering

(a) 5-10

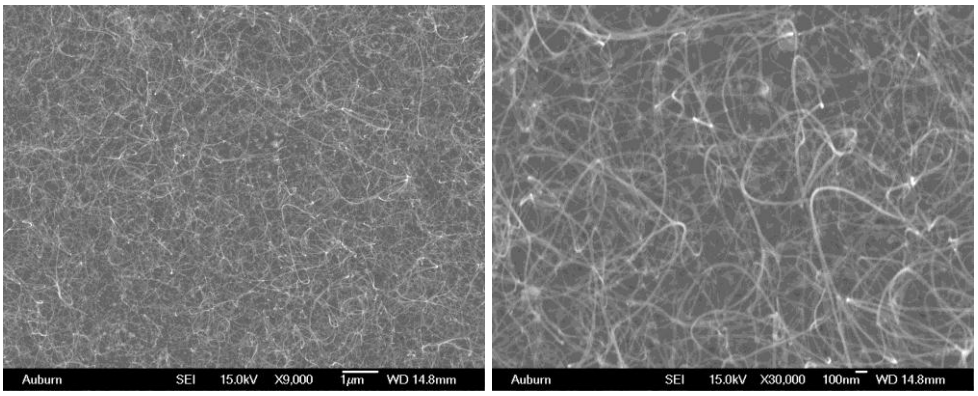

(b) 5-20

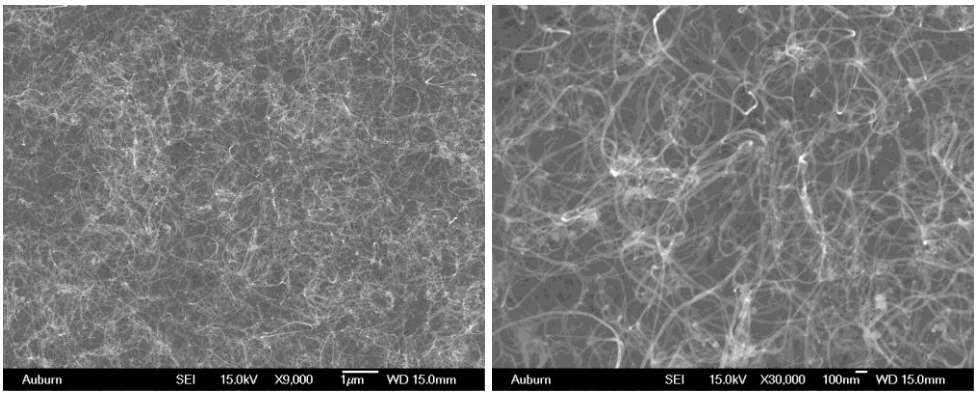

(c) 5-40

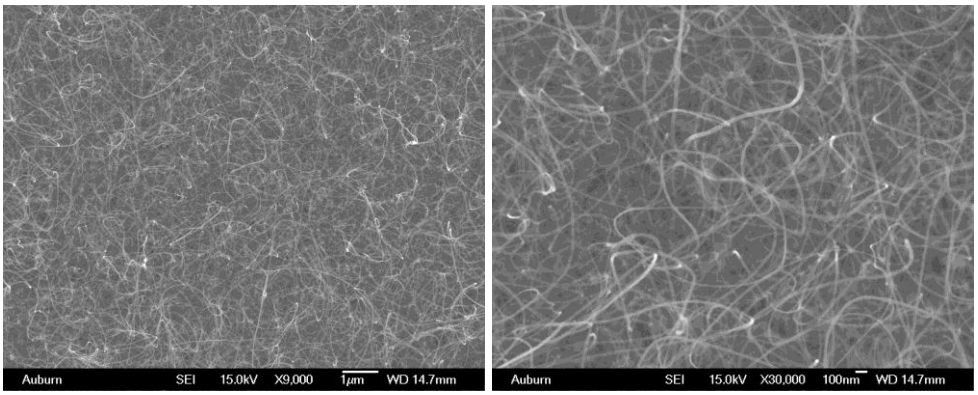

(d) 5-80

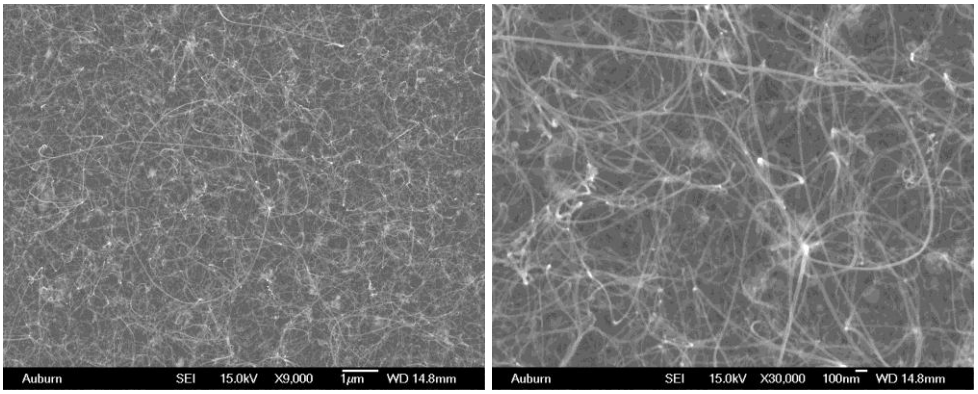

(e) 5-120

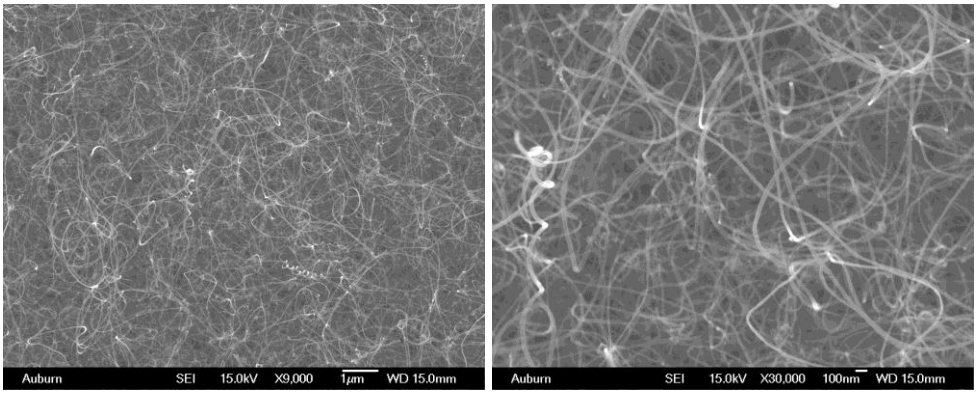

(f) 5-240

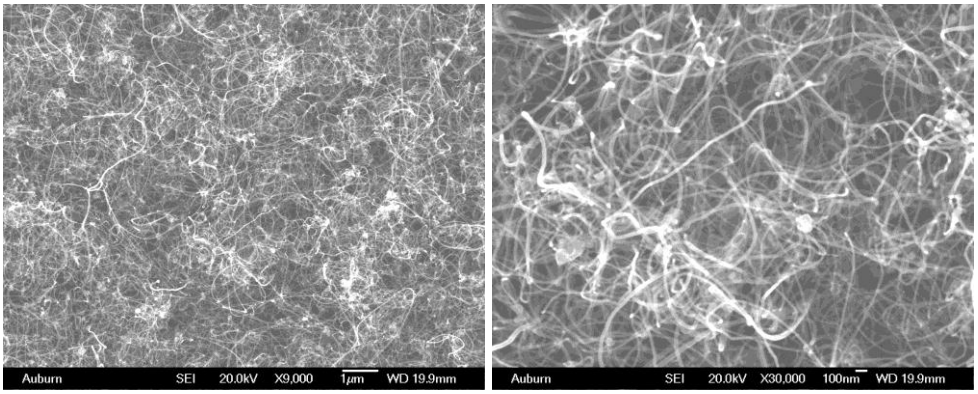

Figure 3.3: Images of CNTs with 5 min sputtering and growth periods (a) 10 min (b) 20 min (c) 40 min (d) 80 min (e) 120 min (f) 240 min Each set is with resolution of 9000X and 30000X.

3.2.1.2 Images of CNTs with 10 min Sputtering

(a) 10-10

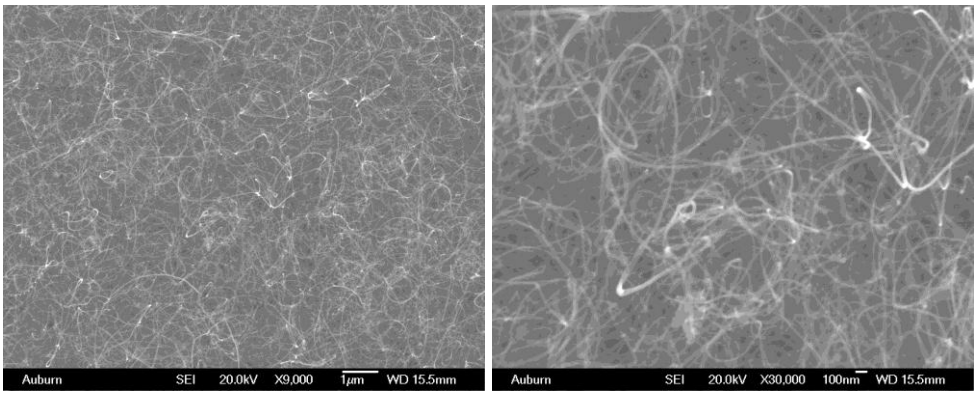

(b) 10-20

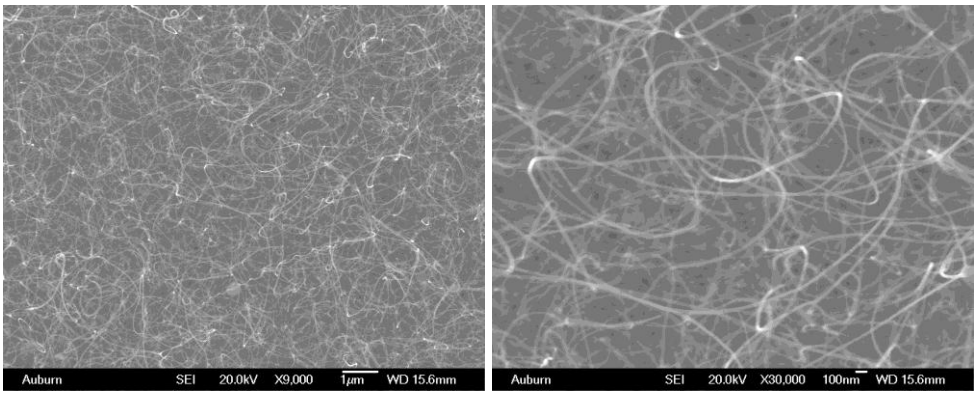

(c) 10-40

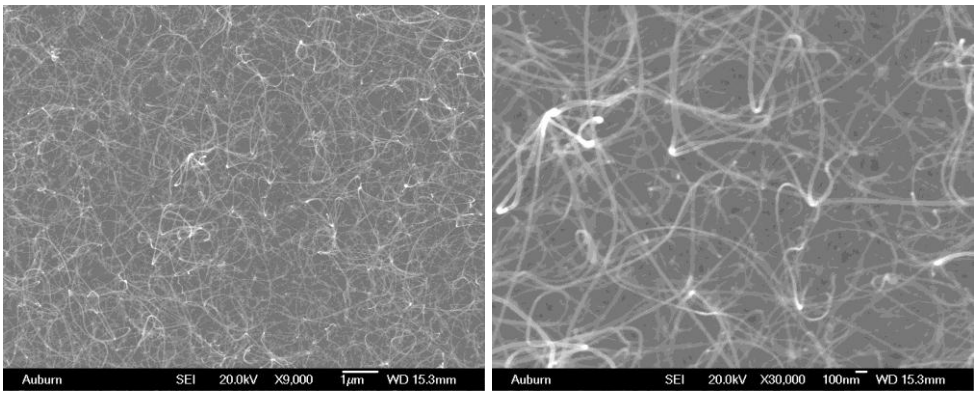

(d) 10-80

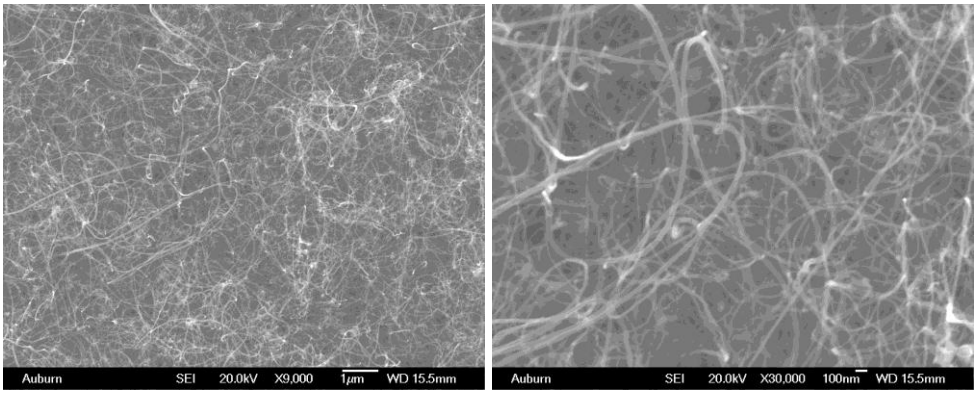

(e) 10-120

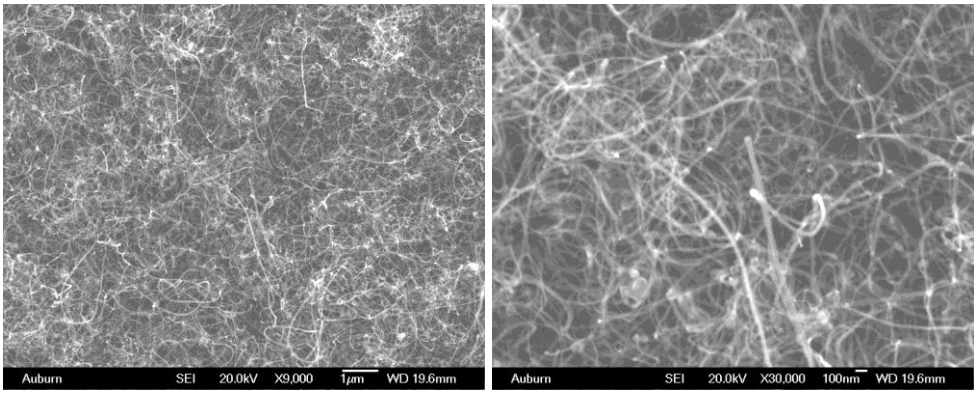

(f) 10-240

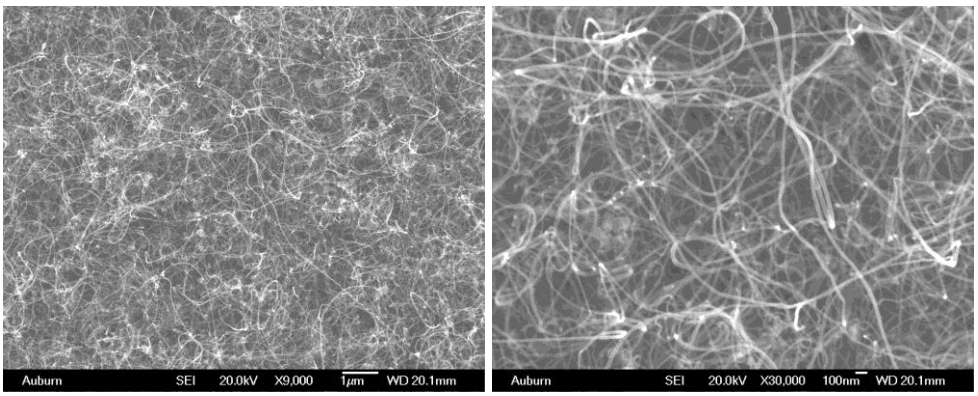

Figure 3.4: Images of CNTs with 10 min sputtering and growth periods (a) 10 min (b) 20 min (c) 40 min (d) 80 min (e) 120 min (f) 240 min. Each set is with resolution of 9000X and 30000X.

3.2.1.3 Images of CNTs with 20 min Sputtering

(a) 20-20

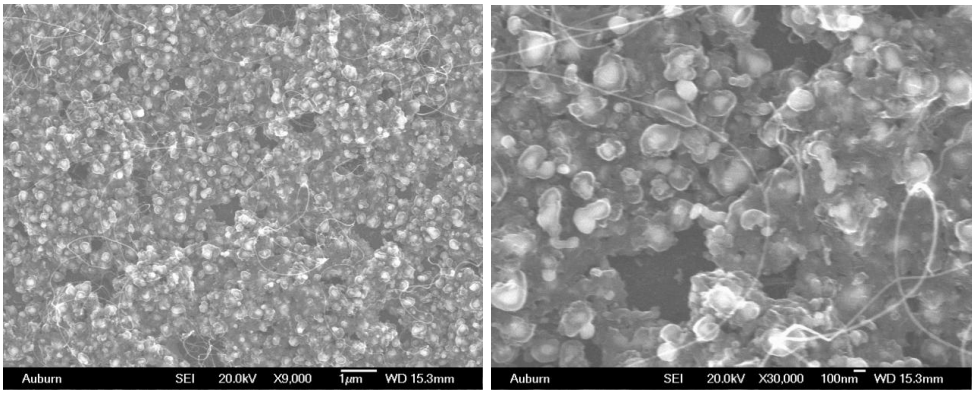

(b) 20-30

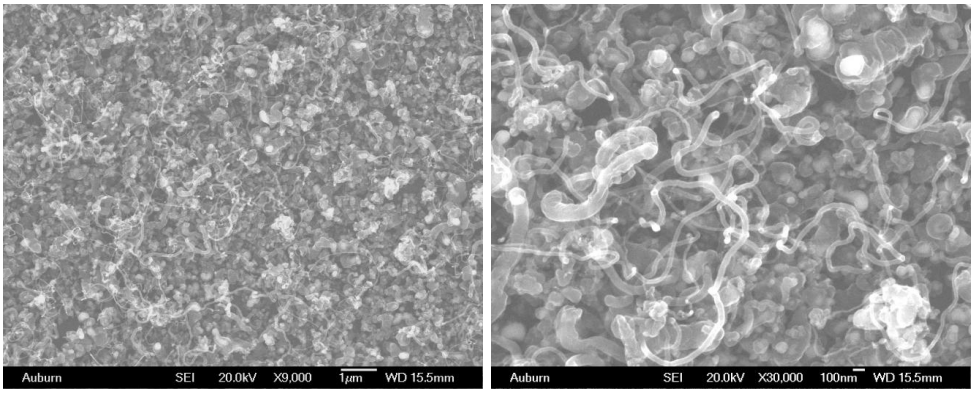

(c) 20-40

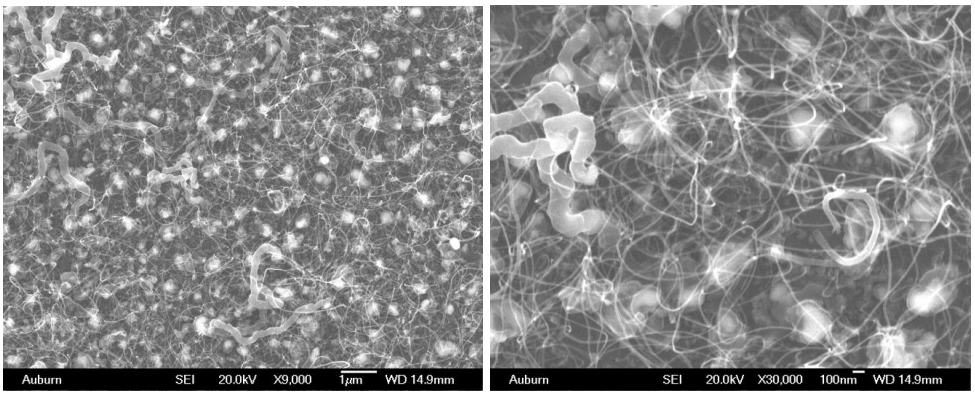

Figure 3.5: Images of CNTs with 20 min sputtering and growth periods (a) 20 min (b) 30 min (c) 40 min. Each set is with resolution of 9000X and 30000X.

3.3 Electron Field Emission Measurement

The CNT samples are loaded into the high vacuum chamber to test their field emission characteristics. The chamber is first pumped by the mechanical pump up to mTorr range and then turbo pump is used to pump down, until the pressure reached to $2x10^{-7}$- $5x10^{-7}$ Torr range. The electron field emission characteristics of carbon nano tube samples are analyzed by a parallel-plate set-up, with the carbon nano tubes sample serving as the electron emitting material, placed on the cathode and a small cylindrical rod with area of collector 0.031415 cm^2 serving as the anode. The sample and the anode are separated by two glass insulating spacers of width 140~150 μm.

(a)

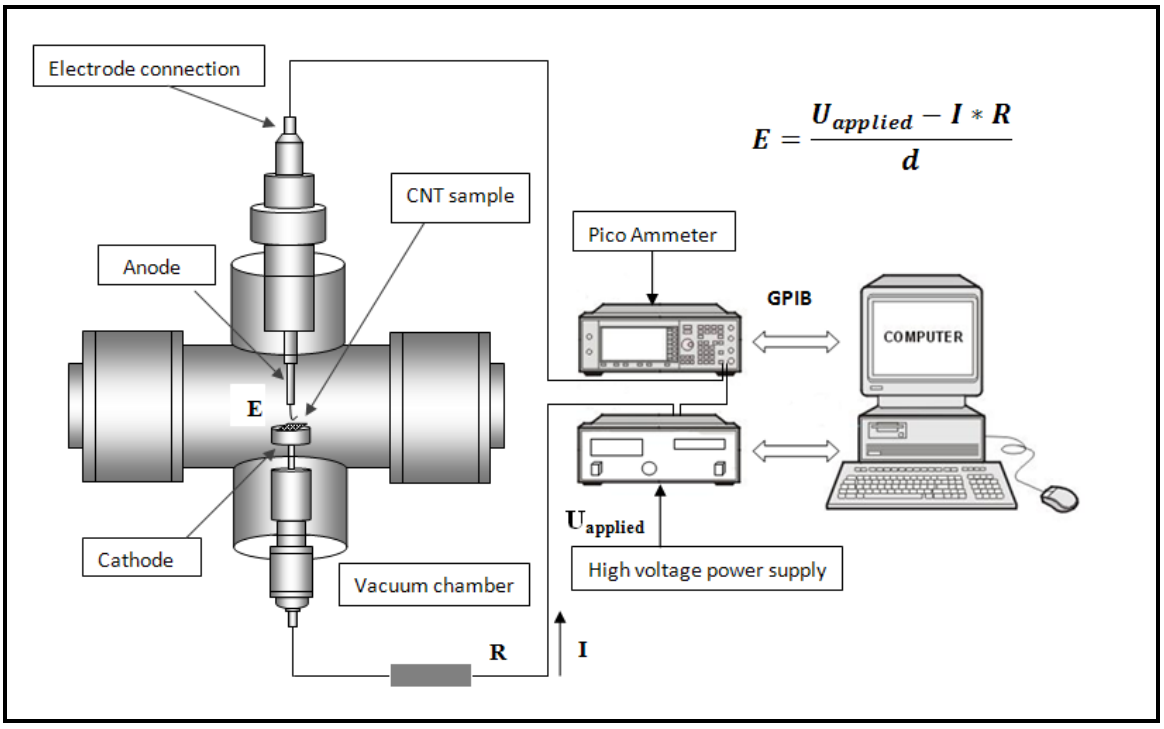

(b)

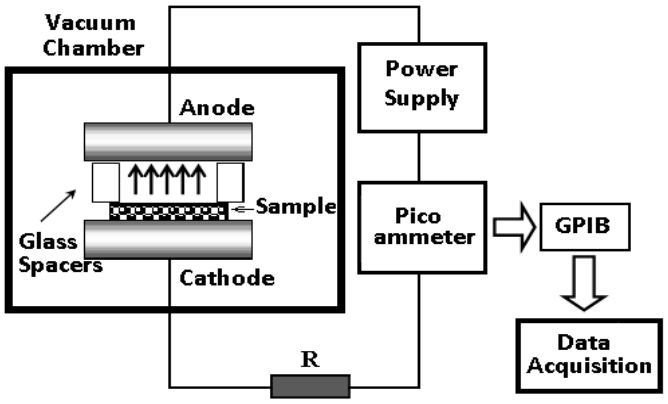

Figure 3.6: Field emission measurement setup (a) Schematic (b) Block diagram

Computer controlled DC voltage source and pico-ammeter are used to measure the *I–E* characteristics. A digital DC power supply (Stanford Research Systems PS235) is used to apply a voltage between the anode and cathode. A Keithley 485 pico-ammeter is used to measure the emission current. For large-area cathode, it was usually masked in such a way to allow a known area of electron emission. In these experiments a cylindrical rod acting as anode with known area of 0.031415 cm^2 collecting surface, is exposed to the CNT sample in order to limit the total current flow within the range of the power supply. The measured electron emission current was divided by the exposed area to calculate the field emission current density.

Initially the chamber is evacuated to a pressure level of ~$5x10^{-7}$ Torr and the field emission characteristics are measured at this vacuum level. Each time the voltage applied from 0 to 1200 V with variable voltage steps depending on the data resolution required in the curve. The field emission curves in vacuum are considered as the base data. Further field emission experiments are carried out in helium and dryair respectively at different pressures ranging from $5x10^{-7}$ to $20x10^{-3}$ Torr. The

pressure of the chamber is varied by inputting the relevant gas each time through gas valves. The field emission data is acquired using the data acquisition system as a function of voltage with respective current. This data is used to plot the field emission curves in the excel spread sheet as a function of current density and electric field. The turn-on electric field and saturation current densities in each case are noted using these plots.

In other case the field emission experiments are carried out over 100 runs (0-1200 V with variable step voltage, to and fro is considered as one run). These runs are to find the stability exhibited by the CNTs in their characteristics. Similar method as above is used to find the turn on saturation current density. These lifetime test experiments are carried out at 20 mTorr pressure for all the samples to test their stability in their characteristics for high pressure applications. The graphs are plotted to find the change in turn-on electric field and saturation current density with respect to the number of runs. The increase in turn-on electric field and decrease in the current density with the number of runs is noted. All comparisons are made with respect to the field emission curves in vacuum.

Experiments are also carried out with constant voltage of 600 V applied for 5hours continuously for the lifetime test, to check the current stability and lifetimes of CNTs. These experiments were carried out at high vacuum conditions and repeated for all the samples with growth periods 10, 20, 40, 80, 120 and 240 min and with two different sputtering times of 5 and 10 min. The degradation in current density is plotted across time to see how long the tubes can withstand constant electric field. The plots for all the samples are presented.

CHAPTER 4

RESULTS AND DISCUSSION

Random aligned multi-walled carbon nano tubes were successfully grown on silicon substrate using chemical vapor deposition method. Nano-tubes with different growth times 10, 20, 40, 80, 120 and 240 min each with set of 5 and 10 min sputtering were grown. These samples were analyzed for their field emission characteristics under different pressure conditions in Helium and dryair. Effects of gas pressures on the field emission properties were investigated and analyzed. A series of field emission experiments with 100 runs were performed on each of these samples at 20 mTorr to find the change in turn-on electric field and saturation current density. These results explained the stability exhibited by the CNTs in their field emission characteristics at high pressure conditions. The lifetime and current stability of all the CNT samples were also tested at high vacuum with constant voltage of 600 V applied to all the samples. Samples with sputtering time 20 min were also grown with 20, 30 and 40 min. These entire samples consisted of impurity clusters such as polydedral graphite nano-particles in the CNTs. Field emission experiments were carried out on these samples to test whether the clusters contribute as the electron emitters with nanotubes or not. Life time stability test were also conducted at vacuum for 100 or more runs to see the stability in their characteristics for turn-on and current density.

4.1 Growth of MWNTs and their Field Emission

In this work we have used thermal CVD method to grow CNTs on <100> silicon wafer with Fe as catalyst approximately 50 nm thick. The SEM image of sputtered wafer is given in Figure 3.1. Though the adhesion of sputtering with Fe catalyst is not very good as electron-beam evaporated Ti/Si/Fe catalyst system, high density of CNTs can also achieved by increasing the growth period [91]. In this research, high density MWNTs with long nanotubes achieved with longer growth periods such as 40 min and above. The increase in density of CNTs was observed to be very minimal beyond 40 min growth time, but their field emission characteristics show a reasonable difference in their turn-on, saturation current density and stability in their lifetime.

Different definitions such as, the applied electric field when the current reaches 10^{-7} A, 10^{-6} A or 10^{-5} A were considered as the turn-on electric field in the literature. In this case we are defining the turn-on electric field as the applied electric field where the current density starts increasing exponentially from the linear, "dark-current" state. The saturation current density is the maximum current density obtained at the applied electric field at 1200 V power supply.

4.2 Field Emission Characteristics of Random Aligned MWNTs

The field emission characteristics of CNTs are tested at different pressures ranging from high vacuum ($2x10^{-7}$ Torr) to high pressures ($20x10^{-3}$ Torr), to observe the change in turn-on electric fields and current densities. These experiments will explain how these CNTs behave when they are used as a cold cathode material of triggering electrode in pseudospark switch at high pressures. Most plasma switches operate in mTorr pressure ranges which are relatively higher

than the vacuum pressure levels. Therefore the field emission experiments are carried out for the samples with under different pressure conditions in helium and dryair.

The following tables show the turn-on electric field and saturation current densities for all the samples for different testing conditions. It can be observed that the turn-on for the CNTs with both 5 min and 10 min sputtering decreases with increase in growth time of the sample. This is observed to be similar case in all different pressures ranging from high vacuum to high pressure. The minimum turn-on field is observed to be 0.53 V/μm for 5 min sputtering and 0.43 V/μm for 10 min sputtering respectively, for the growth time of 240 min sample. But the turn-on field was found to be low for all the cases beyond 20 min growth time. There is definite increase in the saturation current density observed with increase in the growth time for both 5 min and 10 min sputtering cases. The emission characteristics seem to be deteriorating with increase in the pressure levels from $5x10^{-7}$ to $20x10^{-3}$ Torr.

Table 4.1: Turn-on Electric field for Samples with 5 min sputtering time

Growth Time(min)	At $5x10^{7}$ Torr	At $2x10^{-6}$ Torr		At $2x10^{-5}$ Torr		At $2x10^{-4}$ Torr		At $20x10^{-3}$ Torr	
	Vacuum (V/μm)	He (V/μm)	Dry air (V/μm)	He (V/μm)	Dry air (V/μm)	He (V/μm)	Dry air (V/μm)	He (V/μm)	Dry air (V/μm)
10	1.71	2.43	2.71	2.78	2.71	3.14	2.78	3.43	3.75
20	1.16	1.86	2.28	1.93	2.36	2.0	2.57	2.57	2.93
40	1.07	1.43	1.54	1.64	1.64	1.86	2.0	2.07	2.50
80	1.07	1.14	1.68	1.40	1.78	1.50	1.89	1.78	2.5
120	0.57	0.64	0.86	0.86	0.96	0.96	1.21	1.36	1.57
240	0.53	0.64	0.64	0.78	0.86	0.86	1.21	1.21	1.28

Table 4.2: Saturation current density for samples with 5 min sputtering time

Growth Time(min)	At $5x10^{-7}$ Torr	At $2x10^{-6}$ Torr		At $2x10^{-5}$ Torr		At $2x10^{-4}$ Torr		At $20x10^{-3}$ Torr	
	Vacuum (mA/cm²)	He (mA/cm²)	Dry air (mA/cm²)	He (mA/cm²)	Dry air (mA/cm²)	He (mA/cm²)	Dry air (mA/cm²)	He (mA/cm²)	Dry air (mA/cm²)
10	2.80	1.52	1.45	1.13	1.35	1.09	0.763	0.93	0.14
20	5.20	3.62	2.65	2.65	2.45	2.65	2.02	1.90	0.84
40	5.40	5.02	2.41	4.50	2.16	3.63	1.82	1.84	0.94
80	5.24	4.35	3.20	3.68	2.73	3.75	2.75	2.31	1.11
120	7.11	7.08	6.11	6.08	4.89	5.73	4.54	5.02	4.44
240	7.56	7.16	7.08	7.02	5.74	6.20	5.28	5.02	4.83

Table 4.3: Turn-on Electric field for Samples with 10 min sputtering time

Growth Time(min)	At $5x10^{7}$ Torr	At $2x10^{-6}$ Torr		At $2x10^{-5}$ Torr		At $2x10^{-4}$ Torr		At $20x10^{-3}$ Torr	
	Vacuum (V/μm)	He (V/μm)	Dry air (V/μm)	He (V/μm)	Dry air (V/μm)	He (V/μm)	Dry air (V/μm)	He (V/μm)	Dry air (V/μm)
10	1.43	1.57	1.86	1.786	1.86	2.11	2.0	2.43	3.0
20	1.04	1.08	1.14	1.18	1.57	1.54	1.71	2.57	3.0
40	1.0	1.0	1.14	1.14	1.29	1.40	1.71	2.21	1.86
80	0.57	0.57	0.57	0.57	0.57	0.57	0.57	0.86	1.29
120	0.57	0.57	1.07	0.78	1.28	1.07	1.36	1.7	1.85
240	0.43	0.57	1.0	0.78	1.21	1.07	1.28	1.5	1.43

Table 4.4: Saturation current density for samples with 10 min sputtering time

Growth Time(min)	At $5x10^{-7}$ Torr	At $2x10^{-6}$ Torr		At $2x10^{-5}$ Torr		At $2x10^{-4}$ Torr		At $20x10^{-3}$ Torr	
	Vacuum (mA/cm²)	He (mA/cm²)	Dry air (mA/cm²)	He (mA/cm²)	Dry air (mA/cm²)	He (mA/cm²)	Dry air (mA/cm²)	He (mA/cm²)	Dry air (mA/cm²)
10	2.86	2.64	0.95	2.58	0.92	2.11	0.82	0.98	0.51
20	5.36	5.38	3.58	4.80	3.11	4.0	2.56	2.07	1.35
40	5.65	5.14	3.75	5.24	3.20	4.10	2.71	2.07	1.17
80	6.95	6.94	5.33	6.58	5.16	6.50	4.44	5.31	3.78
120	7.40	7.19	5.46	6.70	5.37	6.09	4.95	5.30	4.47
240	7.67	7.30	5.91	6.72	5.74	6.10	5.38	5.63	4.70

4.2.1 Field Emission Comparisons with respect to Pressures and Background Gases

The field emission properties of the sample with 5 min sputtering and 10 min growth time were analyzed under different pressures and back ground gases and are compared below. Field emission measurements of MWNTs were first carried out at $5x10^{-7}$ Torr with gap spacing 140 μm. The following figures shows the typical field emission curves of MWNTs under high vacuum and partial vacuum conditions in both helium and dryair gases compared with the applied electric field scanned from 0 to 1200 V.

From the curves it can be seen that the turn on electric field shifts towards the right with increase in pressure. There is obvious increase in turn-on electric field from 1.71 V/μm at $5x10^{-7}$ Torr to 3.75 V/μm at 20 mTorr in dryair for 5 min sputtered-10 min growth sample. Careful interpretation reveals that the turn-on at the pressure $2x10^{-6}$ Torr is almost the same for both helium and dryair ambience which is 2.71 V/μm. On the other hands from the pressures $2x10^{-5}$ Torr to 20 mTorr range, it is low in case of helium compared to the dryair. Similar pattern is observed for all the cases with different growth times samples, except the turn-on electric field is low, and the current density is improved for the sample with larger growth time.

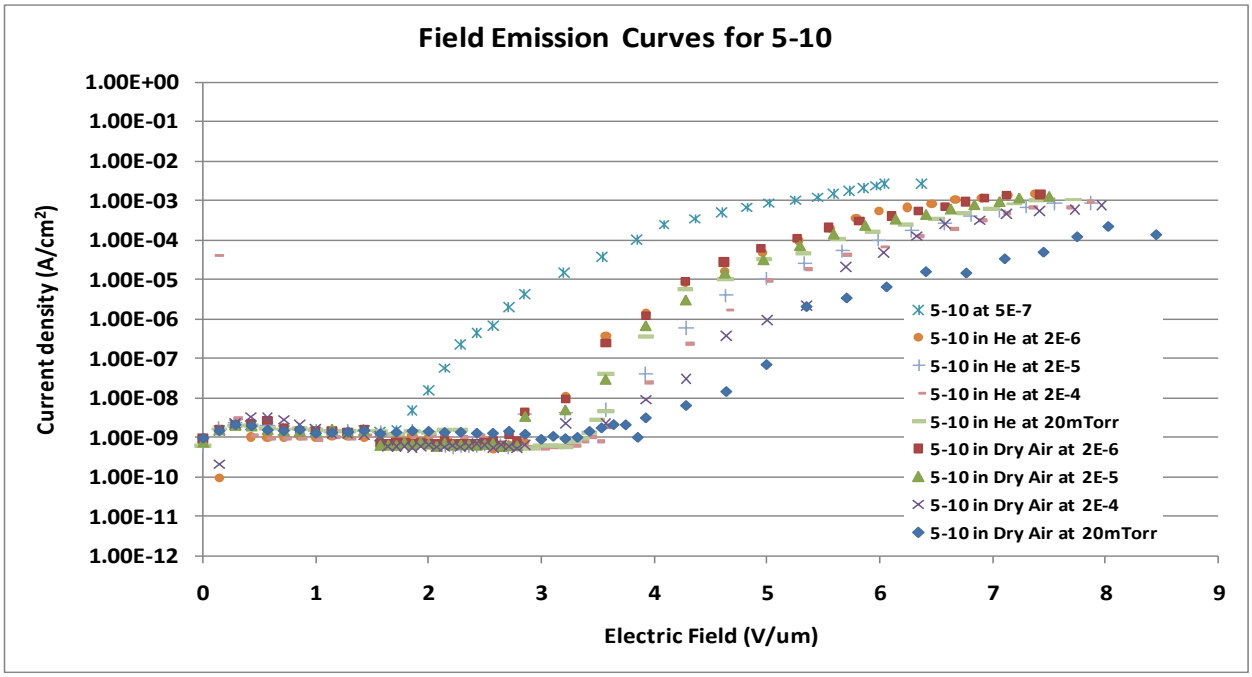
Field Emission Curves for 5-10
Current density (A/cm²)
1.00E+00
1.00E-01
1.00E-02
1.00E-03
1.00E-04
1.00E-05
1.00E-06
1.00E-07
1.00E-08
1.00E-09
1.00E-10
1.00E-11
1.00E-12
0
1
2
3
4
5
6
7
8
9
Electric Field (V/um)
5-10 at 5E-7
5-10 in He at 2E-6
5-10 in He at 2E-5
5-10 in He at 2E-4
5-10 in He at 20mTorr
5-10 in Dry Air at 2E-6
5-10 in Dry Air at 2E-5
5-10 in Dry Air at 2E-4
5-10 in Dry Air at 20mTorr

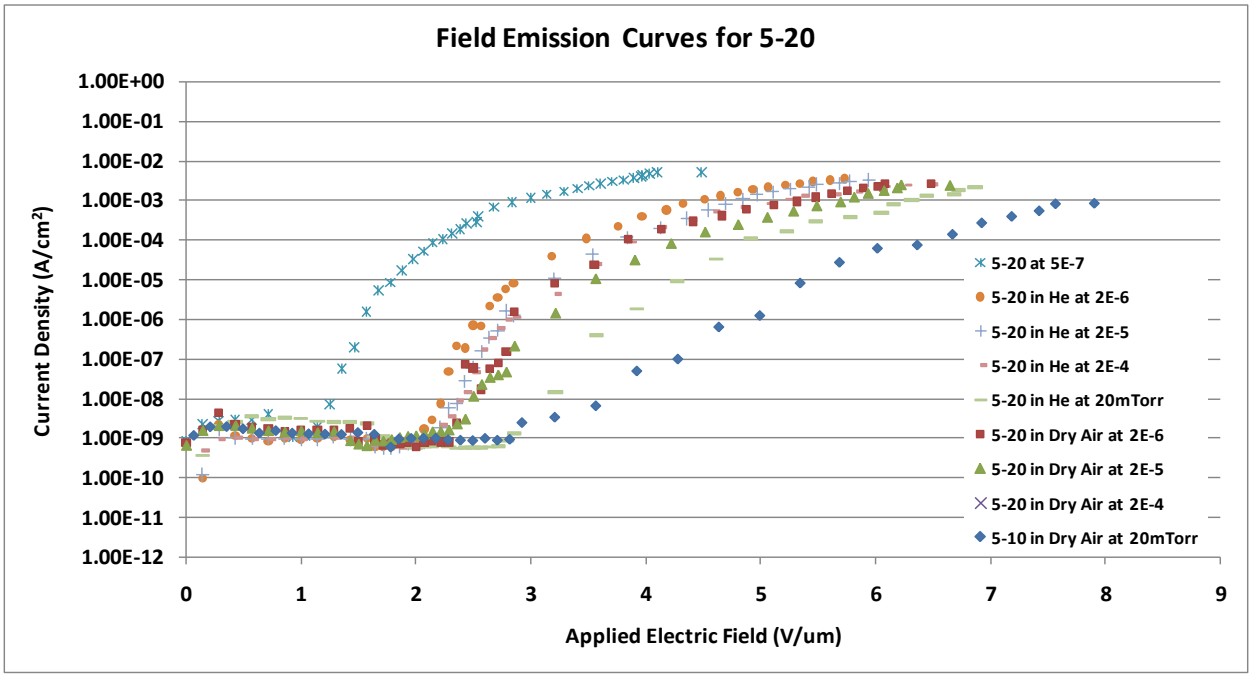
Field Emission Curves for 5-20
Current Density (A/cm²)
1.00E+00
1.00E-01
1.00E-02
1.00E-03
1.00E-04
1.00E-05
1.00E-06
1.00E-07
1.00E-08
1.00E-09
1.00E-10
1.00E-11
1.00E-12
0
1
2
3
4
5
6
7
8
9
Applied Electric Field (V/um)
5-20 at 5E-7
5-20 in He at 2E-6
5-20 in He at 2E-5
5-20 in He at 2E-4
5-20 in He at 20mTorr
5-20 in Dry Air at 2E-6
5-20 in Dry Air at 2E-5
5-20 in Dry Air at 2E-4
5-10 in Dry Air at 20mTorr

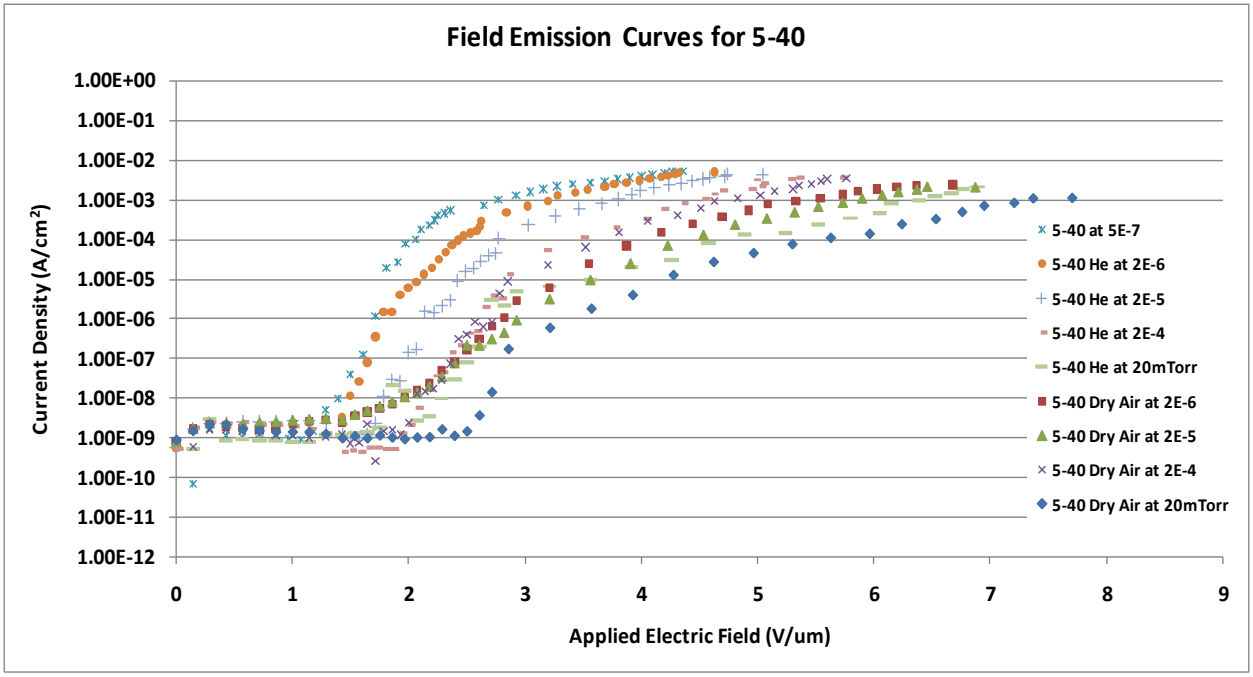
Field Emission Curves for 5-40
Current Density (A/cm²)
1.00E+00
1.00E-01
1.00E-02
1.00E-03
1.00E-04
1.00E-05
1.00E-06
1.00E-07
1.00E-08
1.00E-09
1.00E-10
1.00E-11
1.00E-12
0
1
2
3
4
5
6
7
8
9
Applied Electric Field (V/um)
5-40 at 5E-7
5-40 He at 2E-6
5-40 He at 2E-5
5-40 He at 2E-4
5-40 He at 20mTorr
5-40 Dry Air at 2E-6
5-40 Dry Air at 2E-5
5-40 Dry Air at 2E-4
5-40 Dry Air at 20mTorr

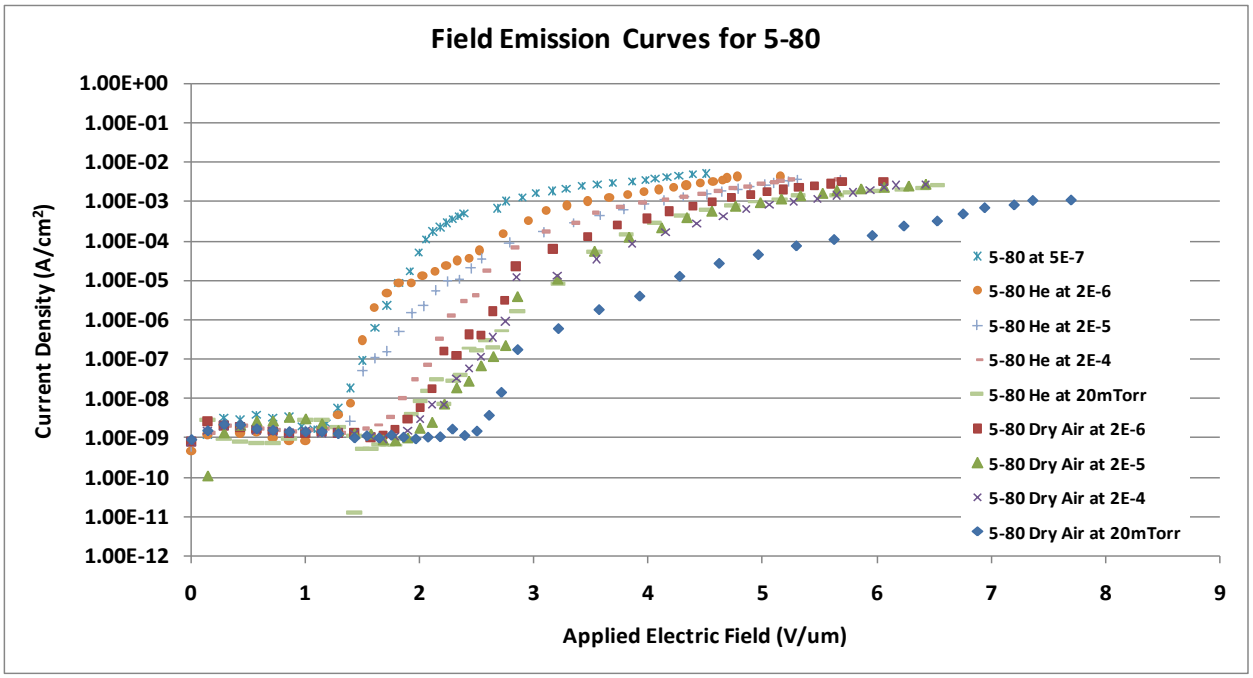
Field Emission Curves for 5-80
Current Density (A/cm²)
1.00E+00
1.00E-01
1.00E-02
1.00E-03
1.00E-04
1.00E-05
1.00E-06
1.00E-07
1.00E-08
1.00E-09
1.00E-10
1.00E-11
1.00E-12
0
1
2
3
4
5
6
7
8
9
Applied Electric Field (V/um)
5-80 at 5E-7
5-80 He at 2E-6
5-80 He at 2E-5
5-80 He at 2E-4
5-80 He at 20mTorr
5-80 Dry Air at 2E-6
5-80 Dry Air at 2E-5
5-80 Dry Air at 2E-4
5-80 Dry Air at 20mTorr

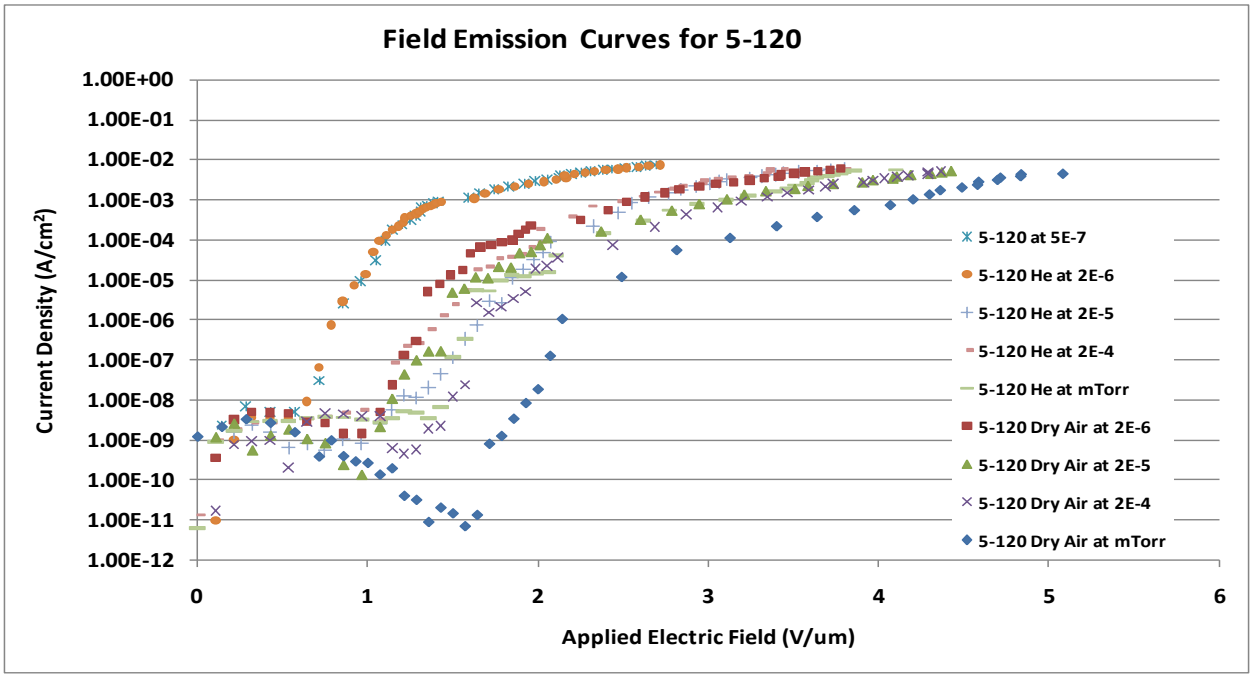
Field Emission Curves for 5-120
Current Density (A/cm²)
1.00E+00
1.00E-01
1.00E-02
1.00E-03
1.00E-04
1.00E-05
1.00E-06
1.00E-07
1.00E-08
1.00E-09
1.00E-10
1.00E-11
1.00E-12
0
1
2
3
4
5
6
Applied Electric Field (V/um)
5-120 at 5E-7
5-120 He at 2E-6
5-120 He at 2E-5
5-120 He at 2E-4
5-120 He at mTorr
5-120 Dry Air at 2E-6
5-120 Dry Air at 2E-5
5-120 Dry Air at 2E-4
5-120 Dry Air at mTorr

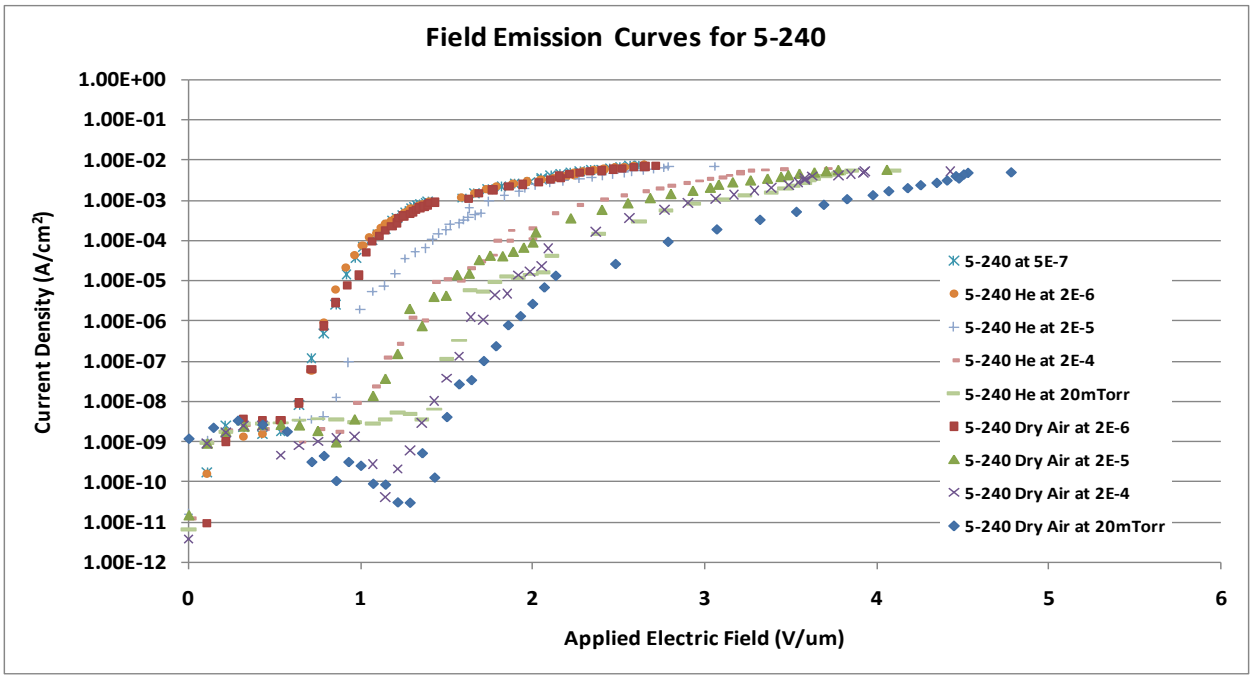
Field Emission Curves for 5-240
Current Density (A/cm²)
1.00E+00
1.00E-01
1.00E-02
1.00E-03
1.00E-04
1.00E-05
1.00E-06
1.00E-07
1.00E-08
1.00E-09
1.00E-10
1.00E-11
1.00E-12
0
1
2
3
4
5
6
Applied Electric Field (V/um)
5-240 at 5E-7
5-240 He at 2E-6
5-240 He at 2E-5
5-240 He at 2E-4
5-240 He at 20mTorr
5-240 Dry Air at 2E-6
5-240 Dry Air at 2E-5
5-240 Dry Air at 2E-4
5-240 Dry Air at 20mTorr

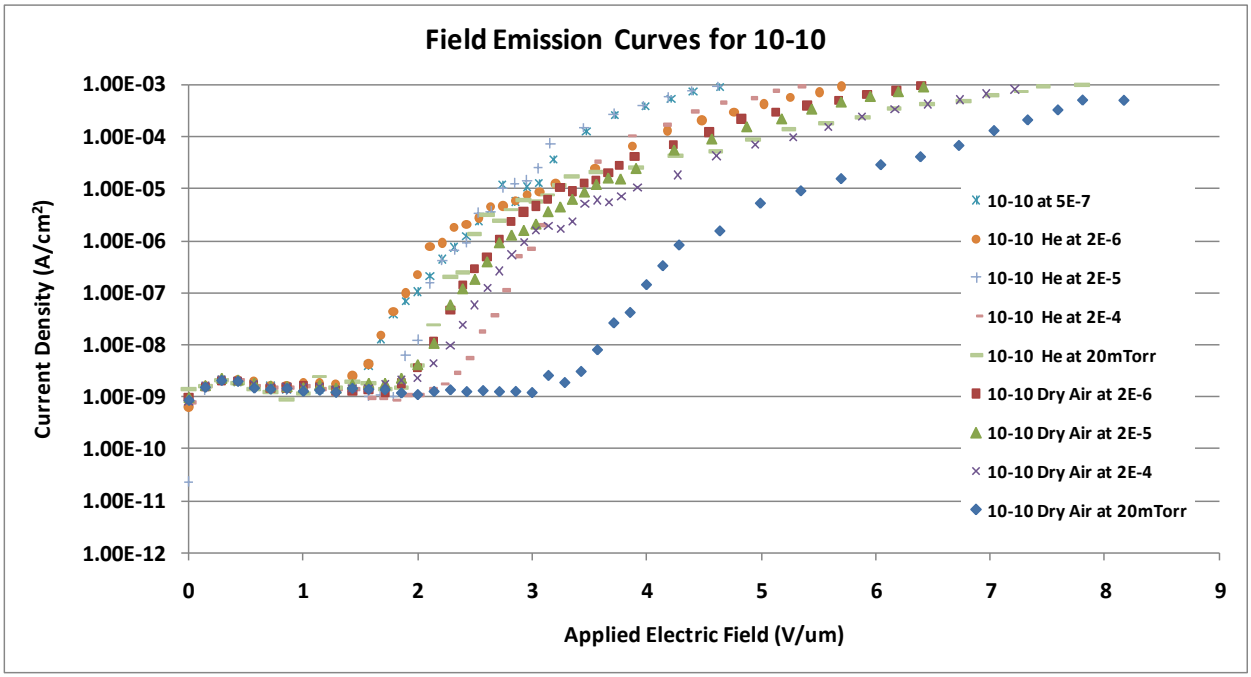
Field Emission Curves for 10-10
Current Density (A/cm²)
1.00E-03
1.00E-04
1.00E-05
1.00E-06
1.00E-07
1.00E-08
1.00E-09
1.00E-10
1.00E-11
1.00E-12
0
1
2
3
4
5
6
7
8
9
Applied Electric Field (V/um)
10-10 at 5E-7
10-10 He at 2E-6
10-10 He at 2E-5
10-10 He at 2E-4
10-10 He at 20mTorr
10-10 Dry Air at 2E-6
10-10 Dry Air at 2E-5
10-10 Dry Air at 2E-4
10-10 Dry Air at 20mTorr

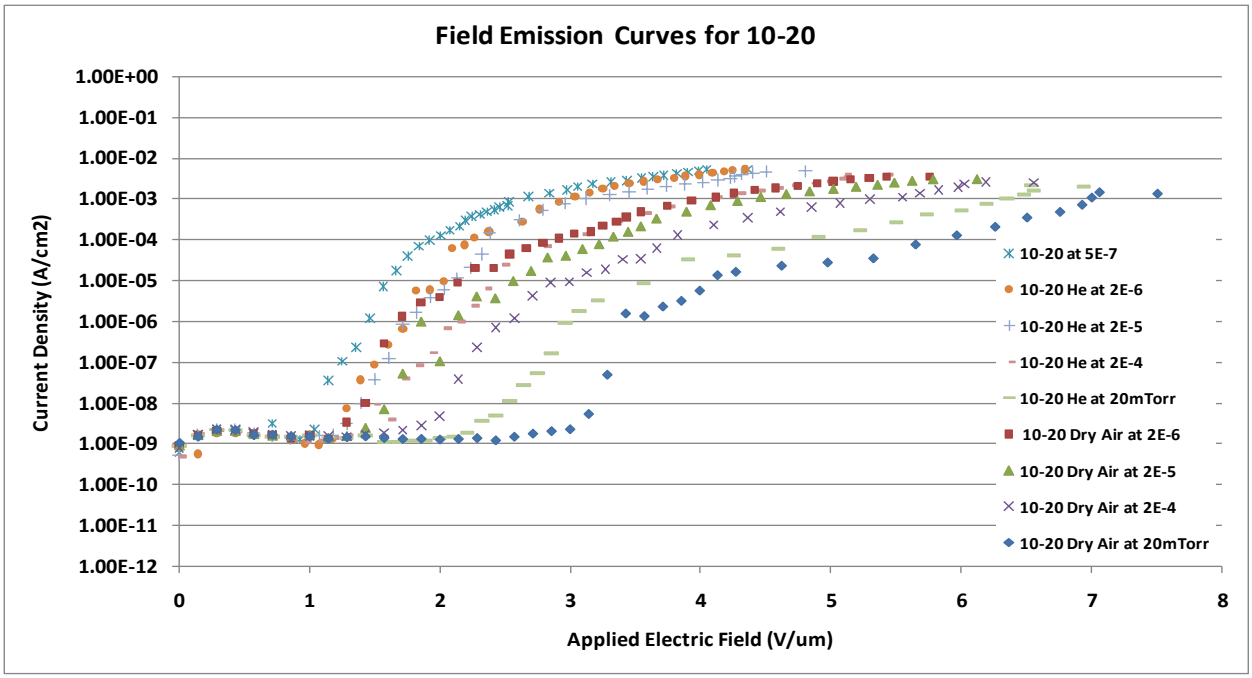
Field Emission Curves for 10-20
Current Density (A/cm2)
1.00E+00
1.00E-01
1.00E-02
1.00E-03
1.00E-04
1.00E-05
1.00E-06
1.00E-07
1.00E-08
1.00E-09
1.00E-10
1.00E-11
1.00E-12
0
1
2
3
4
5
6
7
8
Applied Electric Field (V/um)
10-20 at 5E-7
10-20 He at 2E-6
10-20 He at 2E-5
10-20 He at 2E-4
10-20 He at 20mTorr
10-20 Dry Air at 2E-6
10-20 Dry Air at 2E-5
10-20 Dry Air at 2E-4
10-20 Dry Air at 20mTorr

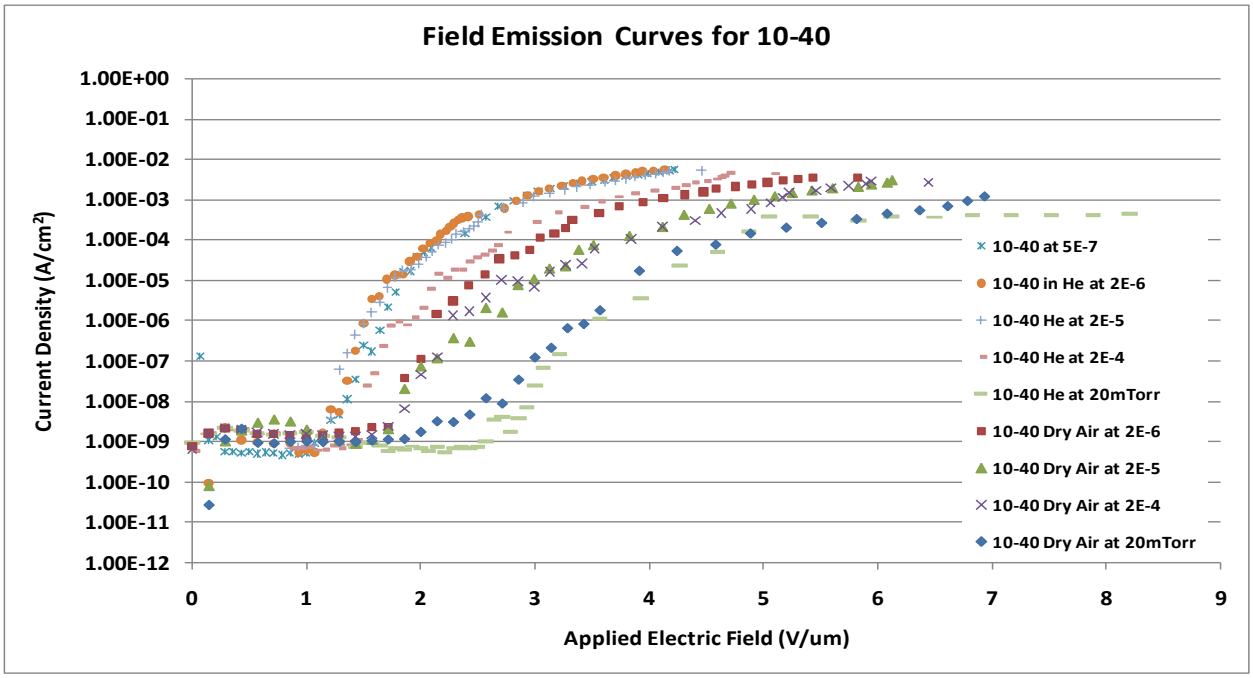
Field Emission Curves for 10-40
Current Density (A/cm²)
1.00E+00
1.00E-01
1.00E-02
1.00E-03
1.00E-04
1.00E-05
1.00E-06
1.00E-07
1.00E-08
1.00E-09
1.00E-10
1.00E-11
1.00E-12
0
1
2
3
4
5
6
7
8
9
Applied Electric Field (V/um)
10-40 at 5E-7
10-40 in He at 2E-6
10-40 He at 2E-5
10-40 He at 2E-4
10-40 He at 20mTorr
10-40 Dry Air at 2E-6
10-40 Dry Air at 2E-5
10-40 Dry Air at 2E-4
10-40 Dry Air at 20mTorr

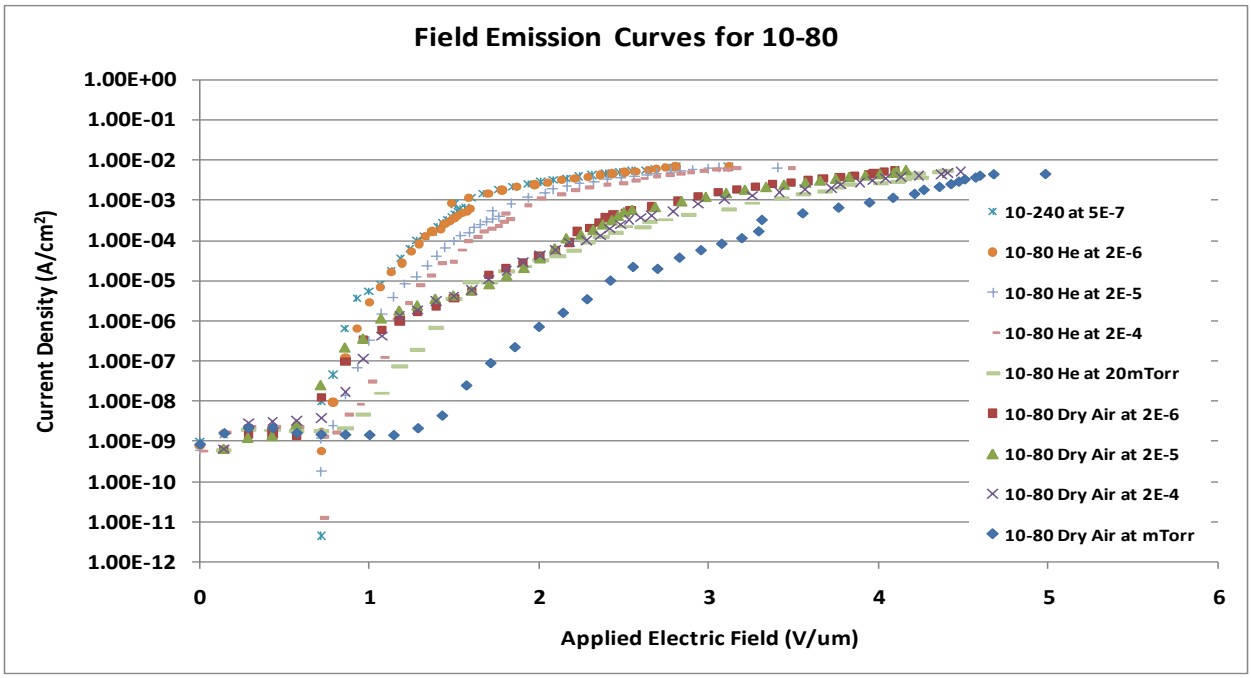
Field Emission Curves for 10-80
Current Density (A/cm²)
1.00E+00
1.00E-01
1.00E-02
1.00E-03
1.00E-04
1.00E-05
1.00E-06
1.00E-07
1.00E-08
1.00E-09
1.00E-10
1.00E-11
1.00E-12
0
1
2
3
4
5
6
Applied Electric Field (V/um)
10-240 at 5E-7
10-80 He at 2E-6
10-80 He at 2E-5
10-80 He at 2E-4
10-80 He at 20mTorr
10-80 Dry Air at 2E-6
10-80 Dry Air at 2E-5
10-80 Dry Air at 2E-4
10-80 Dry Air at mTorr

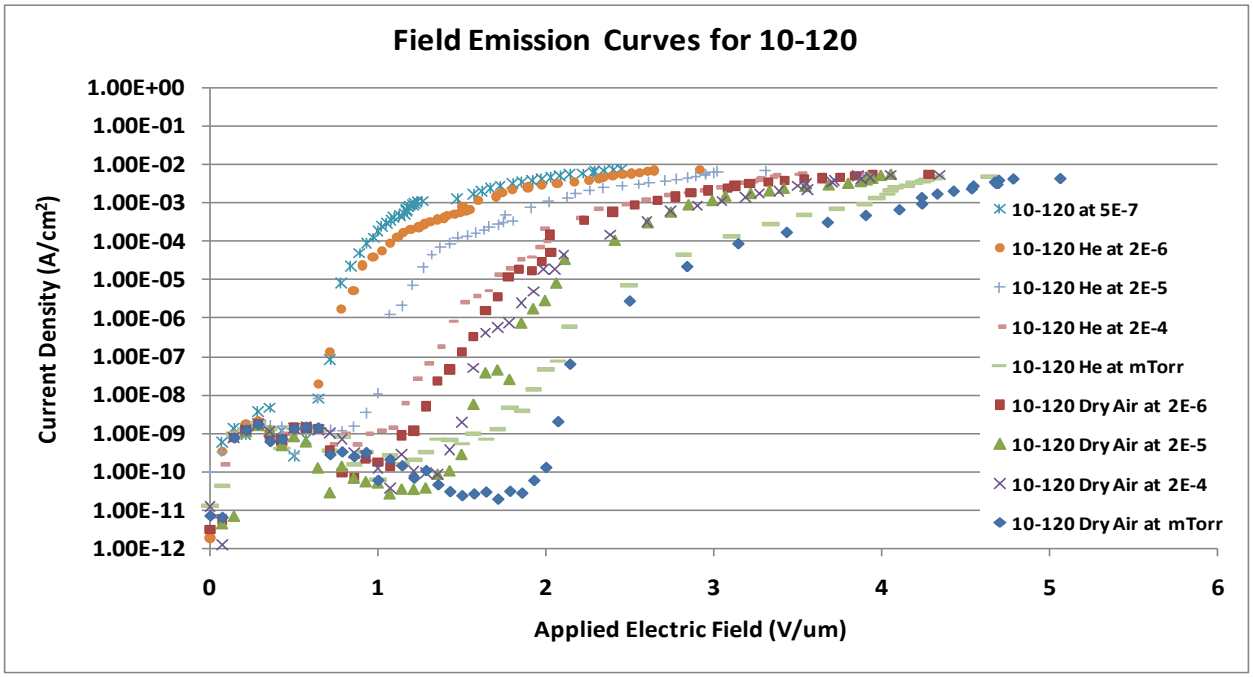

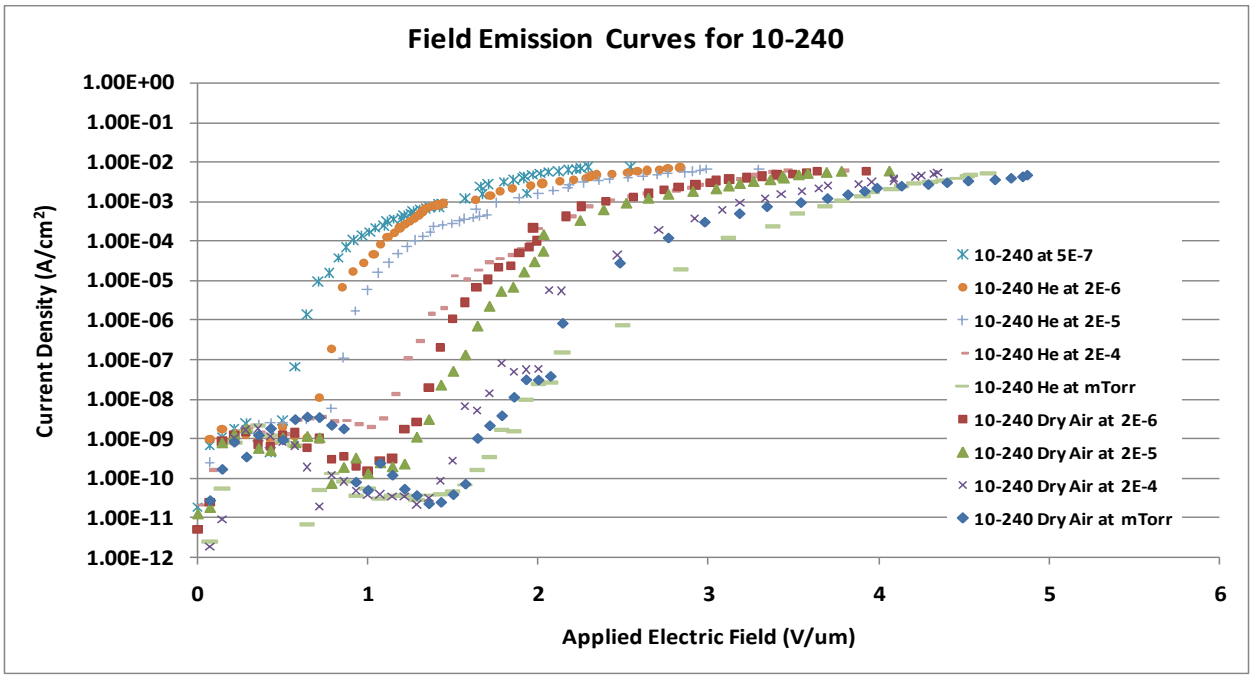

Figure 4.1: Field emission curves comparison with respect to pressures and gases for (a) 5 min sputtering samples (b) 10 min sputtering samples.

4.3 Fowler-Nordheim Curves Comparison

The morphology and density of CNTs depend on the method of fabrication and growth conditions. Many repeated experiments were carried out with large number of samples with different sputtering periods and growth period. The surface topology of CNTs was illustrated by SEM images, as shown in the Figure 3.3, Figure 3.4 and Figure 3.5. The SEM images show that there is obvious difference in the morphologies and the lengths of CNTs grown with different growth conditions. The longer nanotubes are observed in the case of CNT samples fabricated with longer growth period than the samples with short growth period.

The field emission curves that are plotted for all the samples explain the changes in turn-on electric fields and saturation current densities at different pressures with different growth conditions. During the field emission process with the application of high electric field, first the electrons are transported from the substrate to the CNTs and should overcome the contact resistance between the substrate and the CNTs. The electrons then pass through the surface of the CNTs and finally emitted into the vacuum towards the anode.

The local electric field is enhanced by a factor of β with sharp needle like emitting structures compared to the flat structures. The enhancement factor β, is determined by the geometric shape of the emitter, and the electric field (F) at the emitter surface given by

$$F = \beta E = \beta V/d$$

where E is the macroscopic field between anode and cathode.

Considering the work function Φ and enhancement factor β, the electron emission current as a function of local electric field is given by

$$I \propto (\beta^2 E^2/\Phi) \exp(-B\Phi^{3/2}/\beta E)$$

The above relationship is also known as Fowler-Nordheim equation.

The small variations of the shape surrounding the emitter determine the field enhancement factor β, and β has great impact on the emission current density because of exponential relationship between them. The change in the surface chemical state will also have impact on emission current density as it influences the work function.

Field enhancement factor β and work function Φ can be estimated by Fowler-Nordheim model by plotting $\ln(I/E^2)$ versus $1/E$ using the following equation.

$$\text{Ln}(I/E2) \propto s\ 1/E \text{……..….} 4.3$$

A straight line can be obtained with the slope s depending on β and Φ, which is given by

$$s = -B\,\Phi^{3/2}/\beta \text{……..…} 4.4$$

Work function for the CNTs is usually in the range 4.5 to 5 eV.

Following are the F-N curves plotted for all the samples with 5 min and 10 min sputtering and all the mentioned growth periods. The F-N curves at high pressure 20 mTorr are compared to curves at $5x10^{-7}$ Torr pressure. The deviation of the measured F-N plots from the Fowler-Nordheim theory is a general phenomenon. The slopes of the F-N curves are smaller when the samples are tested in high vacuum. This slope is observed to be increasing with increasing in the operating pressure conditions. The curves for the dry air test at 20 mTorr are the steepest, with high turn-on electric field. When the samples of 5 min and 10 min sputtering with different growth periods are compared, the slope of the curves appears to be decreasing with increase in the growth time. High density of nanotubes with large area of emission surface could be reason for decrease in the slope of F-N curves. Because of large area of emission surface, electrons are easily emitted from the surface of nanotubes, which is also responsible for increased current density. The I-V characteristics followed Fowler-Nordheim behavior in low current region with straight line and few scattered points of current observed in case of curves with high pressures.

This could be because of the gas molecules at high pressure affecting the normal emission electrons moving towards anode. In the higher current region the F-N slope becomes smaller and emission current appears to saturate. This deviation might be also due to space charge effects or non metallic characteristics of the emitters. The CNTs has the space charge effect appears to play minor role. Thus the non-metallic nature and the presence of localized states at the tip of the emitter are the reasons of the deviation.

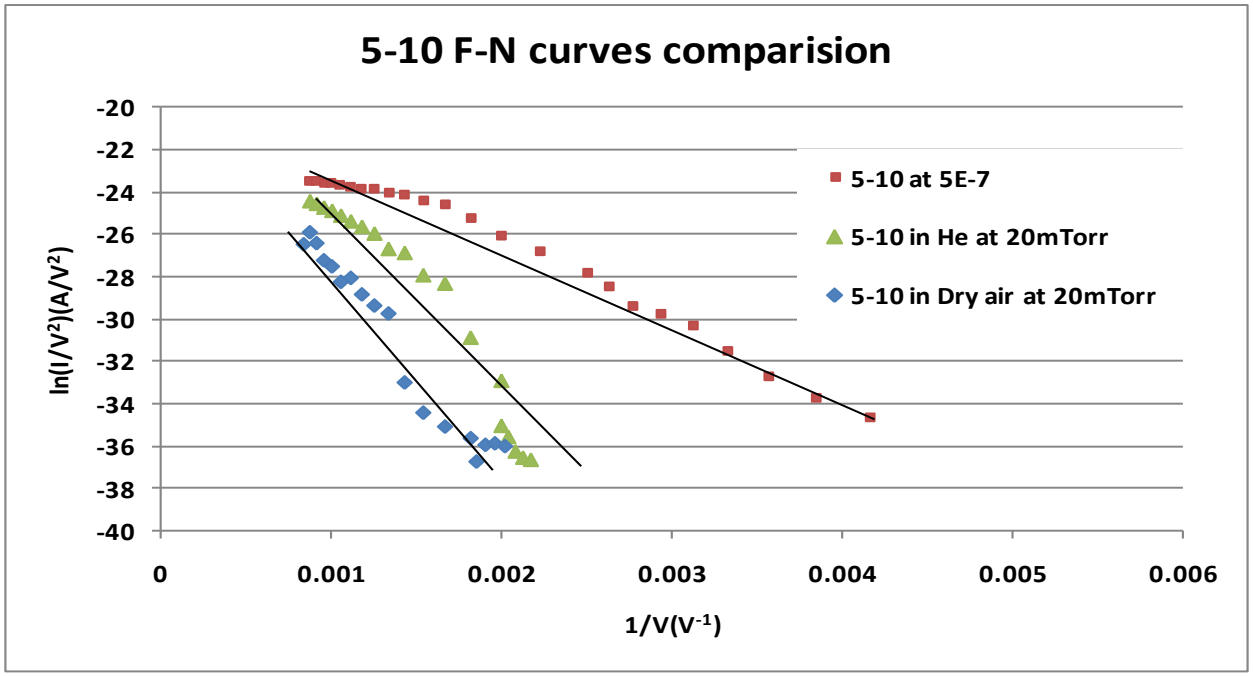

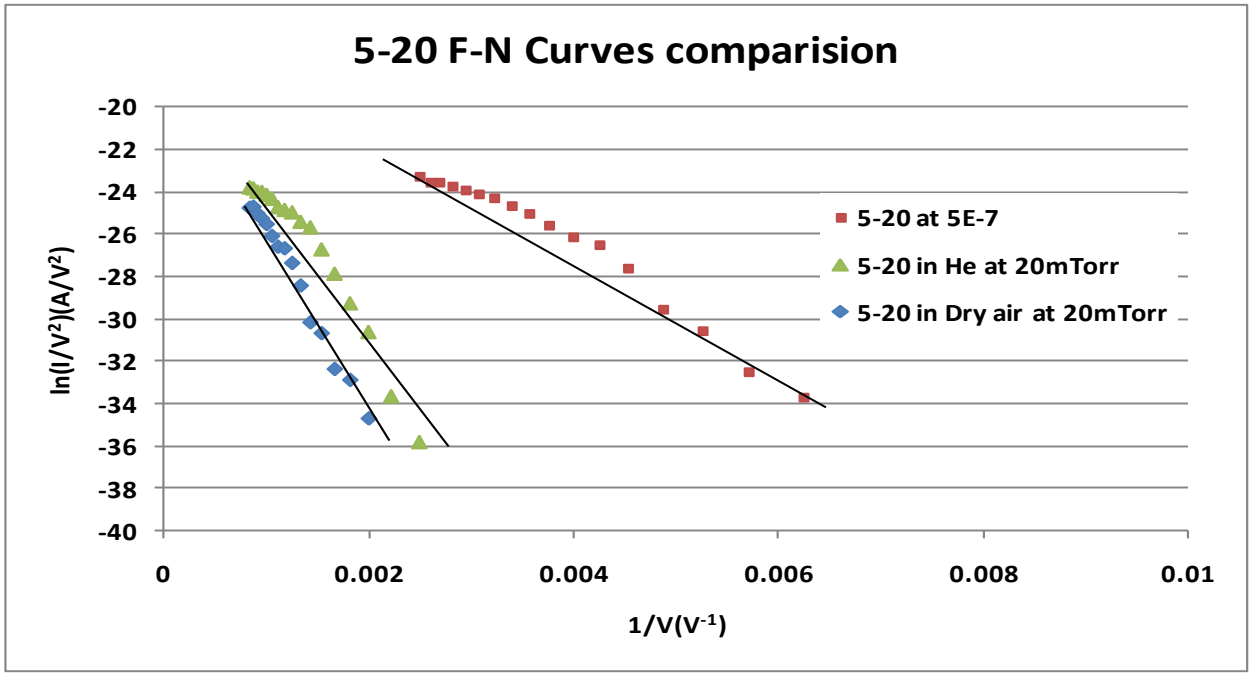
5-20 F-N Curves comparision
-20
-22
-24
-26
-28
-30
-32
-34
-36
-38
-40
ln(I/V²)(A/V²)
0
0.002
0.004
0.006
0.008
0.01
1/V(V⁻¹)
5-20 at 5E-7
5-20 in He at 20mTorr
5-20 in Dry air at 20mTorr

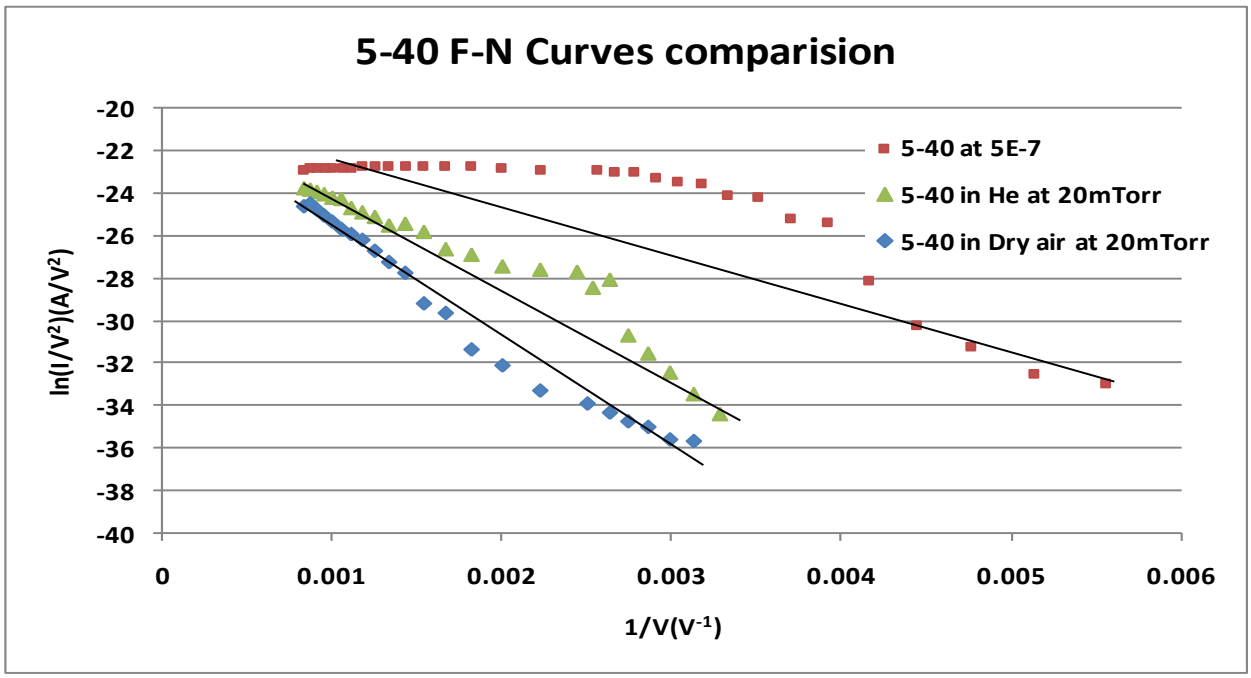
5-40 F-N Curves comparision
-20
-22
-24
-26
-28
-30
-32
-34
-36
-38
-40
ln(I/V²)(A/V²)
0
0.001
0.002
0.003
0.004
0.005
0.006
1/V(V⁻¹)
5-40 at 5E-7
5-40 in He at 20mTorr
5-40 in Dry air at 20mTorr

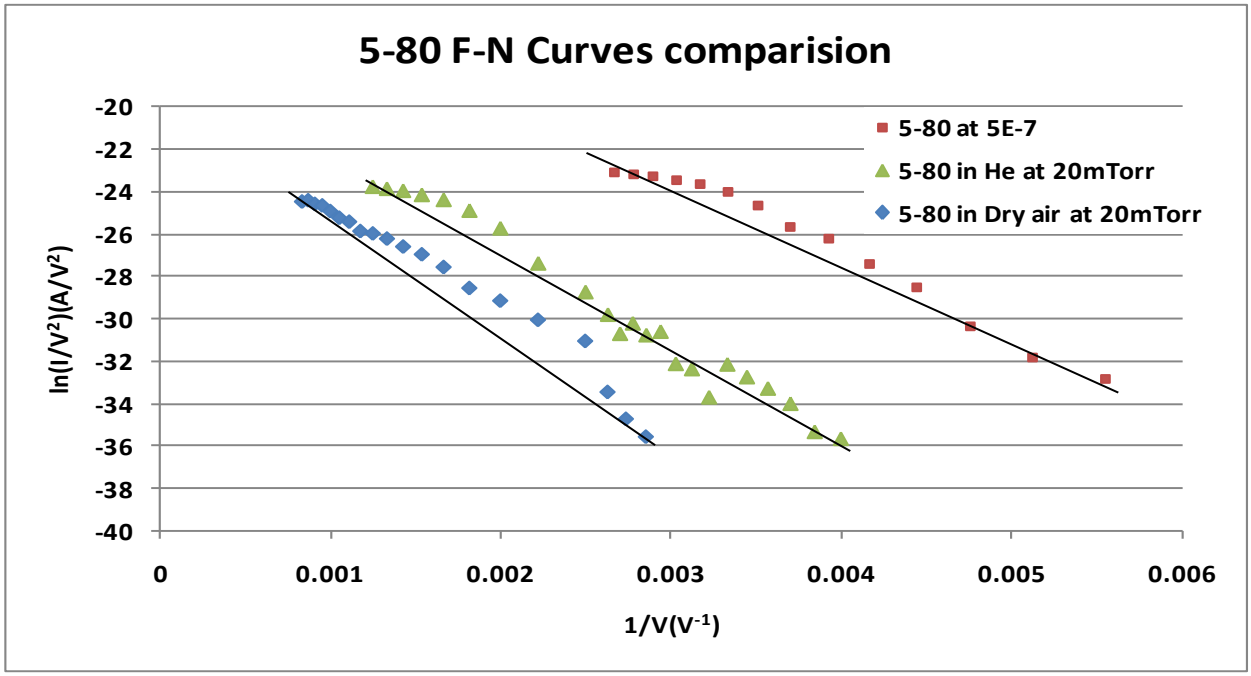
5-80 F-N Curves comparision
-20
-22
-24
-26
-28
-30
-32
-34
-36
-38
-40
ln(I/V²)(A/V²)
0
0.001
0.002
0.003
0.004
0.005
0.006
1/V(V⁻¹)
5-80 at 5E-7
5-80 in He at 20mTorr
5-80 in Dry air at 20mTorr

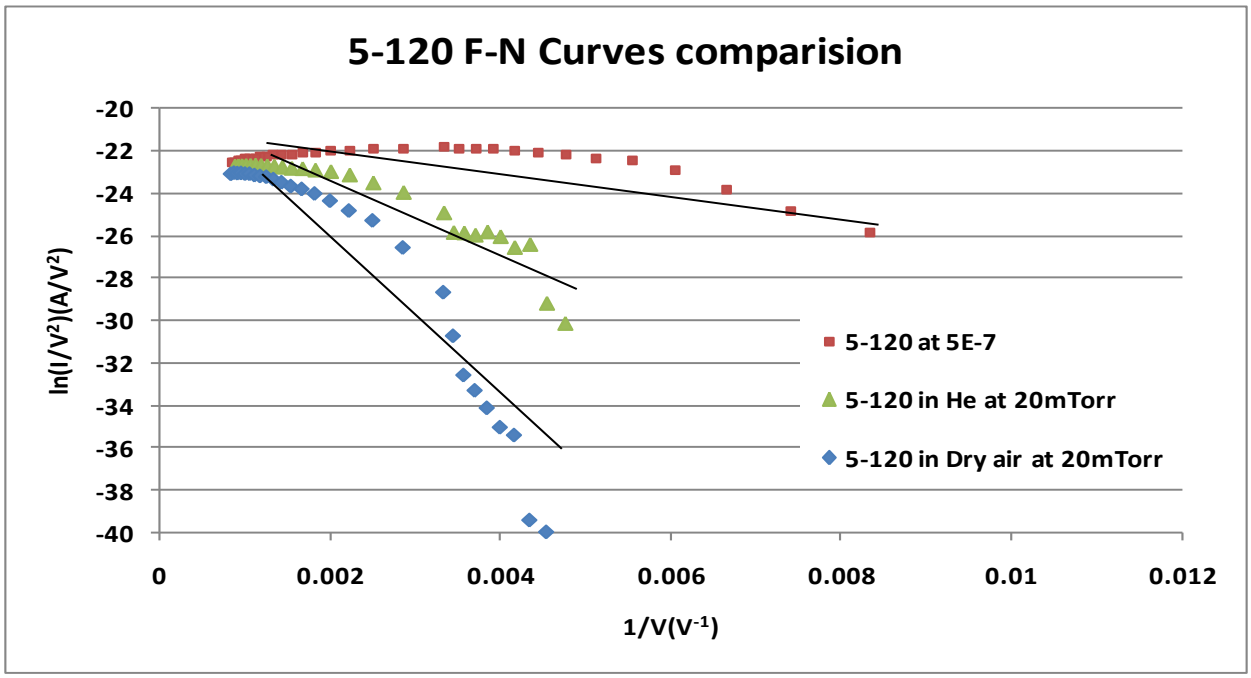
5-120 F-N Curves comparision
-20
-22
-24
-26
-28
-30
-32
-34
-36
-38
-40
ln(I/V²)(A/V²)
0
0.002
0.004
0.006
0.008
0.01
0.012
1/V(V⁻¹)
5-120 at 5E-7
5-120 in He at 20mTorr
5-120 in Dry air at 20mTorr

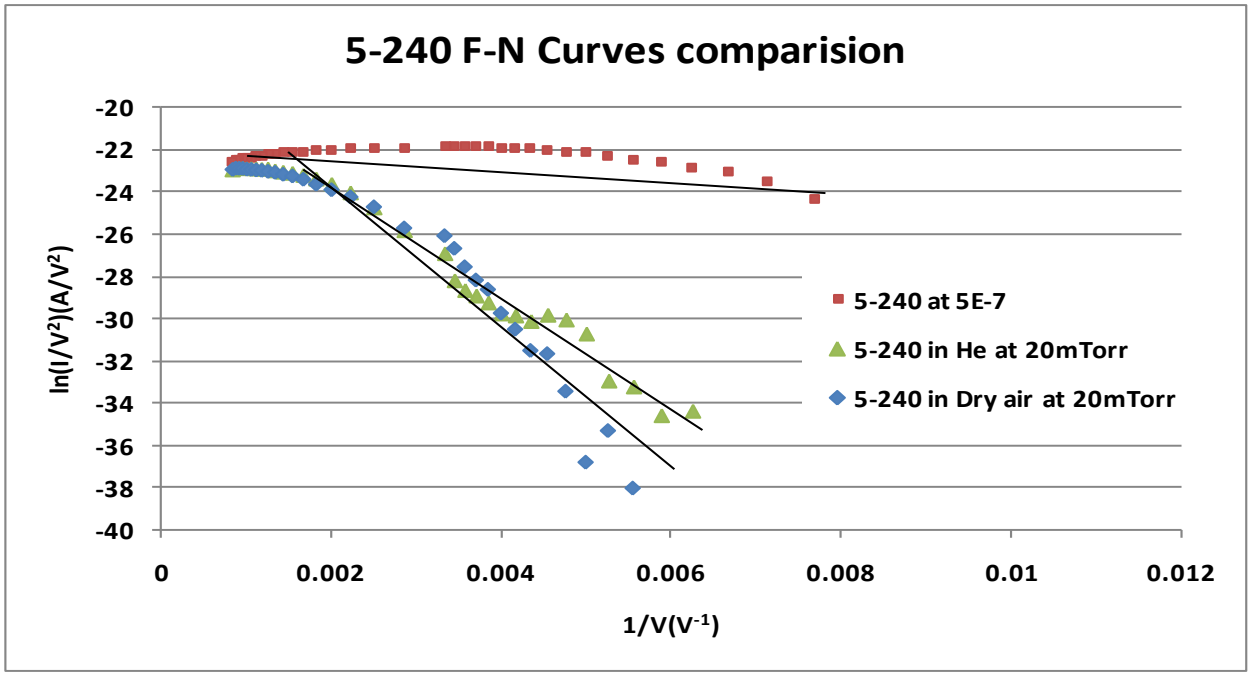
5-240 F-N Curves comparision
-20
-22
-24
-26
-28
-30
-32
-34
-36
-38
-40
ln(I/V²)(A/V²)
0
0.002
0.004
0.006
0.008
0.01
0.012
1/V(V⁻¹)
5-240 at 5E-7
5-240 in He at 20mTorr
5-240 in Dry air at 20mTorr

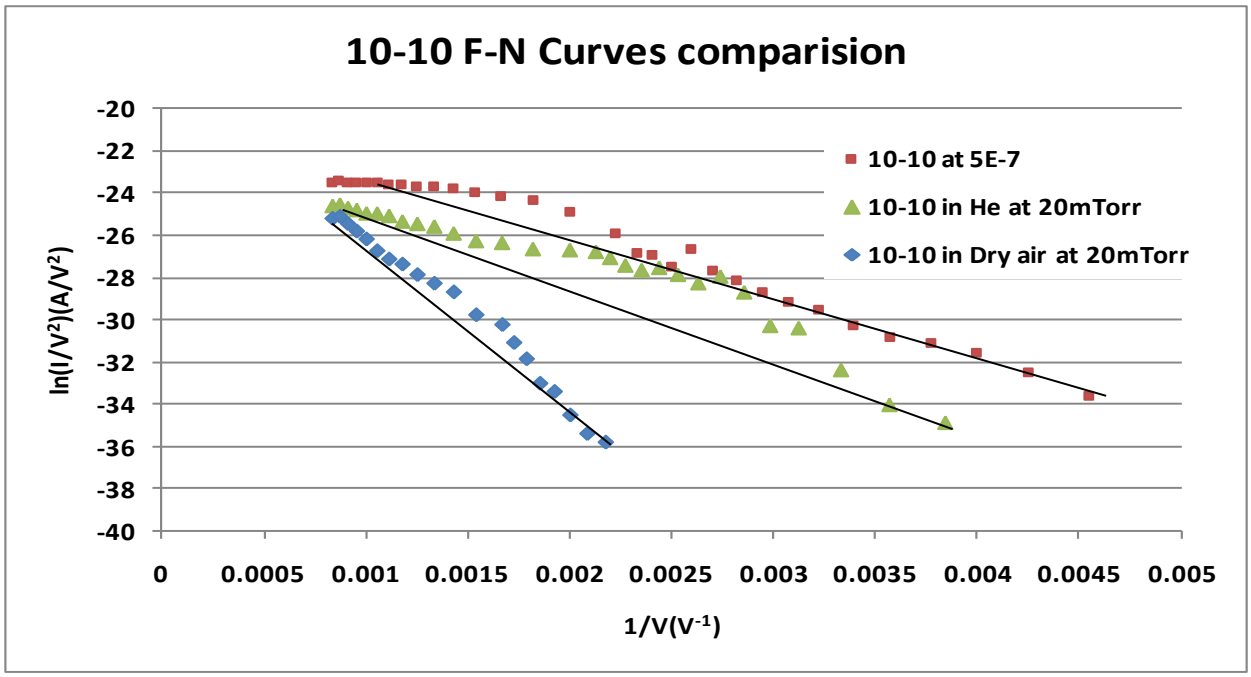
10-10 F-N Curves comparision
-20
-22
-24
-26
-28
-30
-32
-34
-36
-38
-40
ln(I/V²)(A/V²)
0
0.0005
0.001
0.0015
0.002
0.0025
0.003
0.0035
0.004
0.0045
0.005
1/V(V⁻¹)
10-10 at 5E-7
10-10 in He at 20mTorr
10-10 in Dry air at 20mTorr

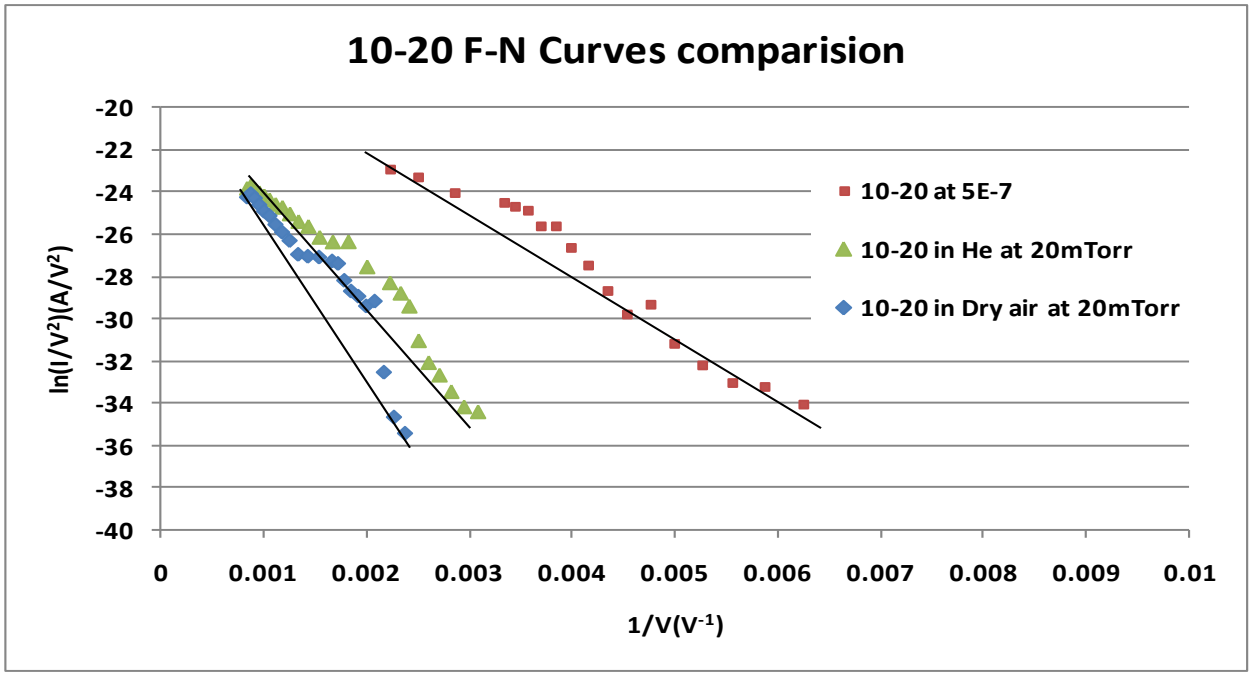
10-20 F-N Curves comparision
-20
-22
-24
-26
-28
-30
-32
-34
-36
-38
-40
ln(I/V²)(A/V²)
0
0.001
0.002
0.003
0.004
0.005
0.006
0.007
0.008
0.009
0.01
1/V(V⁻¹)
10-20 at 5E-7
10-20 in He at 20mTorr
10-20 in Dry air at 20mTorr

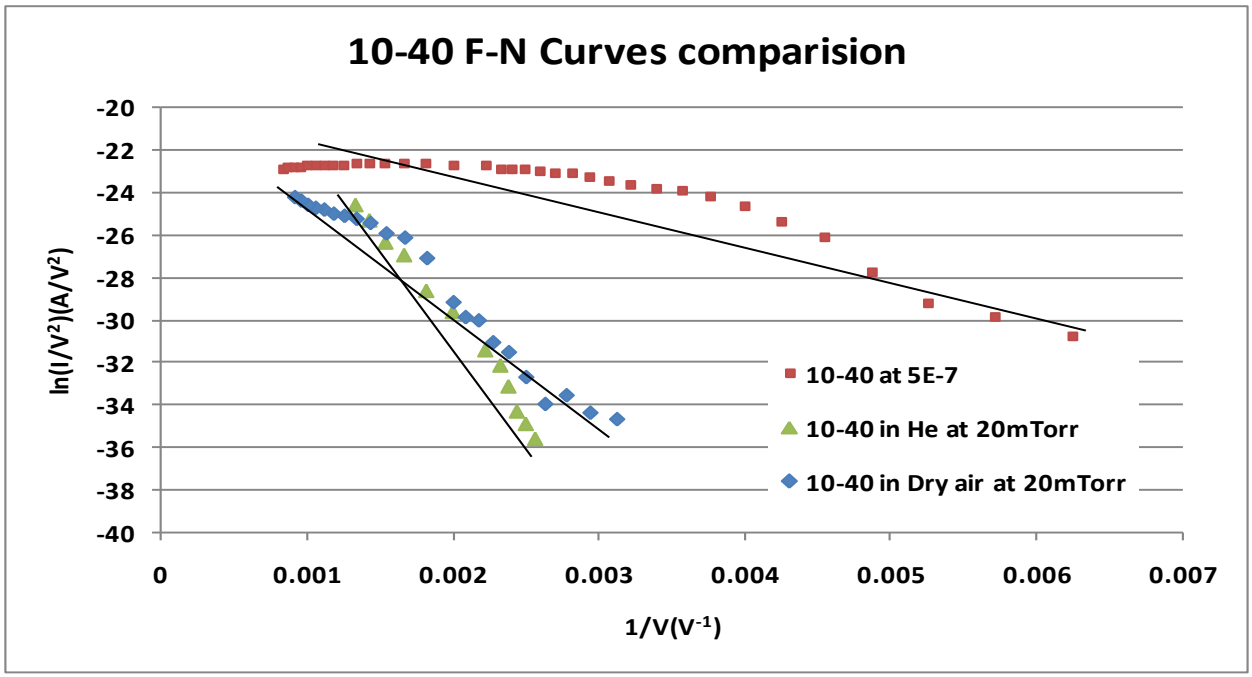
10-40 F-N Curves comparision
-20
-22
-24
-26
-28
-30
-32
-34
-36
-38
-40
ln(I/V²)(A/V²)
0
0.001
0.002
0.003
0.004
0.005
0.006
0.007
1/V(V⁻¹)
10-40 at 5E-7
10-40 in He at 20mTorr
10-40 in Dry air at 20mTorr

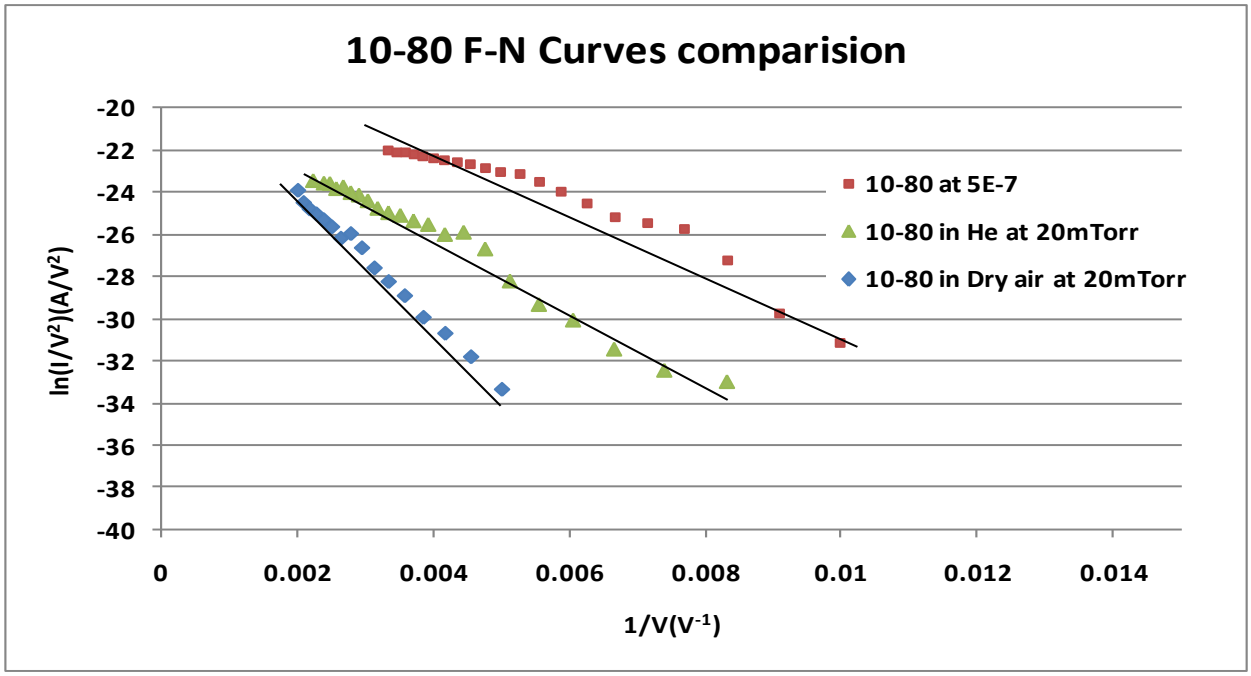
10-80 F-N Curves comparision
-20
-22
-24
-26
-28
-30
-32
-34
-36
-38
-40
ln(I/V²)(A/V²)
0
0.002
0.004
0.006
0.008
0.01
0.012
0.014
1/V(V⁻¹)
10-80 at 5E-7
10-80 in He at 20mTorr
10-80 in Dry air at 20mTorr

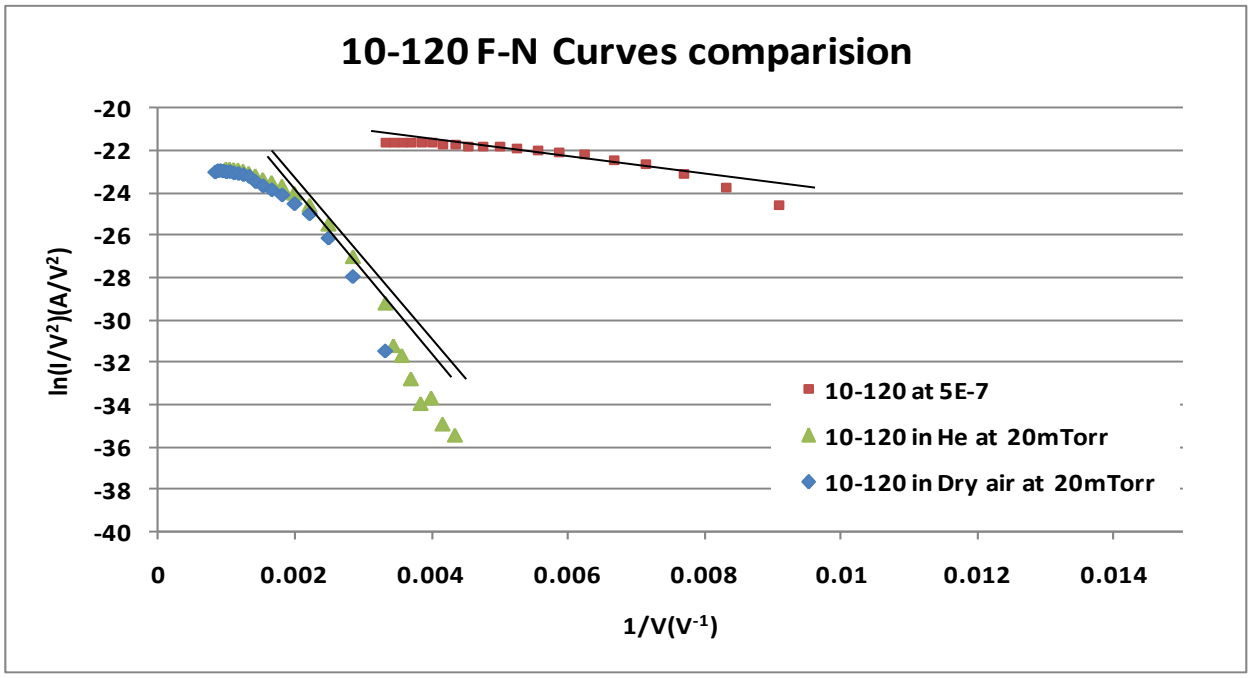
10-120 F-N Curves comparision
-20
-22
-24
-26
-28
-30
-32
-34
-36
-38
-40
ln(I/V²)(A/V²)
0
0.002
0.004
0.006
0.008
0.01
0.012
0.014
1/V(V⁻¹)
10-120 at 5E-7
10-120 in He at 20mTorr
10-120 in Dry air at 20mTorr

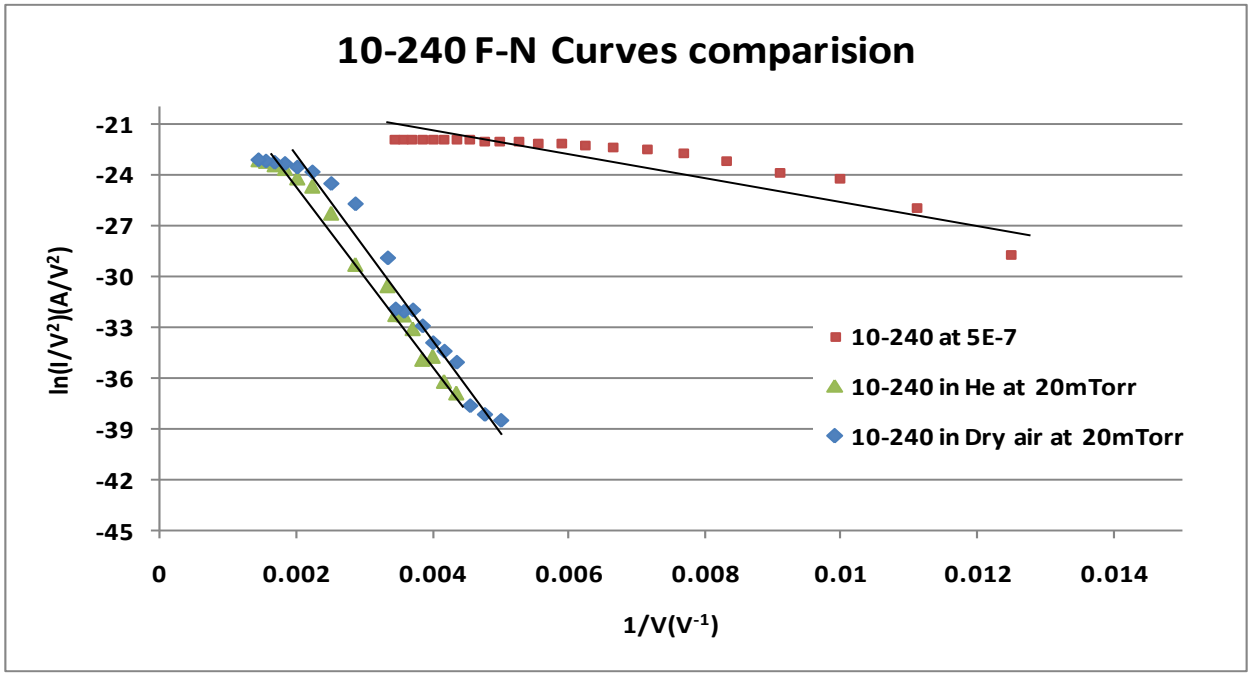

Figure 4.2: F-N curves comparisons at different pressures for (a) 5 min sputtering samples (b) 10 min sputtering samples.

4.4 Field Emission Comparison with respect to Growth Time

Field emission characteristics are plotted for all the samples with respect to the growth times for both 5 min and 10 min sputtering samples. In most cases the turn-on electric field for the samples with higher growth time has low value compared to the samples grown for less time. The turn-on for sample with 10 min growth time has high value in all cases where as the turn-on for 20, 40, and 80 min falls approximately in the same range. Lower turn-on electric fields were observed in case of samples with 80 min and longer growth periods but the lowest was observed in case of 10 min sputtering, 240 min growth time which is 0.43 V/μm. The current densities observed to be increasing with increase in the growth times. This clearly suggests that the increase in the density of CNTs and long tubes provide larger area for the emission of electrons and thus increase in the current density. The lowest current density was observed to be 0.14 mA/cm^2 for 5 min sputtering and 10 min growth time at 20 mTorr pressure where as the highest

is 7.67 mA/cm^2 for 10 min sputtering and 240 min growth time. Below are the curves compared with their growth times in vacuum, Helium and dryair at different pressures. The turn-on is observed to be increasing with change in gas, from vacuum to He and to dry air respectively along with the pressures.

4.4.1 Growth Time Effect for 5 min Sputtering Samples

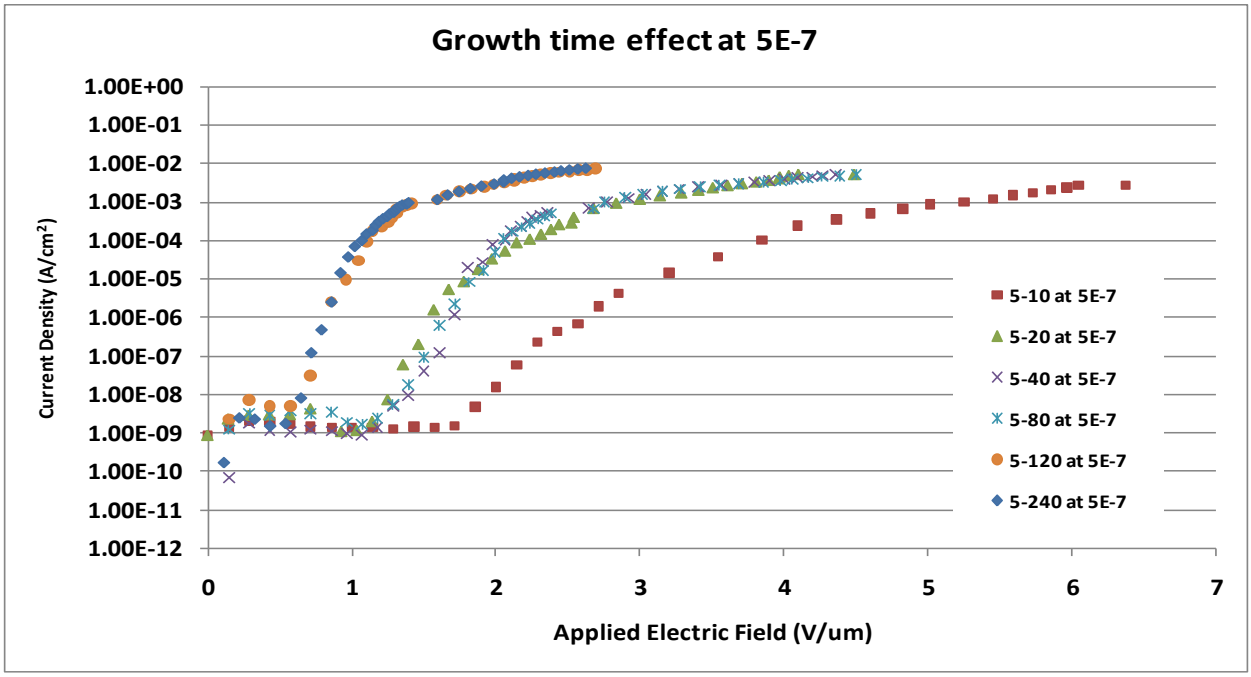

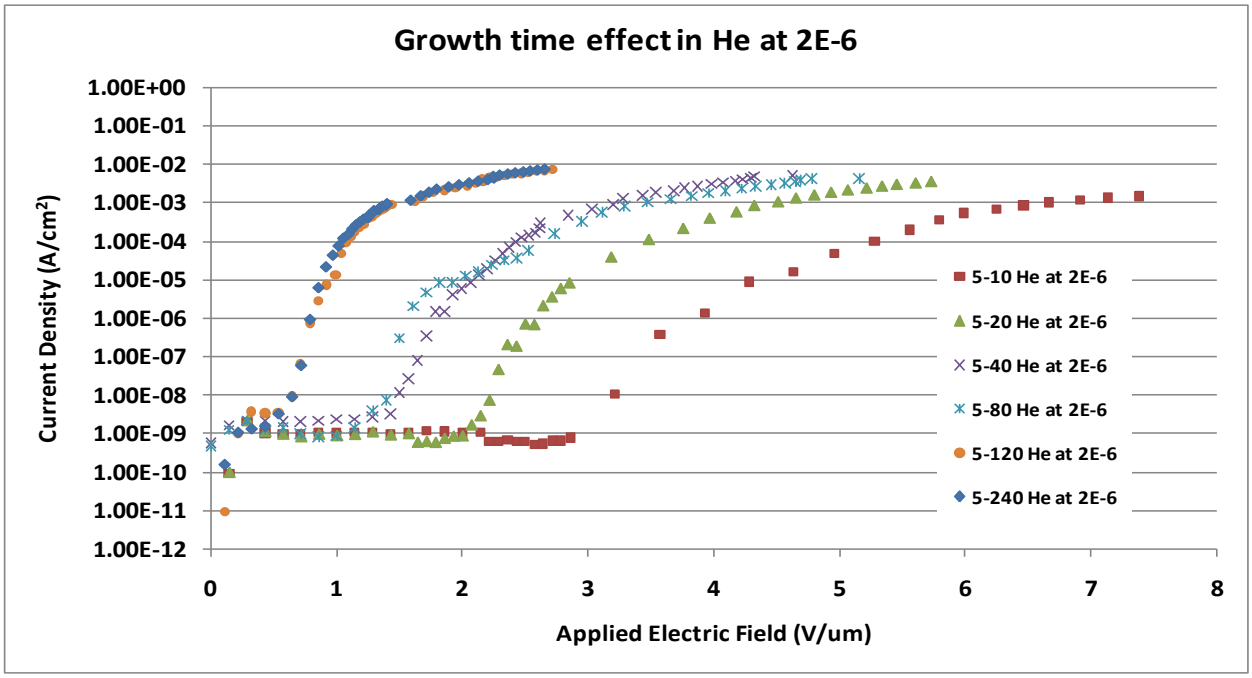
Growth time effect in He at 2E-6
Current Density (A/cm²)
1.00E+00
1.00E-01
1.00E-02
1.00E-03
1.00E-04
1.00E-05
1.00E-06
1.00E-07
1.00E-08
1.00E-09
1.00E-10
1.00E-11
1.00E-12
0
1
2
3
4
5
6
7
8
Applied Electric Field (V/um)
5-10 He at 2E-6
5-20 He at 2E-6
5-40 He at 2E-6
5-80 He at 2E-6
5-120 He at 2E-6
5-240 He at 2E-6

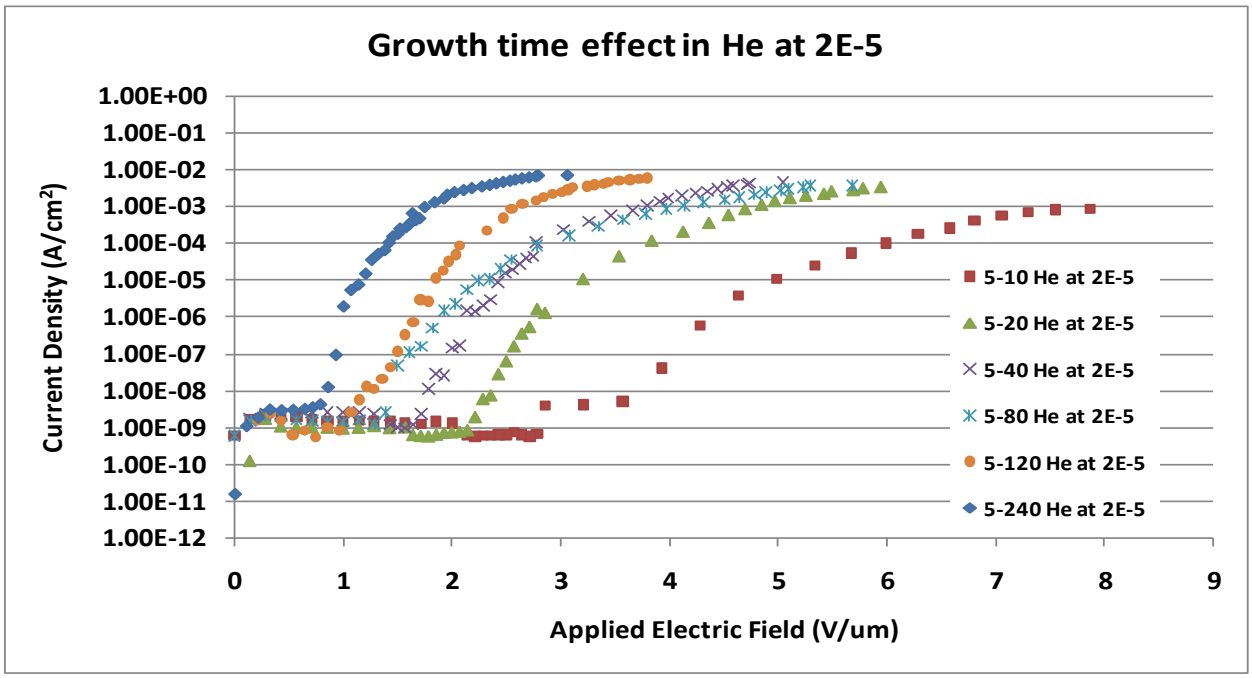
Growth time effect in He at 2E-5
Current Density (A/cm²)
1.00E+00
1.00E-01
1.00E-02
1.00E-03
1.00E-04
1.00E-05
1.00E-06
1.00E-07
1.00E-08
1.00E-09
1.00E-10
1.00E-11
1.00E-12
0
1
2
3
4
5
6
7
8
9
Applied Electric Field (V/um)
5-10 He at 2E-5
5-20 He at 2E-5
5-40 He at 2E-5
5-80 He at 2E-5
5-120 He at 2E-5
5-240 He at 2E-5

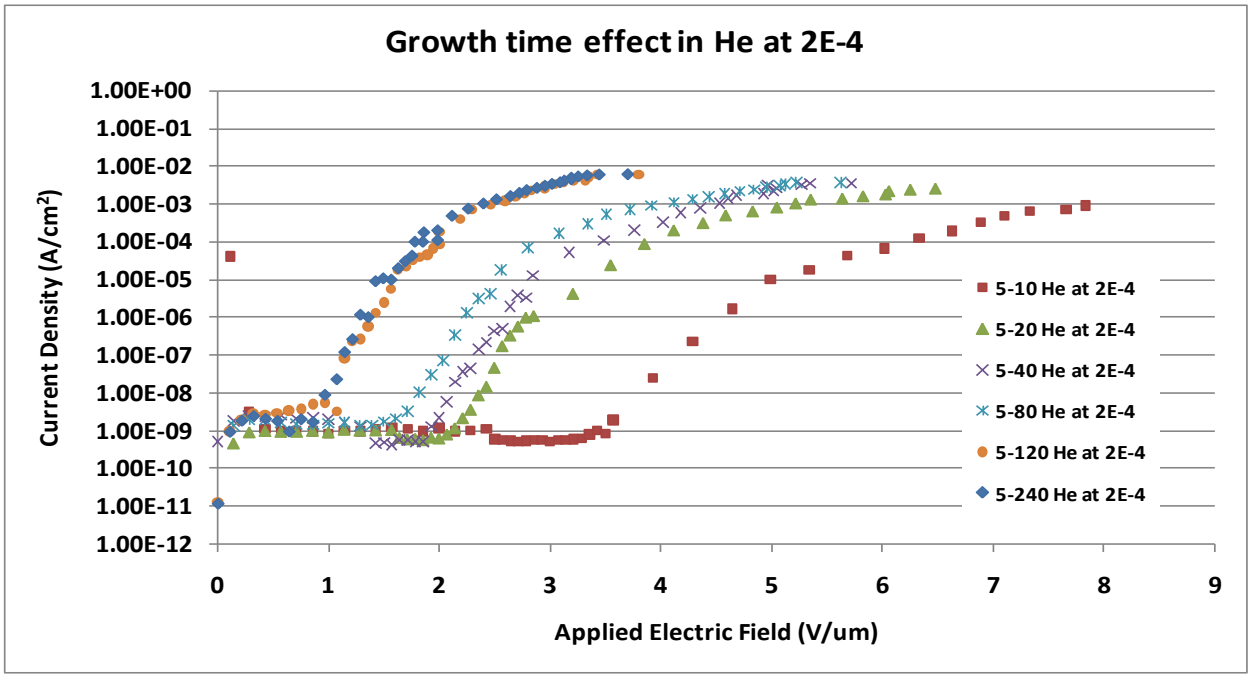
Growth time effect in He at 2E-4
Current Density (A/cm²)
1.00E+00
1.00E-01
1.00E-02
1.00E-03
1.00E-04
1.00E-05
1.00E-06
1.00E-07
1.00E-08
1.00E-09
1.00E-10
1.00E-11
1.00E-12
0
1
2
3
4
5
6
7
8
9
Applied Electric Field (V/um)
5-10 He at 2E-4
5-20 He at 2E-4
5-40 He at 2E-4
5-80 He at 2E-4
5-120 He at 2E-4
5-240 He at 2E-4

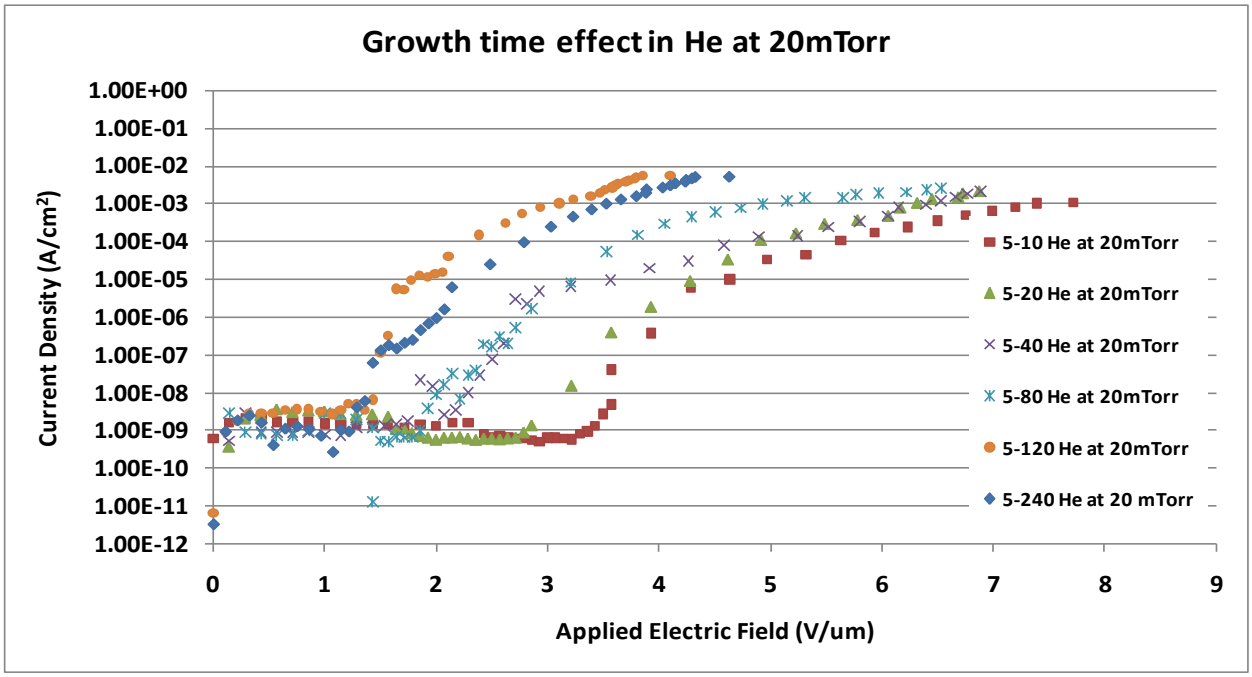
Growth time effect in He at 20mTorr
Current Density (A/cm²)
1.00E+00
1.00E-01
1.00E-02
1.00E-03
1.00E-04
1.00E-05
1.00E-06
1.00E-07
1.00E-08
1.00E-09
1.00E-10
1.00E-11
1.00E-12
0
1
2
3
4
5
6
7
8
9
Applied Electric Field (V/um)
5-10 He at 20mTorr
5-20 He at 20mTorr
5-40 He at 20mTorr
5-80 He at 20mTorr
5-120 He at 20mTorr
5-240 He at 20 mTorr

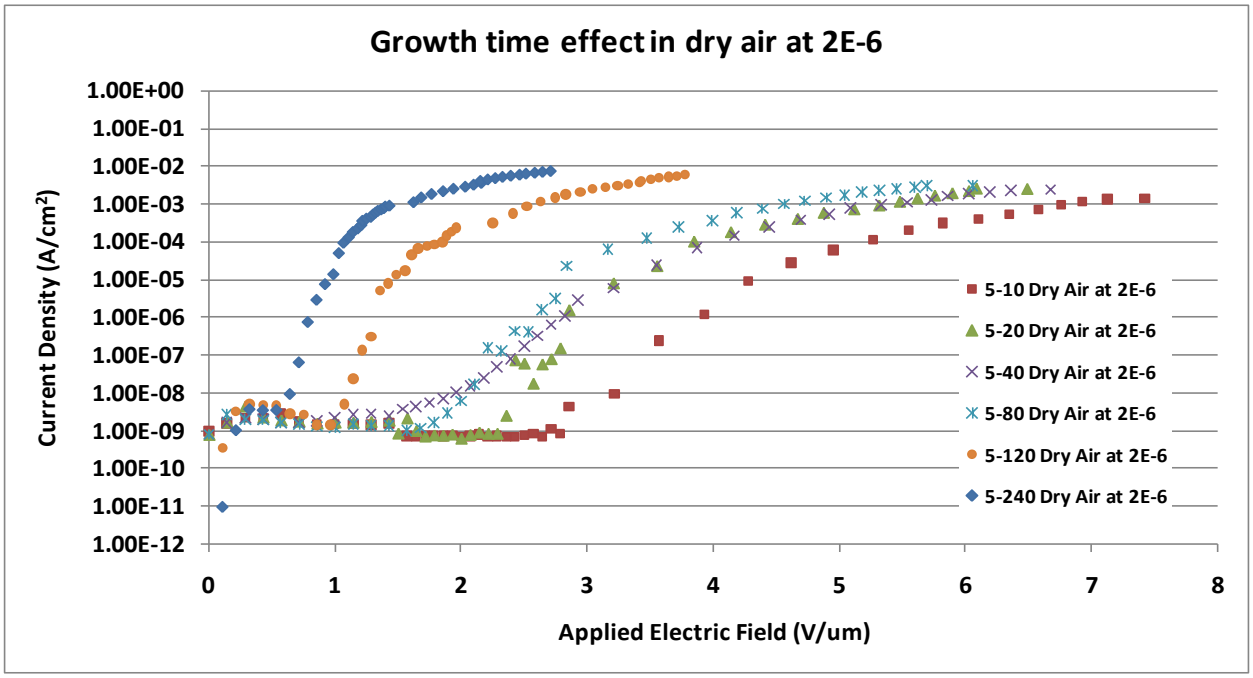
Growth time effect in dry air at 2E-6
Current Density (A/cm²)
1.00E+00
1.00E-01
1.00E-02
1.00E-03
1.00E-04
1.00E-05
1.00E-06
1.00E-07
1.00E-08
1.00E-09
1.00E-10
1.00E-11
1.00E-12
0
1
2
3
4
5
6
7
8
Applied Electric Field (V/um)
5-10 Dry Air at 2E-6
5-20 Dry Air at 2E-6
5-40 Dry Air at 2E-6
5-80 Dry Air at 2E-6
5-120 Dry Air at 2E-6
5-240 Dry Air at 2E-6

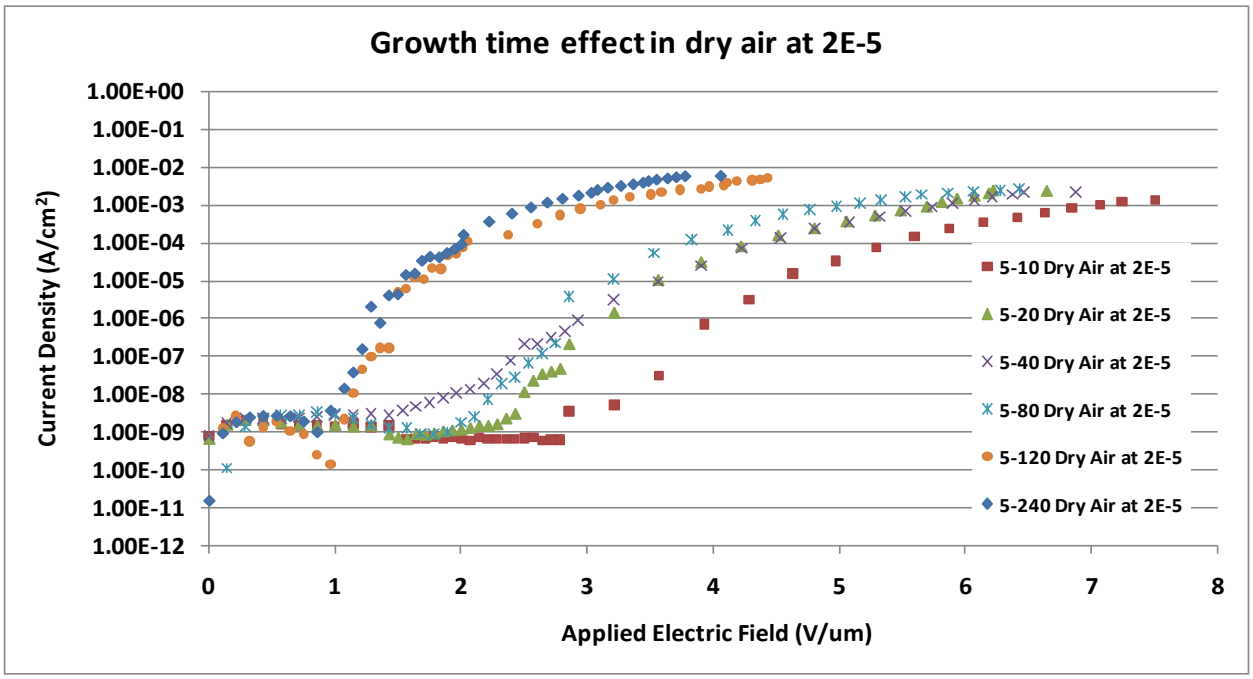
Growth time effect in dry air at 2E-5
Current Density (A/cm²)
1.00E+00
1.00E-01
1.00E-02
1.00E-03
1.00E-04
1.00E-05
1.00E-06
1.00E-07
1.00E-08
1.00E-09
1.00E-10
1.00E-11
1.00E-12
0
1
2
3
4
5
6
7
8
Applied Electric Field (V/um)
5-10 Dry Air at 2E-5
5-20 Dry Air at 2E-5
5-40 Dry Air at 2E-5
5-80 Dry Air at 2E-5
5-120 Dry Air at 2E-5
5-240 Dry Air at 2E-5

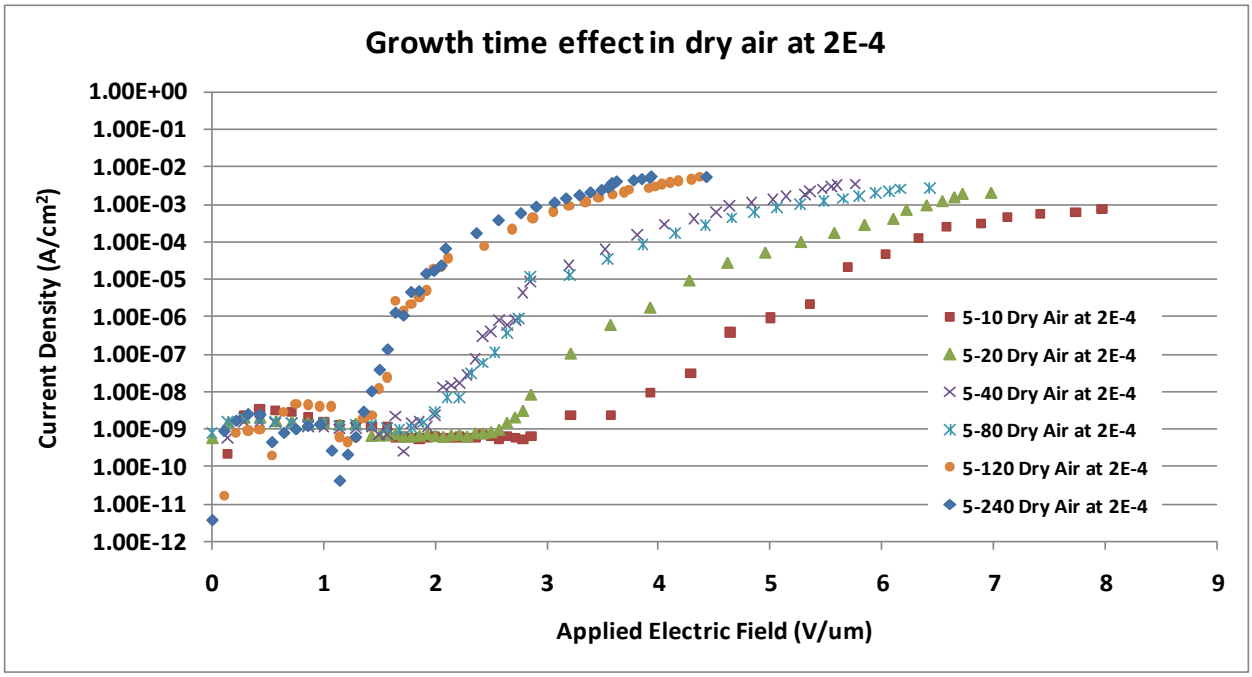
Growth time effect in dry air at 2E-4
Current Density (A/cm²)
1.00E+00
1.00E-01
1.00E-02
1.00E-03
1.00E-04
1.00E-05
1.00E-06
1.00E-07
1.00E-08
1.00E-09
1.00E-10
1.00E-11
1.00E-12
0
1
2
3
4
5
6
7
8
9
Applied Electric Field (V/um)
5-10 Dry Air at 2E-4
5-20 Dry Air at 2E-4
5-40 Dry Air at 2E-4
5-80 Dry Air at 2E-4
5-120 Dry Air at 2E-4
5-240 Dry Air at 2E-4

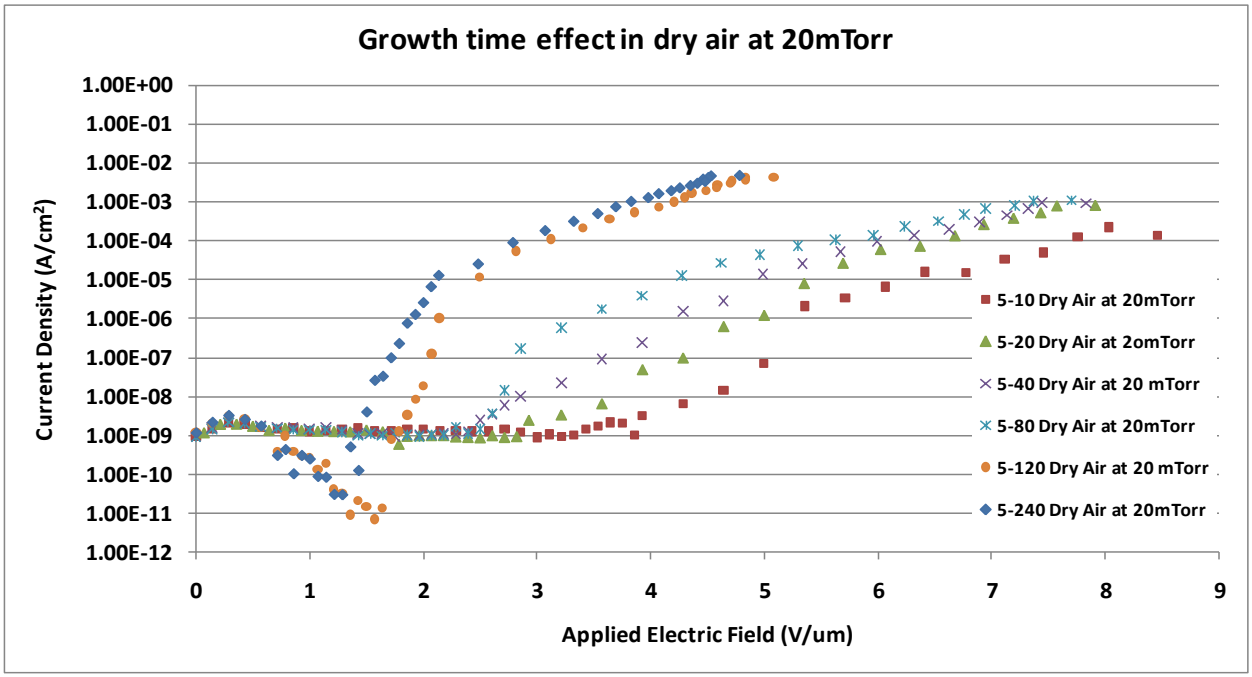
Growth time effect in dry air at 20mTorr
Current Density (A/cm²)
1.00E+00
1.00E-01
1.00E-02
1.00E-03
1.00E-04
1.00E-05
1.00E-06
1.00E-07
1.00E-08
1.00E-09
1.00E-10
1.00E-11
1.00E-12
0
1
2
3
4
5
6
7
8
9
Applied Electric Field (V/um)
5-10 Dry Air at 20mTorr
5-20 Dry Air at 2omTorr
5-40 Dry Air at 20 mTorr
5-80 Dry Air at 20mTorr
5-120 Dry Air at 20 mTorr
5-240 Dry Air at 20mTorr

4.4.2 Growth time effect for 10 min sputtering samples

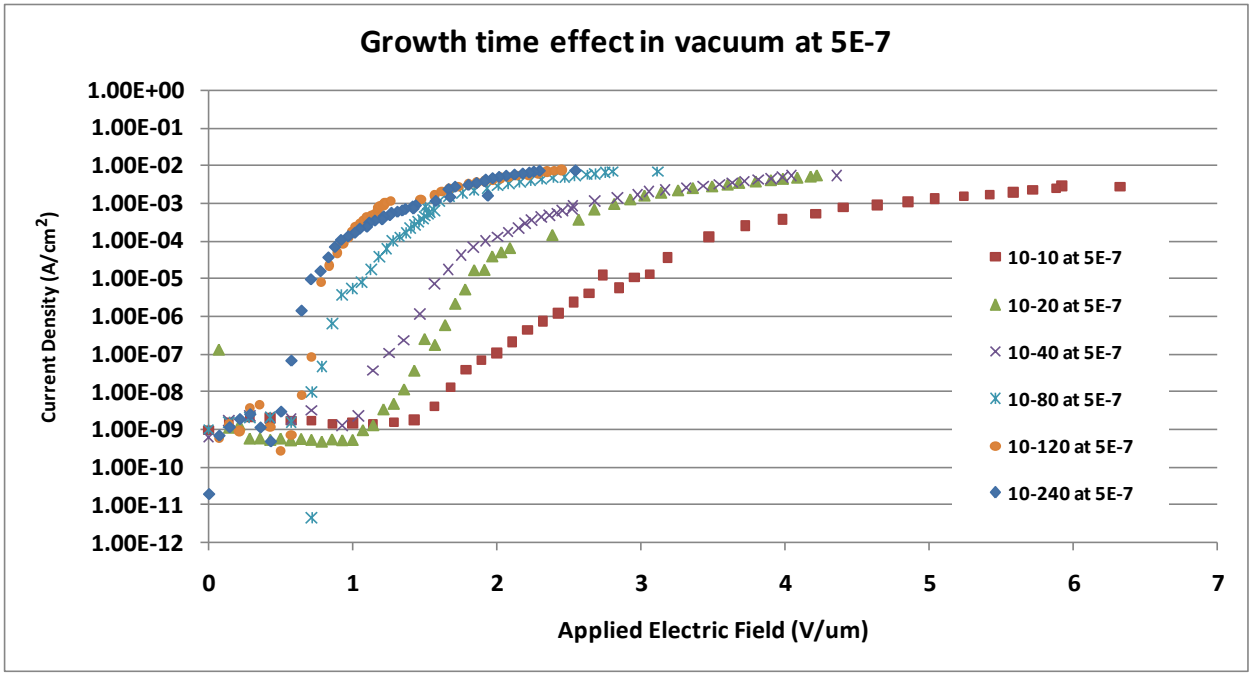

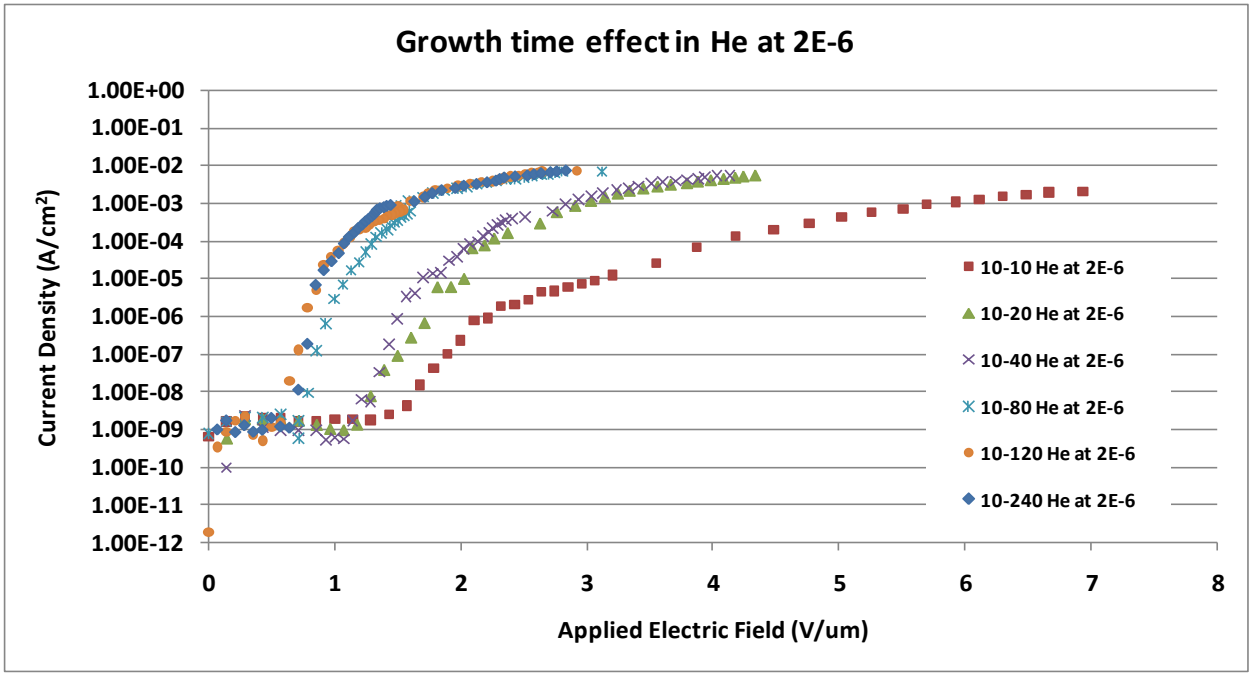

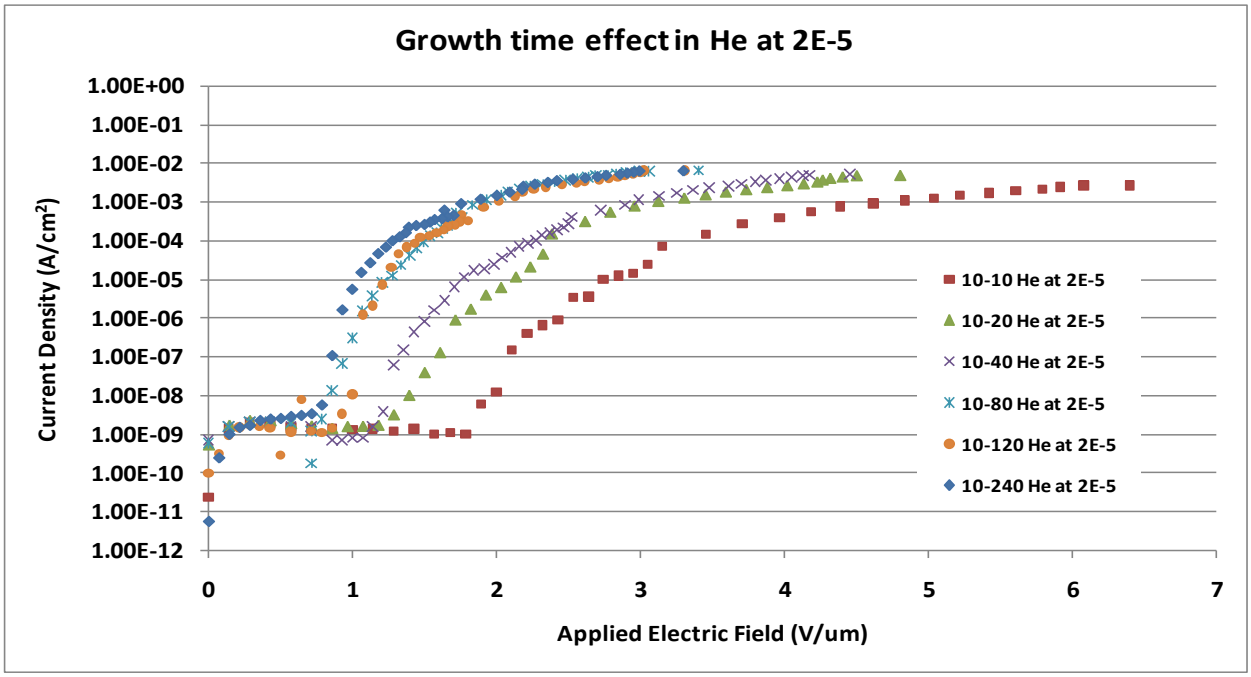
Growth time effect in He at 2E-5
Current Density (A/cm²)
1.00E+00
1.00E-01
1.00E-02
1.00E-03
1.00E-04
1.00E-05
1.00E-06
1.00E-07
1.00E-08
1.00E-09
1.00E-10
1.00E-11
1.00E-12
0
1
2
3
4
5
6
7
Applied Electric Field (V/um)
10-10 He at 2E-5
10-20 He at 2E-5
10-40 He at 2E-5
10-80 He at 2E-5
10-120 He at 2E-5
10-240 He at 2E-5

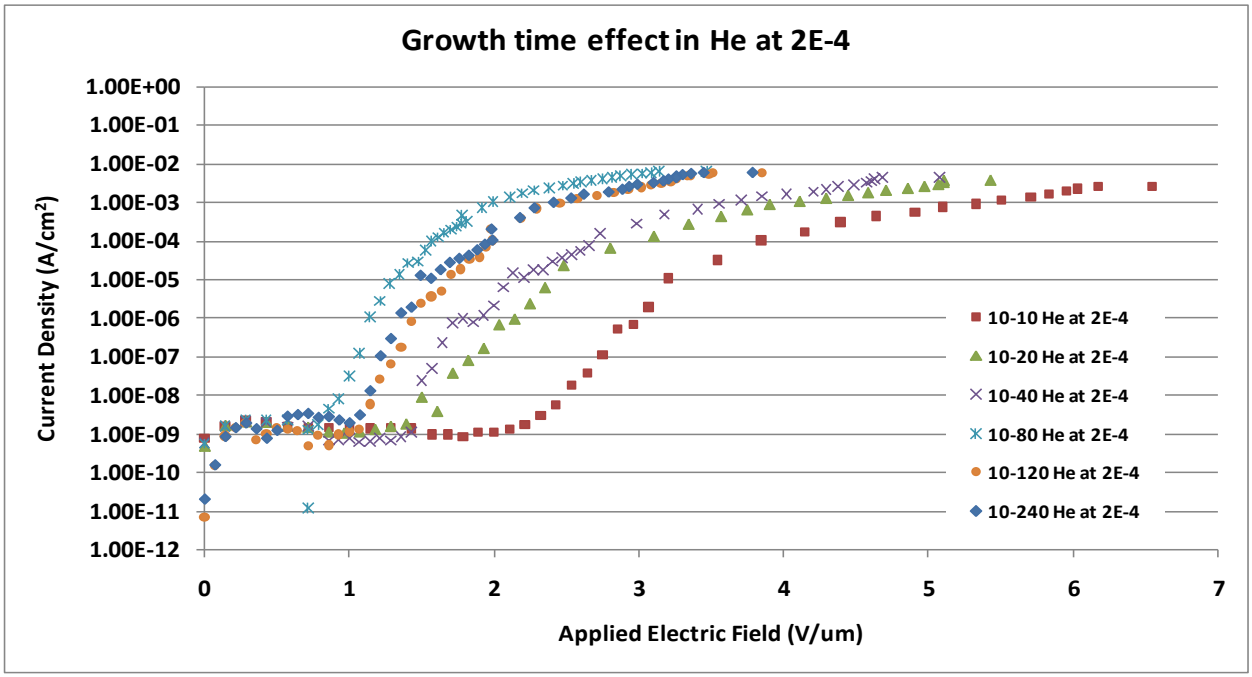
Growth time effect in He at 2E-4
Current Density (A/cm²)
1.00E+00
1.00E-01
1.00E-02
1.00E-03
1.00E-04
1.00E-05
1.00E-06
1.00E-07
1.00E-08
1.00E-09
1.00E-10
1.00E-11
1.00E-12
0
1
2
3
4
5
6
7
Applied Electric Field (V/um)
10-10 He at 2E-4
10-20 He at 2E-4
10-40 He at 2E-4
10-80 He at 2E-4
10-120 He at 2E-4
10-240 He at 2E-4

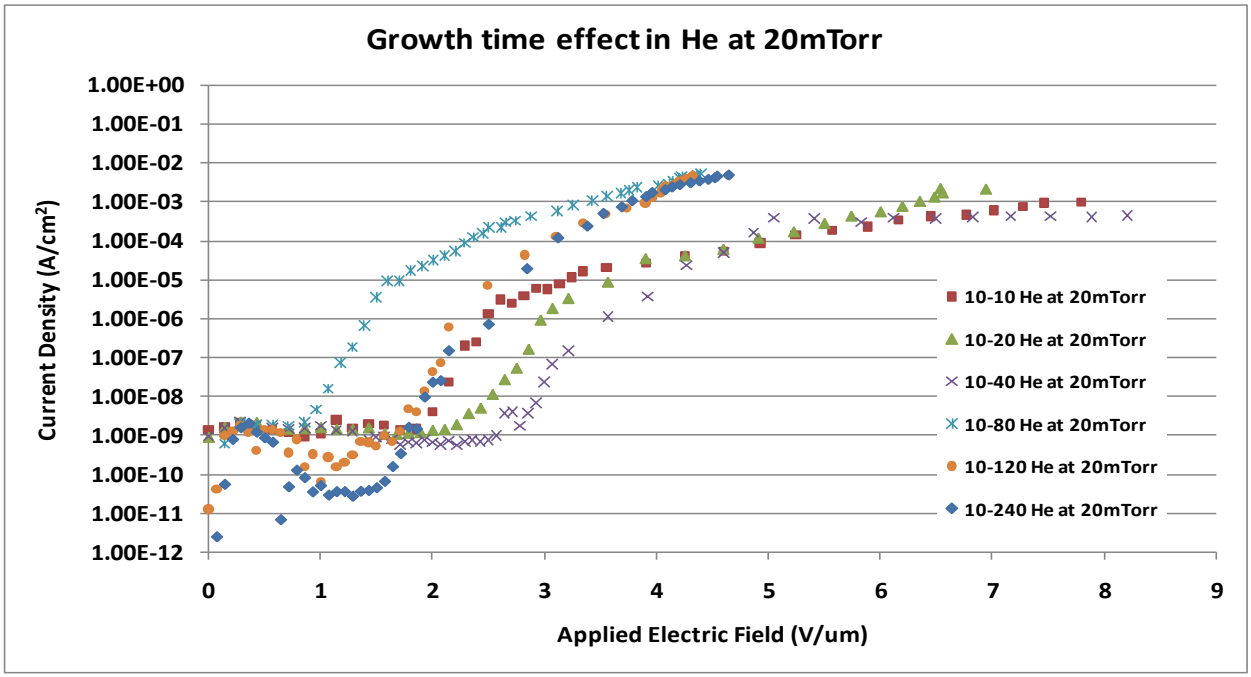
Growth time effect in He at 20mTorr
Current Density (A/cm²)
1.00E+00
1.00E-01
1.00E-02
1.00E-03
1.00E-04
1.00E-05
1.00E-06
1.00E-07
1.00E-08
1.00E-09
1.00E-10
1.00E-11
1.00E-12
0
1
2
3
4
5
6
7
8
9
Applied Electric Field (V/um)
10-10 He at 20mTorr
10-20 He at 20mTorr
10-40 He at 20mTorr
10-80 He at 20mTorr
10-120 He at 20mTorr
10-240 He at 20mTorr

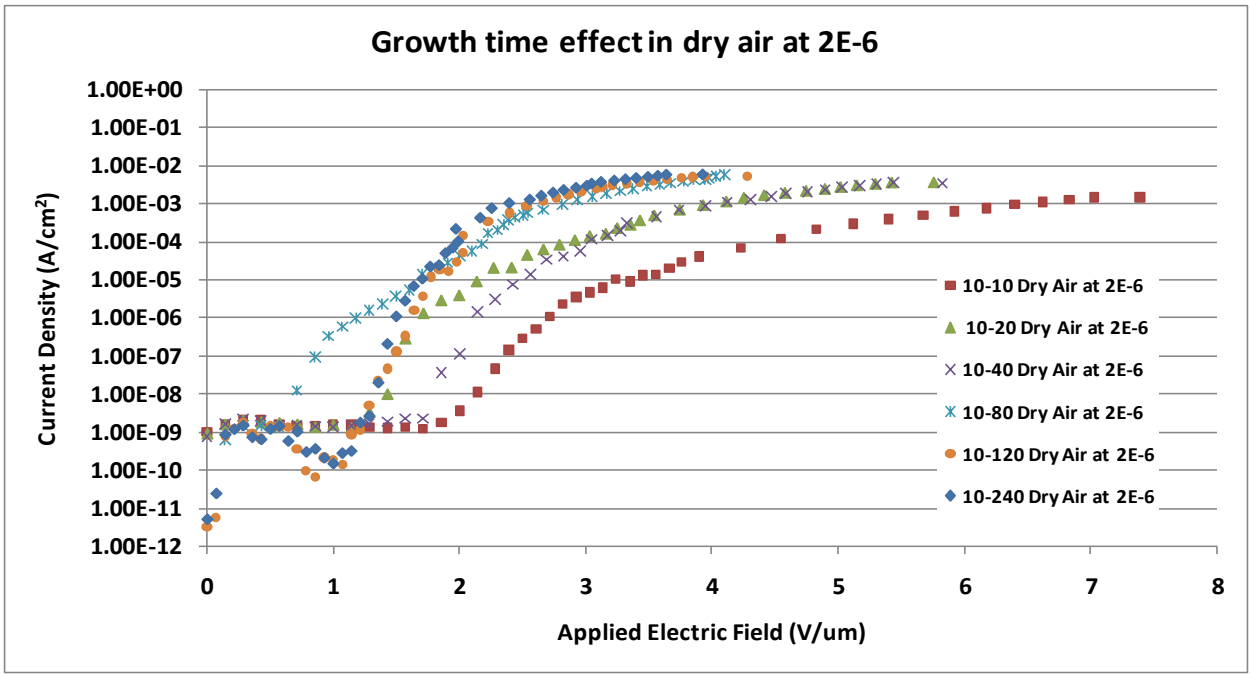
Growth time effect in dry air at 2E-6
Current Density (A/cm²)
1.00E+00
1.00E-01
1.00E-02
1.00E-03
1.00E-04
1.00E-05
1.00E-06
1.00E-07
1.00E-08
1.00E-09
1.00E-10
1.00E-11
1.00E-12
0
1
2
3
4
5
6
7
8
Applied Electric Field (V/um)
10-10 Dry Air at 2E-6
10-20 Dry Air at 2E-6
10-40 Dry Air at 2E-6
10-80 Dry Air at 2E-6
10-120 Dry Air at 2E-6
10-240 Dry Air at 2E-6

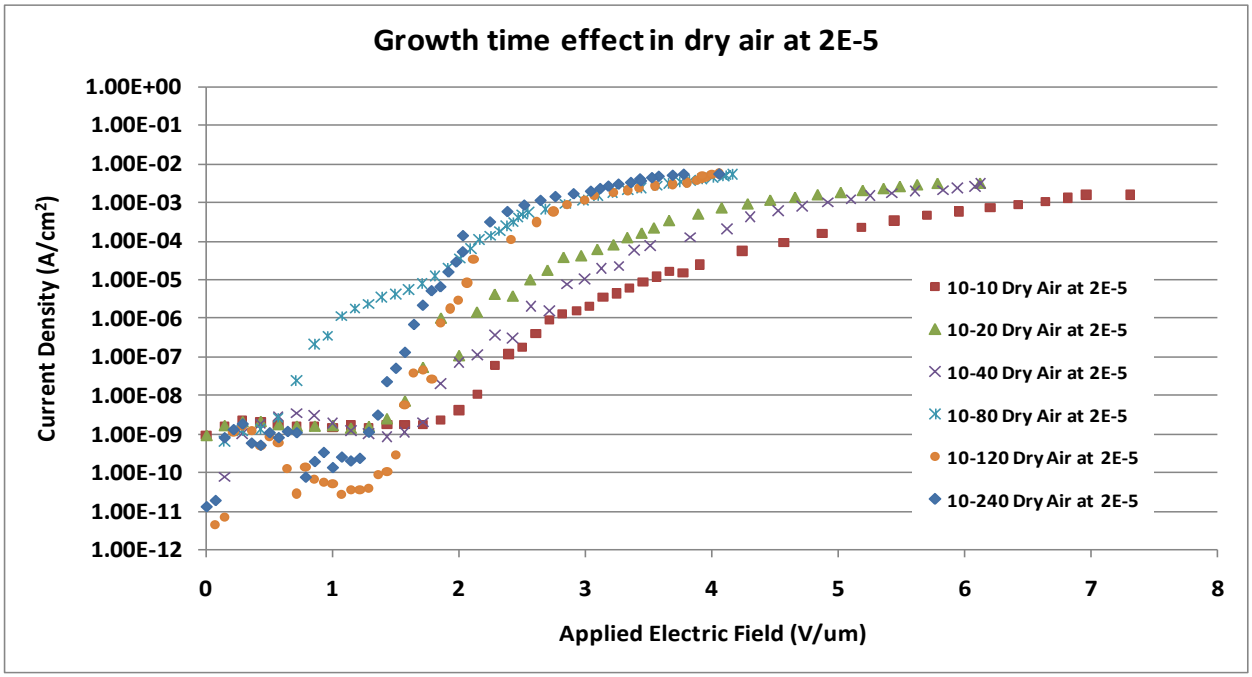
Growth time effect in dry air at 2E-5
Current Density (A/cm²)
1.00E+00
1.00E-01
1.00E-02
1.00E-03
1.00E-04
1.00E-05
1.00E-06
1.00E-07
1.00E-08
1.00E-09
1.00E-10
1.00E-11
1.00E-12
0
1
2
3
4
5
6
7
8
Applied Electric Field (V/um)
10-10 Dry Air at 2E-5
10-20 Dry Air at 2E-5
10-40 Dry Air at 2E-5
10-80 Dry Air at 2E-5
10-120 Dry Air at 2E-5
10-240 Dry Air at 2E-5

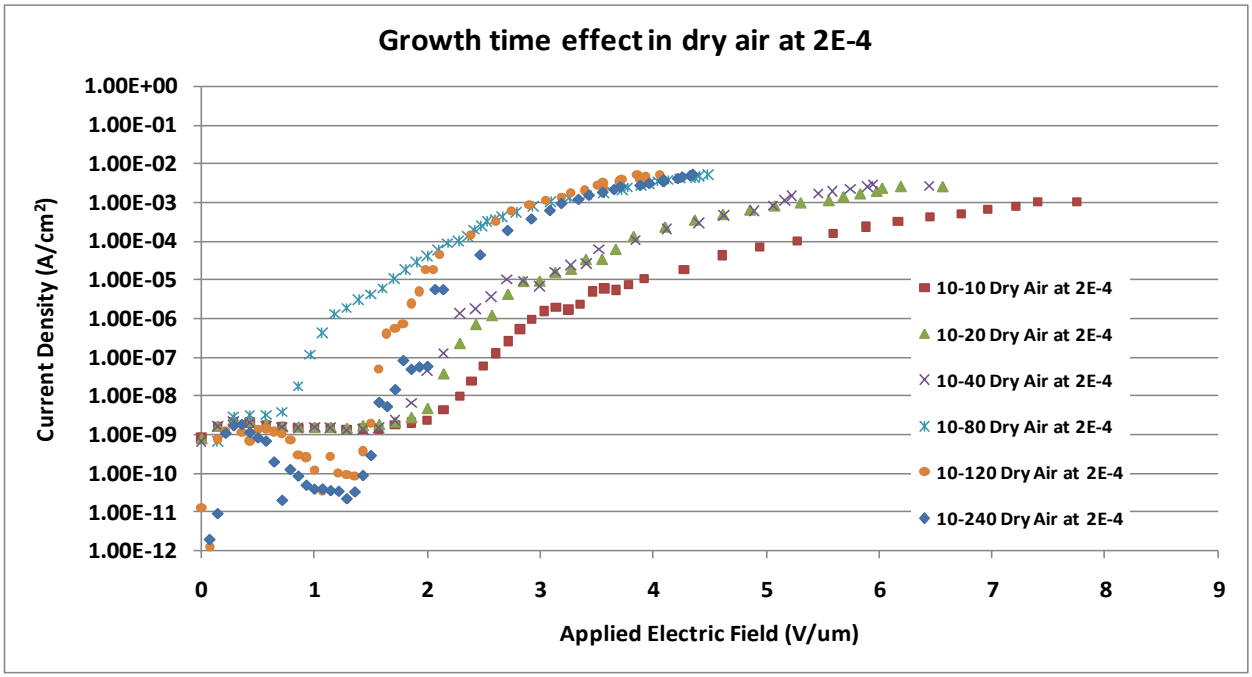
Growth time effect in dry air at 2E-4
Current Density (A/cm²)
1.00E+00
1.00E-01
1.00E-02
1.00E-03
1.00E-04
1.00E-05
1.00E-06
1.00E-07
1.00E-08
1.00E-09
1.00E-10
1.00E-11
1.00E-12
0
1
2
3
4
5
6
7
8
9
Applied Electric Field (V/um)
10-10 Dry Air at 2E-4
10-20 Dry Air at 2E-4
10-40 Dry Air at 2E-4
10-80 Dry Air at 2E-4
10-120 Dry Air at 2E-4
10-240 Dry Air at 2E-4

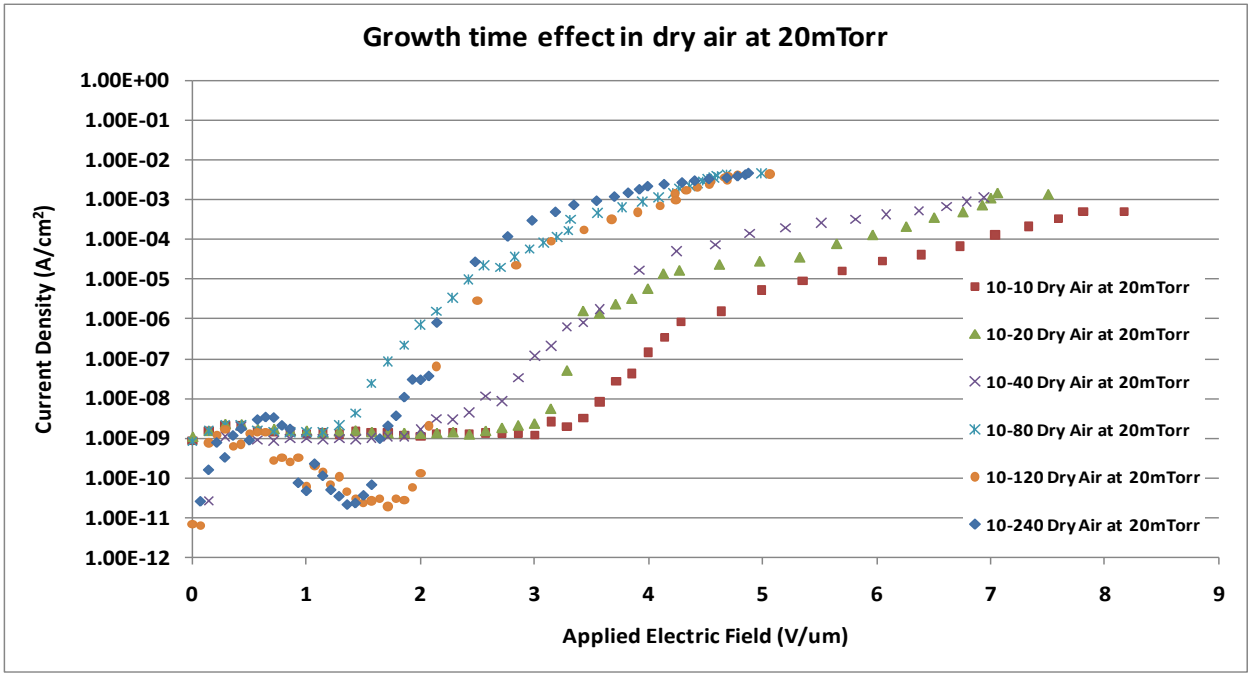

Figure 4.3: Growth time effect on the field emission characteristics of CNTs in different gases and pressures for (a) 5 min sputtering samples (b) 10 min sputtering samples.

4.5 Lifetime and Current Stability Test at Constant Voltage

In many high voltage applications, the constant electron emission from cold cathode for a given range of applied electric field, over long run is important. The change in electron emission from the cathode surface with respect to the applied electric field over time influences the turn-on electric field which is not desired in many applications. Study of saturation current density and its variation at the steady state level with respect to the applied electric field over long run gives important information about the turn-on electric field and the lifetime of a cold cathode. To know the amount of deviation in the turn-on electric field and the effective lifetime of CNT cold cathode over which it remains as a constant field emitter, the saturation current density is considered.

All the samples were tested for their lifetime and current stability by applying constant voltage of 600 V at high vacuum conditions. Current densities of all the samples were plotted

with respect to time to see if there is any degradation in their characteristics. In all the cases it can be observed that there was very little degradation in their emission current. Even there is very little difference in the amount of current all the samples with different growth times are emitted except the sample with 5 min sputtering and 10 min growth. This could be because of the runs that were performed for previous tests had impact on the tubes resulting in the low current density. If we observe for the degradation keeping aside the amount of current emission, all the samples exhibit a stable emission for 5 hours or more. Similar phenomenon is observed with case of 10 min sputtering samples. The plots are shown below.

4.5.1 Lifetime Test at Constant Voltage for Samples with 5 min Sputtering

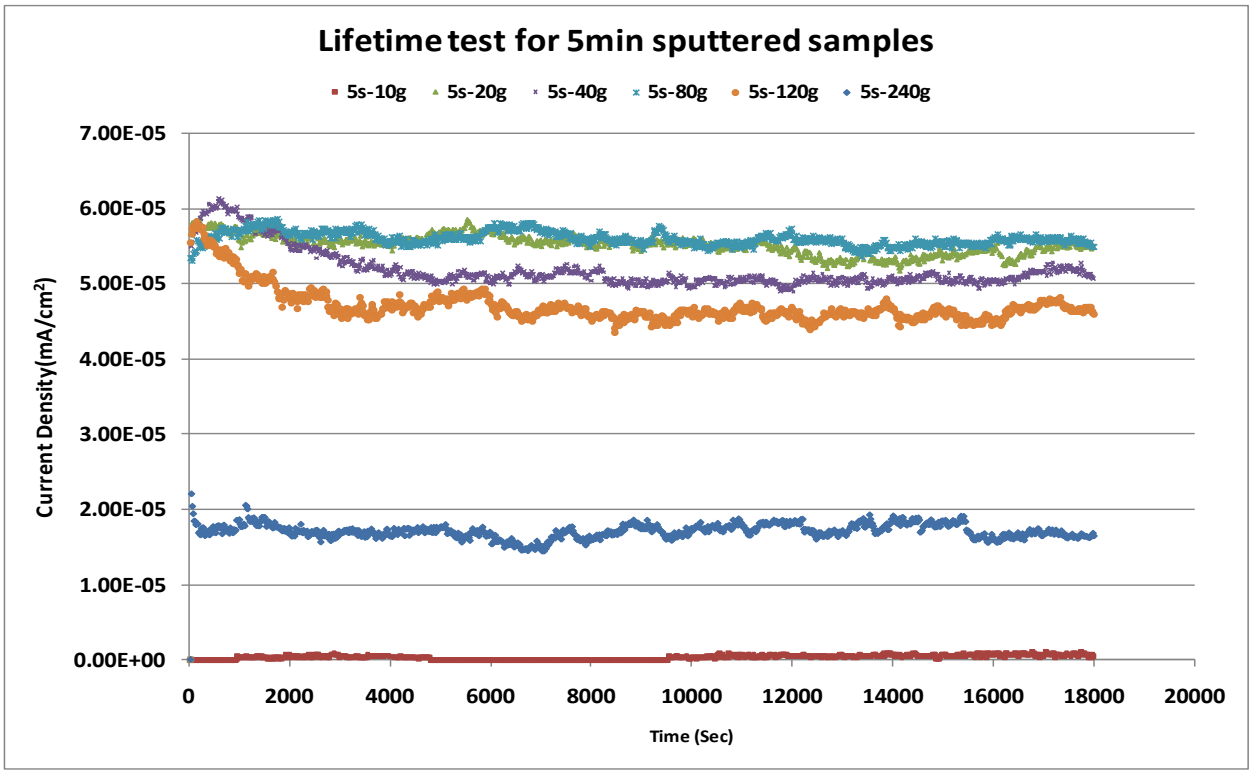

4.5.2 Lifetime Test at Constant Voltage for Samples with 10 min Sputtering

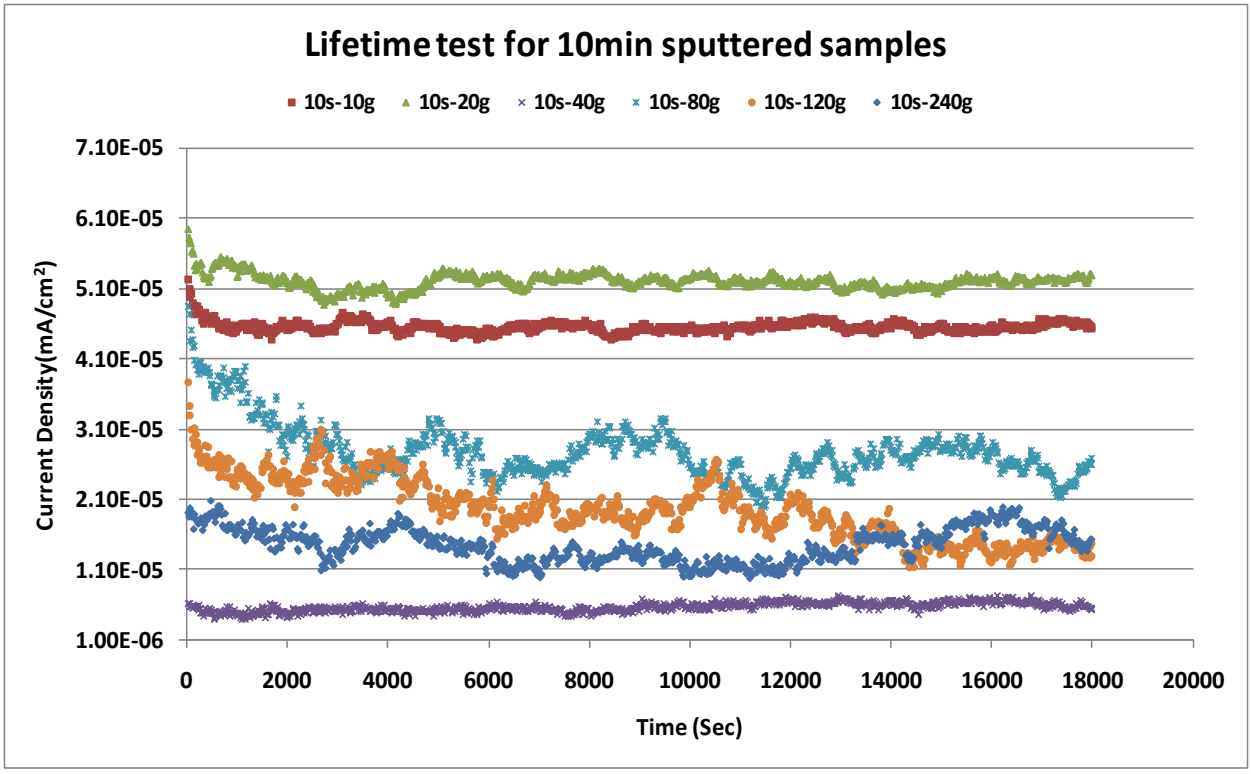

Figure 4.4: Lifetime test at constant voltage in vacuum for different growth time samples for (a) 5 min sputtering (b) 10 min sputtering.

4.6 Effect of Sputtering Time on the Field Emission

The amount of metal catalyst that is sputtered to grow CNTs has a clear impact on the fabrication of CNTs. The variation in the densities of impurities (Polyhedral) in CNTs is observed with the change in sputtering time of the sample. The impurity clusters observed in grown CNTs when the substrate was sputtered (with iron target) for 20 min or more. The carbon clusters probably could be the result of higher decomposition rate of hydrocarbons than that of CNTs growth rate [7]. In these experiments CNTs were grown with sputtering times 5 min and 10 min, and in both cases the CNTs were cluster free. The field emission curves in high vacuum were compared to see if there is any effect on the turn-on and current density with change in

sputtering time during its growth. The effect of sputtering time for both 5 min and 10 min is so minimal for all growth conditions. The turn-on for 10 min sputtering samples was little bit lower compared to 5 min sputtering samples in few cases, but taking all the conditions (such as the age of sample, the no. of runs performed before the particular runs) into consideration the effect is said to be very minimal and not substantial. The field emission curves compared with respect to sputtering times for all the growth times are presented.

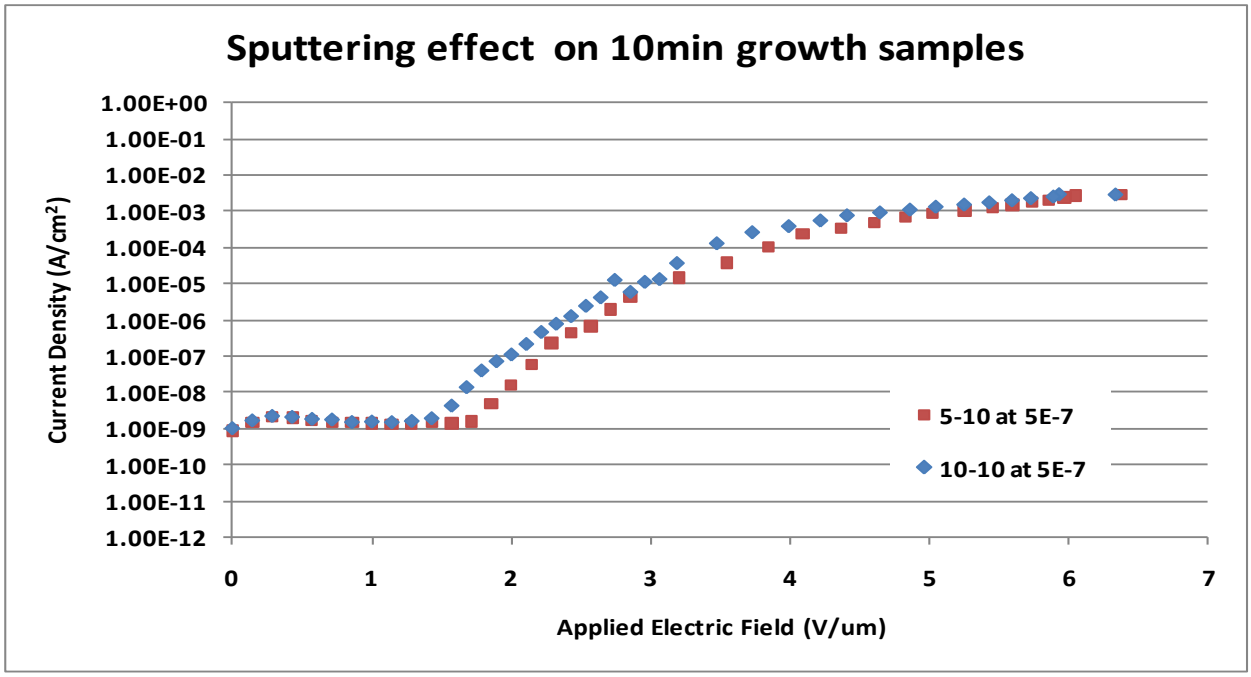

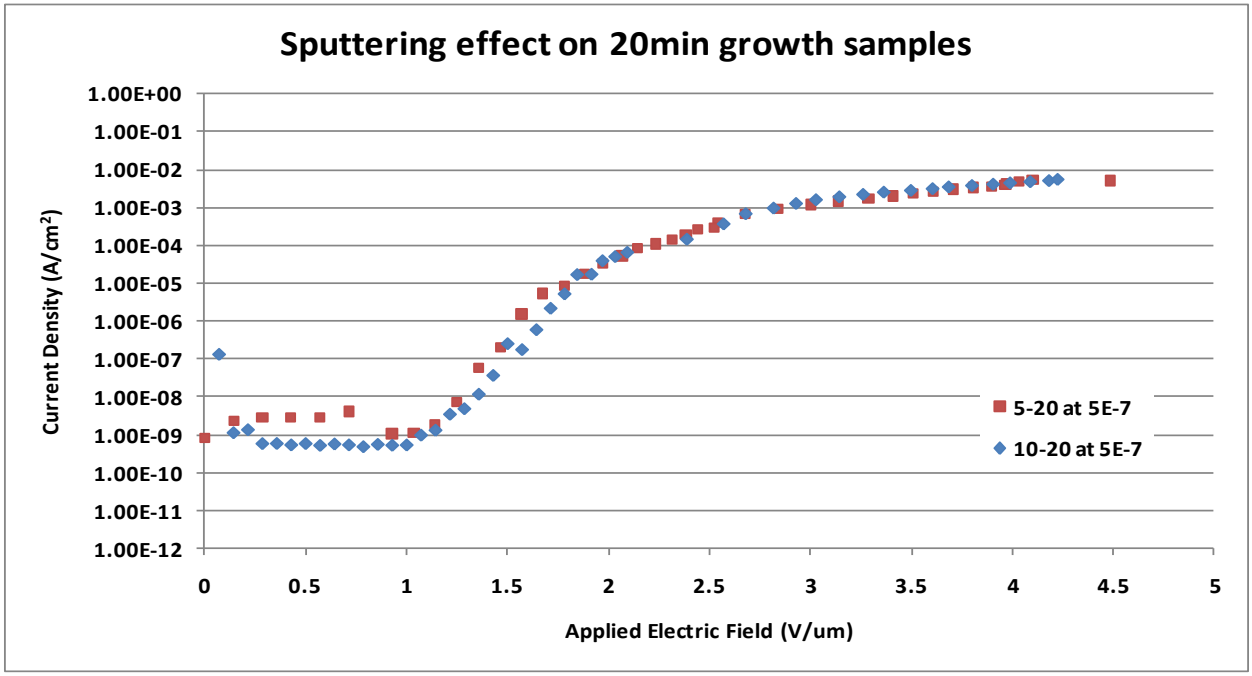
Sputtering effect on 20min growth samples
Current Density (A/cm²)
1.00E+00
1.00E-01
1.00E-02
1.00E-03
1.00E-04
1.00E-05
1.00E-06
1.00E-07
1.00E-08
1.00E-09
1.00E-10
1.00E-11
1.00E-12
0
0.5
1
1.5
2
2.5
3
3.5
4
4.5
5
Applied Electric Field (V/um)
5-20 at 5E-7
10-20 at 5E-7

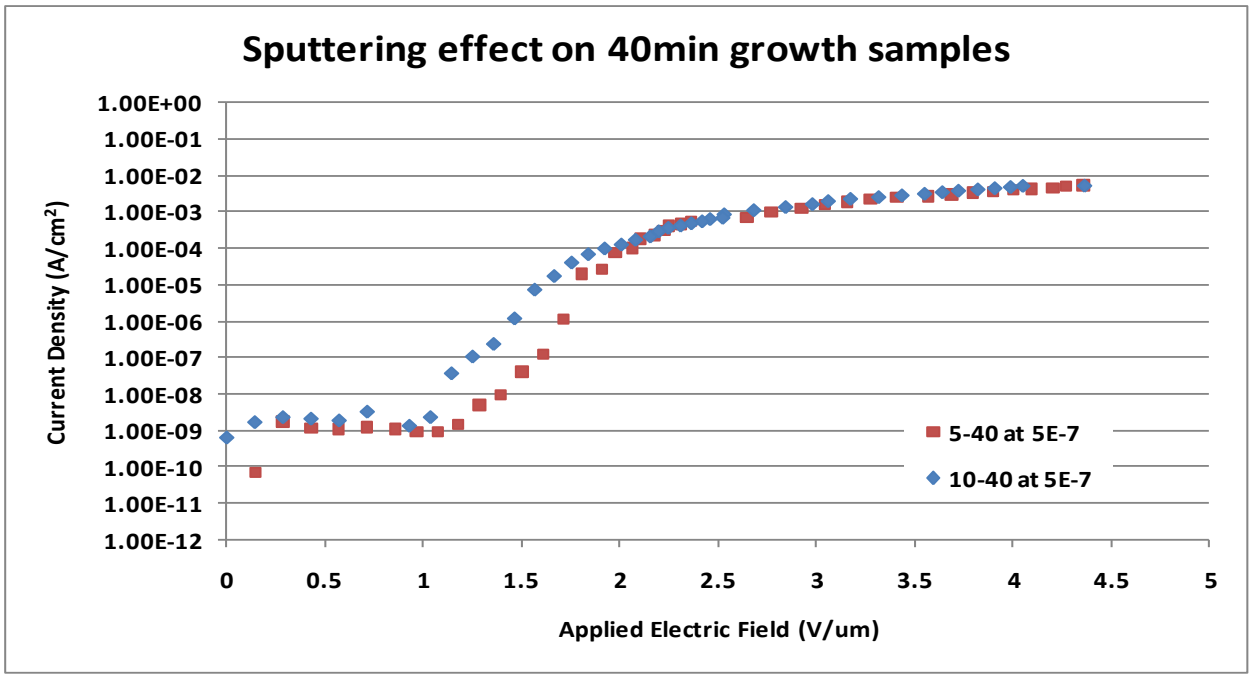
Sputtering effect on 40min growth samples
Current Density (A/cm²)
1.00E+00
1.00E-01
1.00E-02
1.00E-03
1.00E-04
1.00E-05
1.00E-06
1.00E-07
1.00E-08
1.00E-09
1.00E-10
1.00E-11
1.00E-12
0
0.5
1
1.5
2
2.5
3
3.5
4
4.5
5
Applied Electric Field (V/um)
5-40 at 5E-7
10-40 at 5E-7

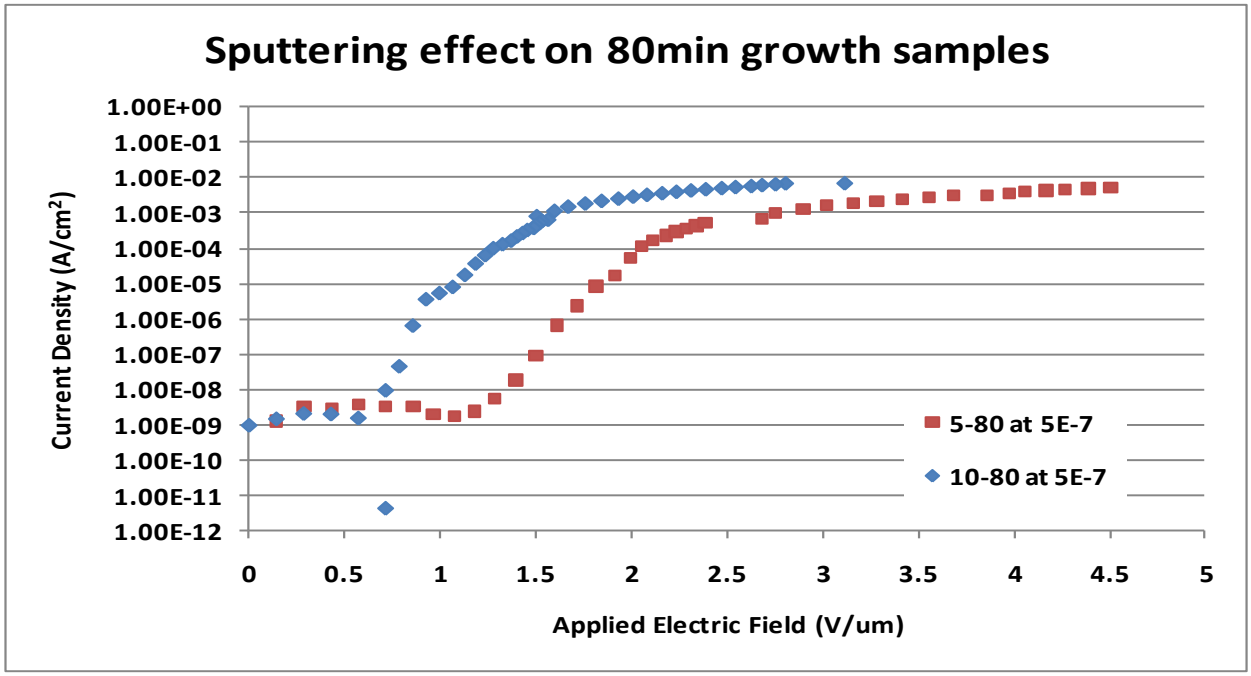
Sputtering effect on 80min growth samples
Current Density (A/cm²)
1.00E+00
1.00E-01
1.00E-02
1.00E-03
1.00E-04
1.00E-05
1.00E-06
1.00E-07
1.00E-08
1.00E-09
1.00E-10
1.00E-11
1.00E-12
0
0.5
1
1.5
2
2.5
3
3.5
4
4.5
5
Applied Electric Field (V/um)
5-80 at 5E-7
10-80 at 5E-7

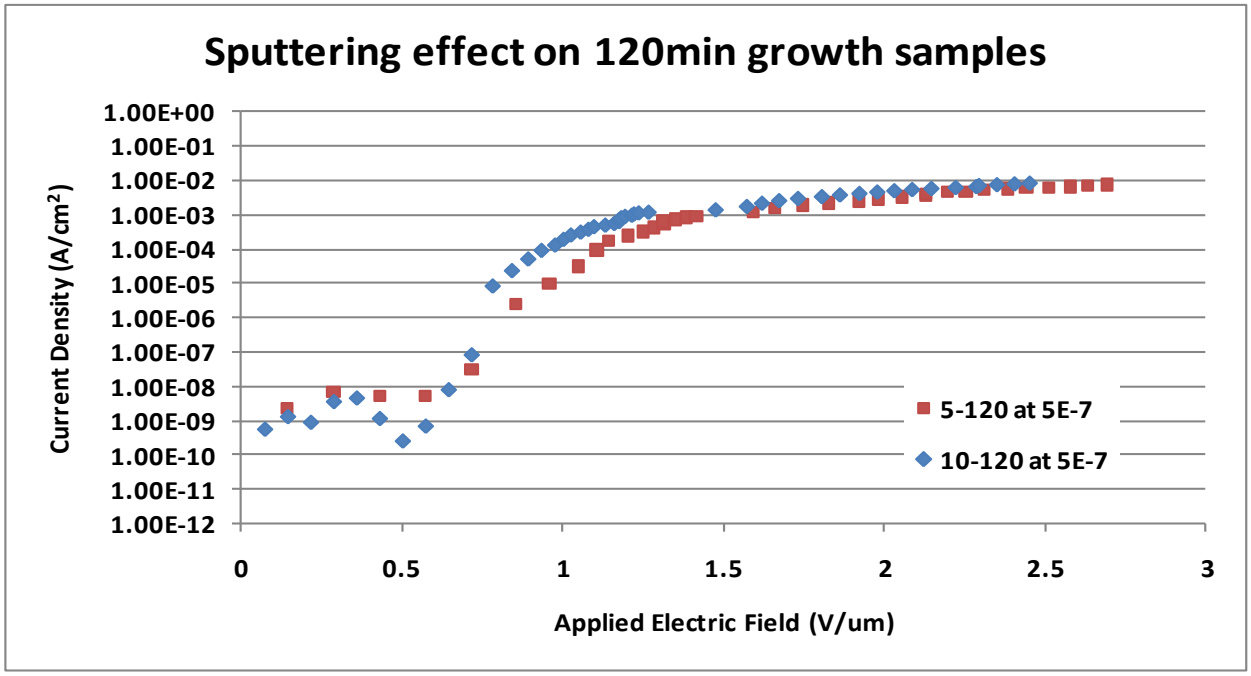
Sputtering effect on 120min growth samples
Current Density (A/cm²)
1.00E+00
1.00E-01
1.00E-02
1.00E-03
1.00E-04
1.00E-05
1.00E-06
1.00E-07
1.00E-08
1.00E-09
1.00E-10
1.00E-11
1.00E-12
0
0.5
1
1.5
2
2.5
3
Applied Electric Field (V/um)
5-120 at 5E-7
10-120 at 5E-7

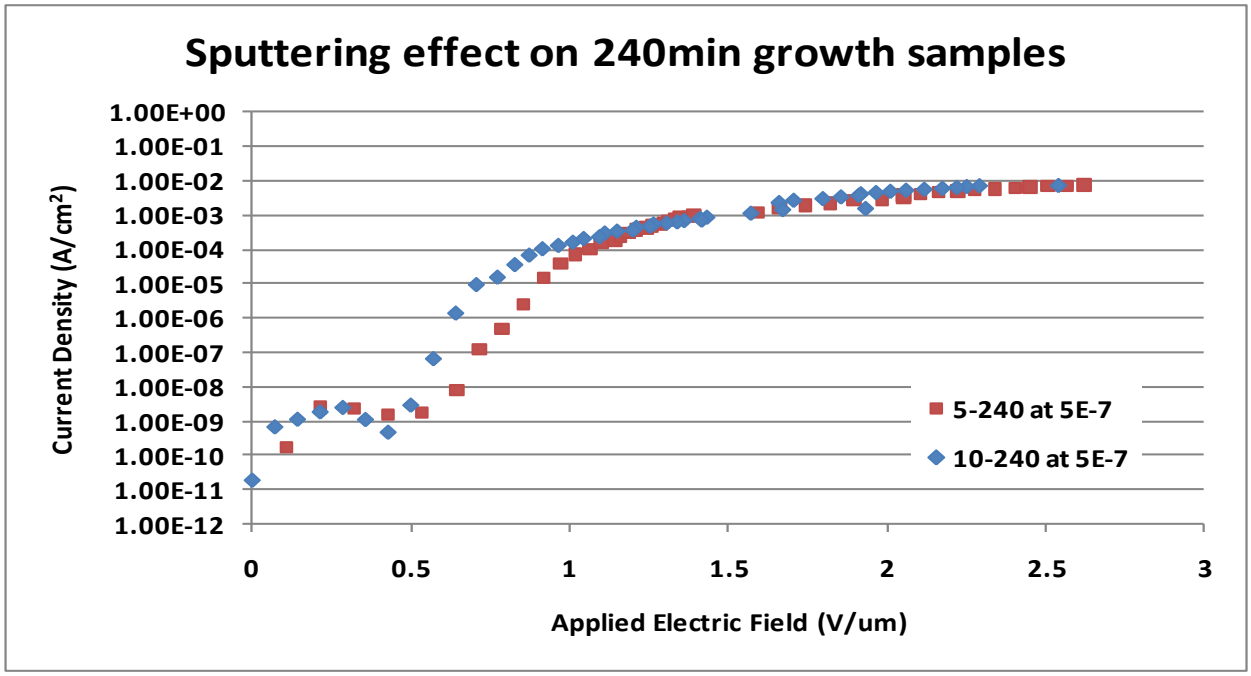

Figure 4.5: Field emission comparison with respect to sputtering times for samples with different growth time.

4.7 Lifetime Test with 100 runs at 20 mTorr

A variety of nano-structured materials have been considered for the efficient field emitters in many applications such as field emission displays (FEDs) and for triggering mechanisms such as pseudospark switches. However the field emission for CNTs exhibits a permanent decrease in the current density and an increase in the turn-on electric field. This degradation greatly impacts the CNTs application in FED and other applications under poor vacuum or low pressure gas filled environments. Therefore, besides best field emission properties in vacuum, thermal stability, ambient insensitivity, and less degradation over time is also important for choosing them as a material for cold cathode applications.

For a cold cathode emitter to be used in applications like pseudospark switch, it is important that the CNT cathode sustain its characteristics, turn-on electric field and saturation current density as constant for over a period of time to sustain the characteristics of the switch. So in

order to test the current stability and lifetime in poor vacuum conditions, the lifetime tests were also performed for all the samples in poor vacuum conditions at 20 m Torr by continuously applying the voltage from 0-1200 V in many runs with variable step voltage on the same sample to see how turn-on electric field and current density curves behaves in long run. Each sample's field emission characteristics were recorded for 100 runs to observe any decay or degradation. Each run took approximately 20 to 25 hours to complete. When the field emission experiments were carried out in dry air, the surface of the anode was completely oxidized. This is because of constant hitting of oxygen in dry air gas with anode during the field emission with application of high voltage. This was not observed when the field emission experiments were carried out in He and, in high vacuum conditions.

From the field emission curves we can see that there is definite degradation in both turn-on electric field and current density for all the samples with the increase in number of runs. It can be observed that data is scattered in current density curves; this could be because of the high pressure conditions where background gas molecules always interact with the electrons that are emitted from the nanotubes.

4.7.1 Samples with 5 min Sputtering

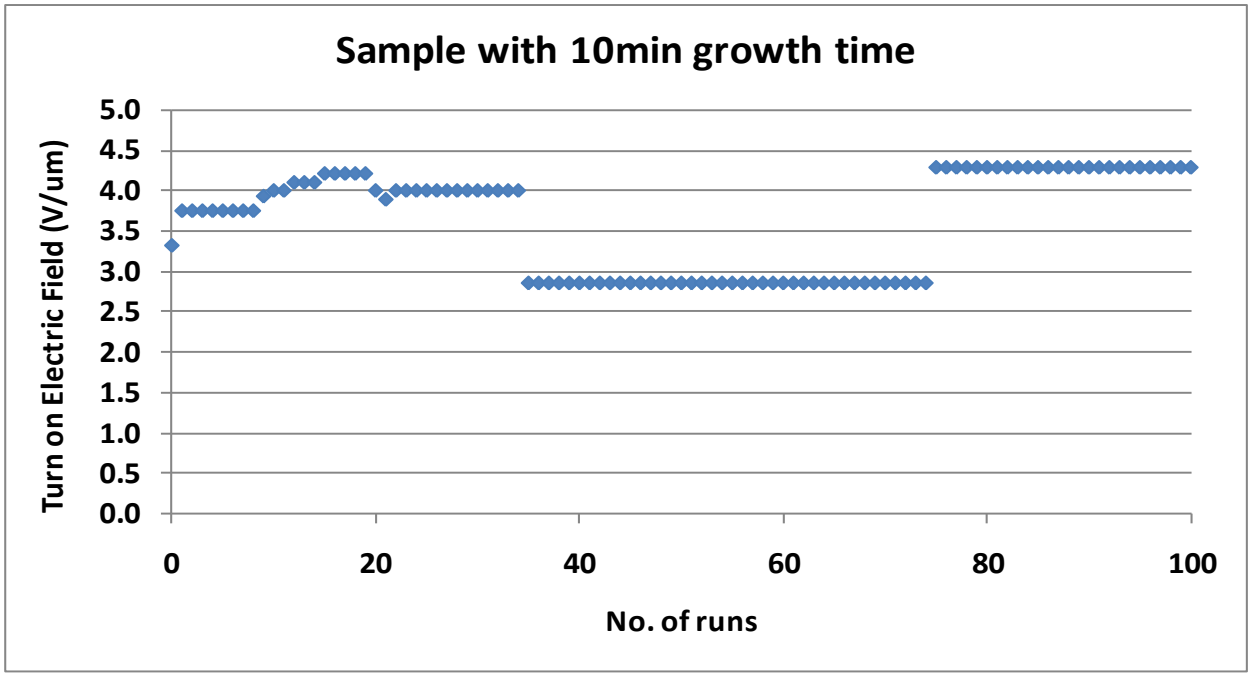

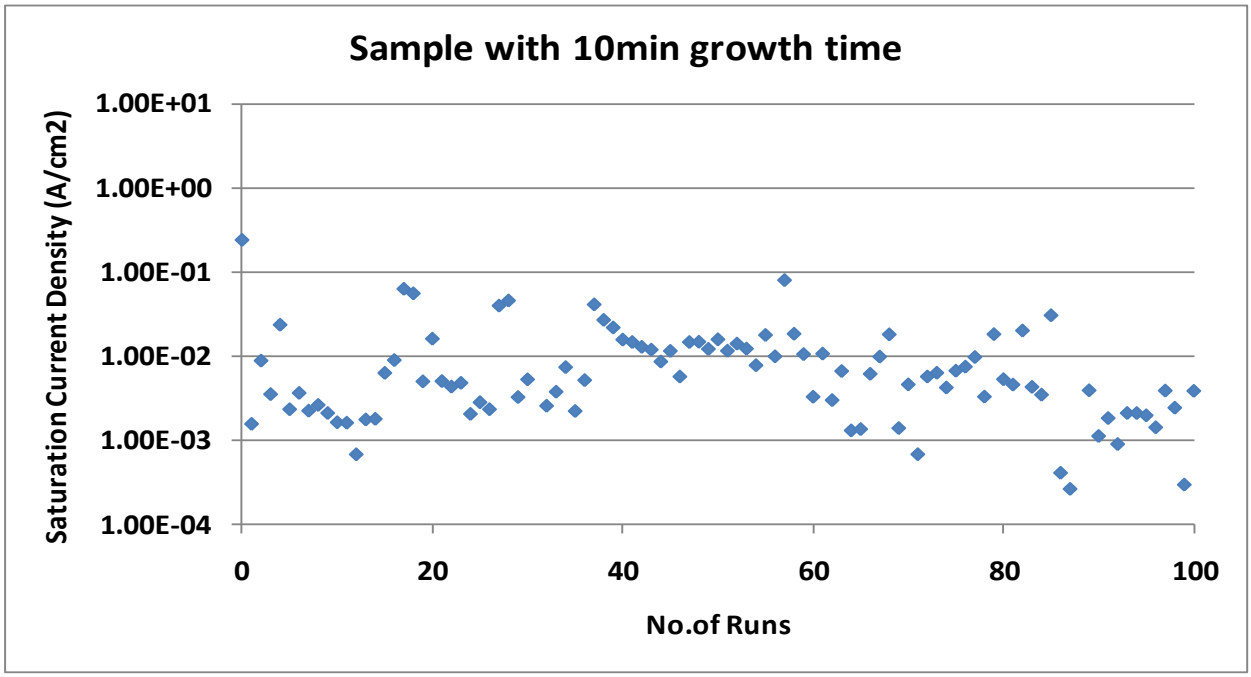

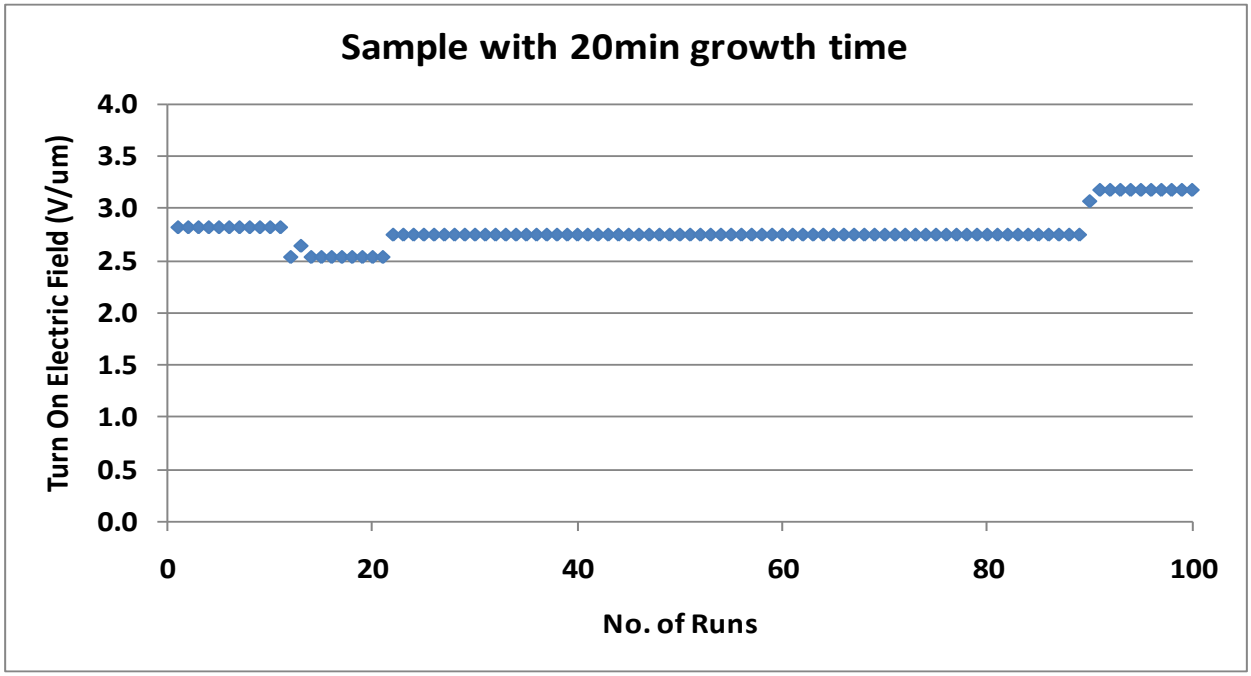
Sample with 20min growth time
Turn On Electric Field (V/um)
4.0
3.5
3.0
2.5
2.0
1.5
1.0
0.5
0.0
0
20
40
60
80
100
No. of Runs

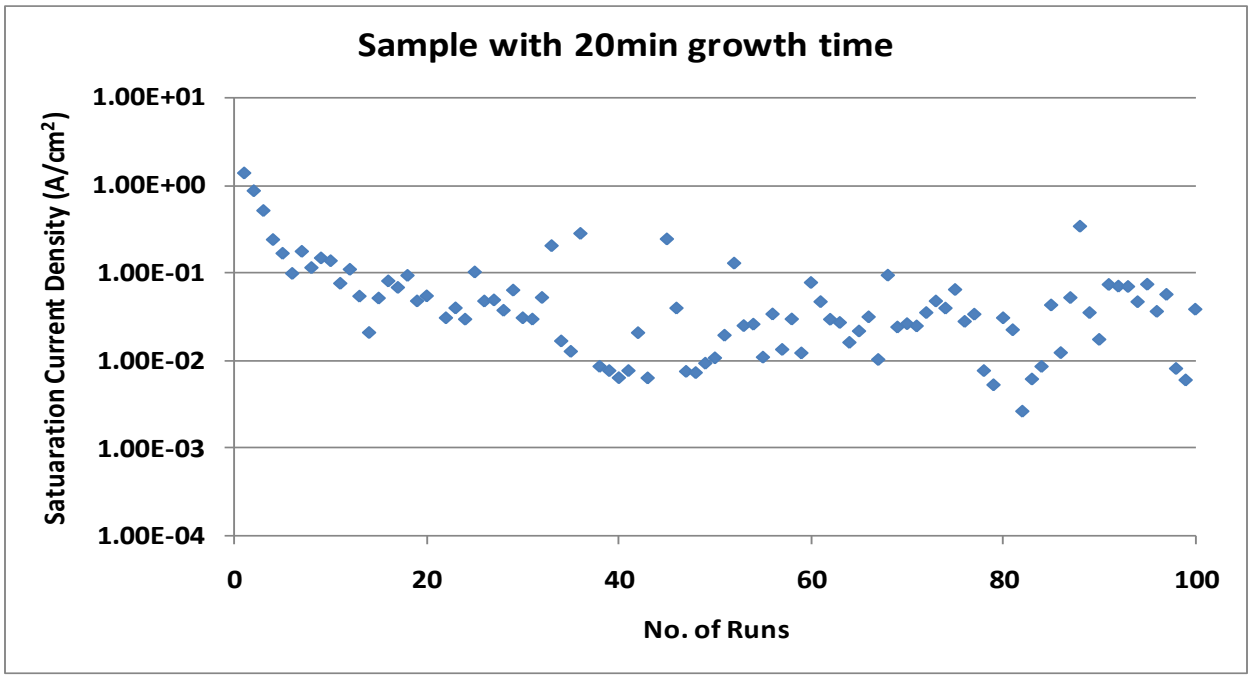
Sample with 20min growth time
Satuaration Current Density (A/cm²)
1.00E+01
1.00E+00
1.00E-01
1.00E-02
1.00E-03
1.00E-04
0
20
40
60
80
100
No. of Runs

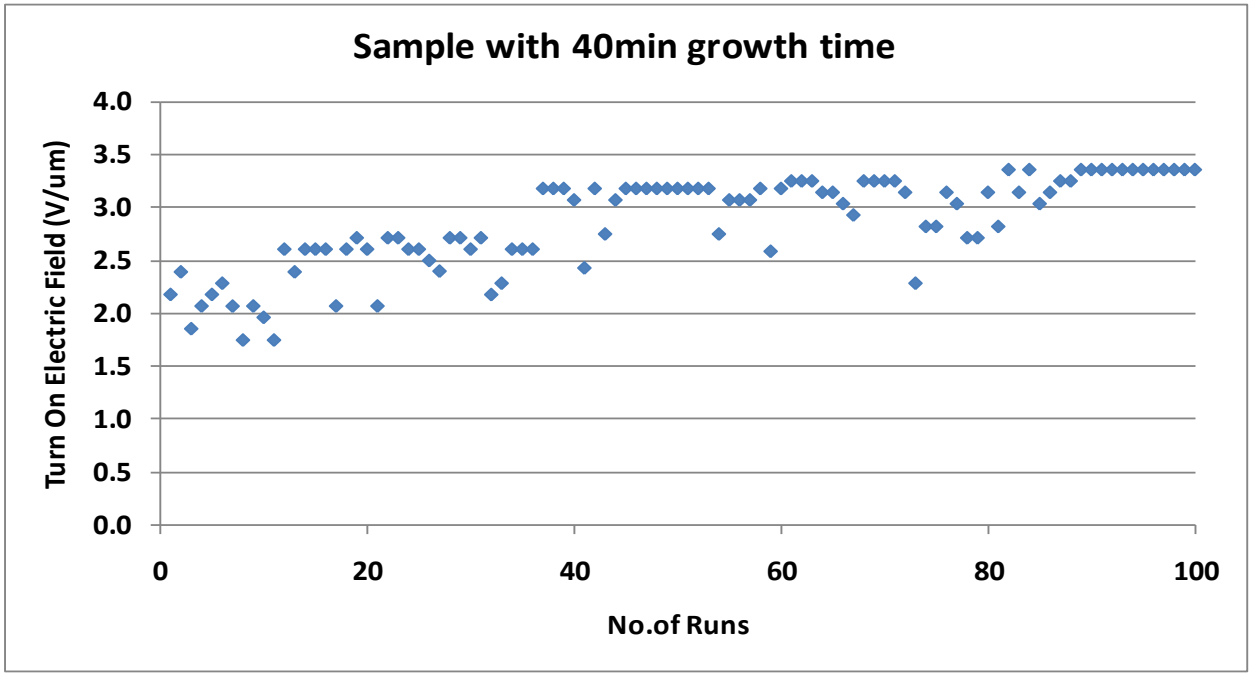
Sample with 40min growth time
Turn On Electric Field (V/um)
4.0
3.5
3.0
2.5
2.0
1.5
1.0
0.5
0.0
0
20
40
60
80
100
No.of Runs

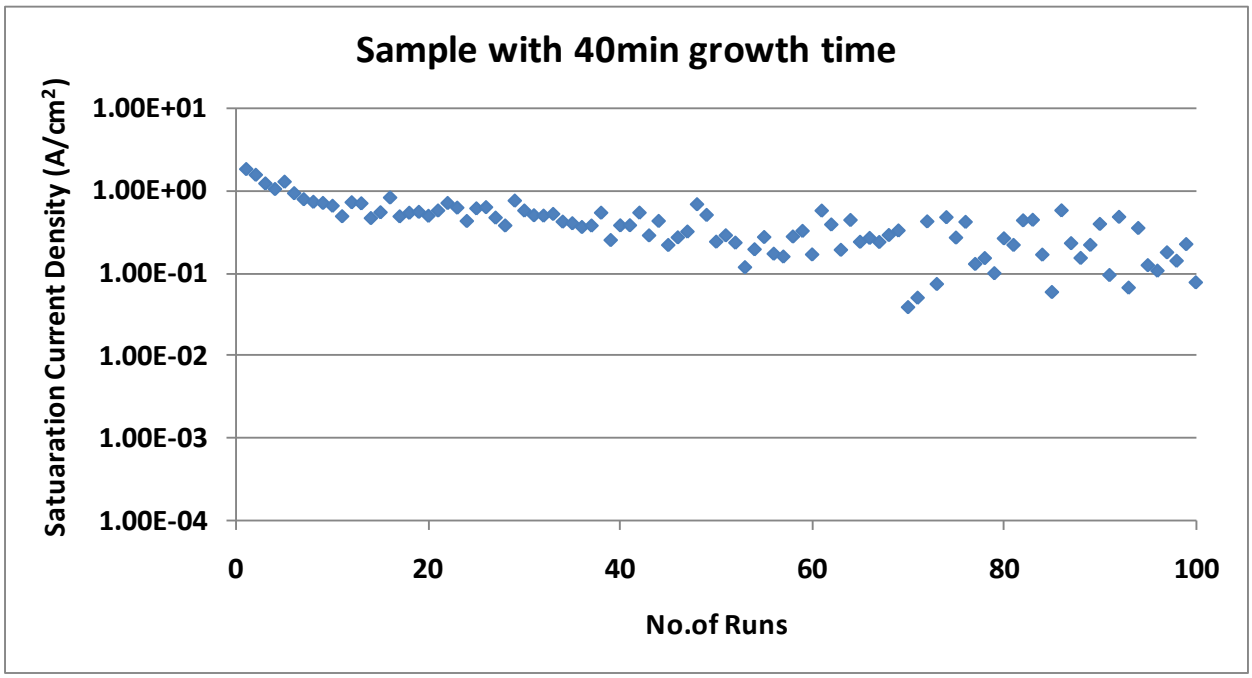
Sample with 40min growth time
Satuaration Current Density (A/cm²)
1.00E+01
1.00E+00
1.00E-01
1.00E-02
1.00E-03
1.00E-04
0
20
40
60
80
100
No.of Runs

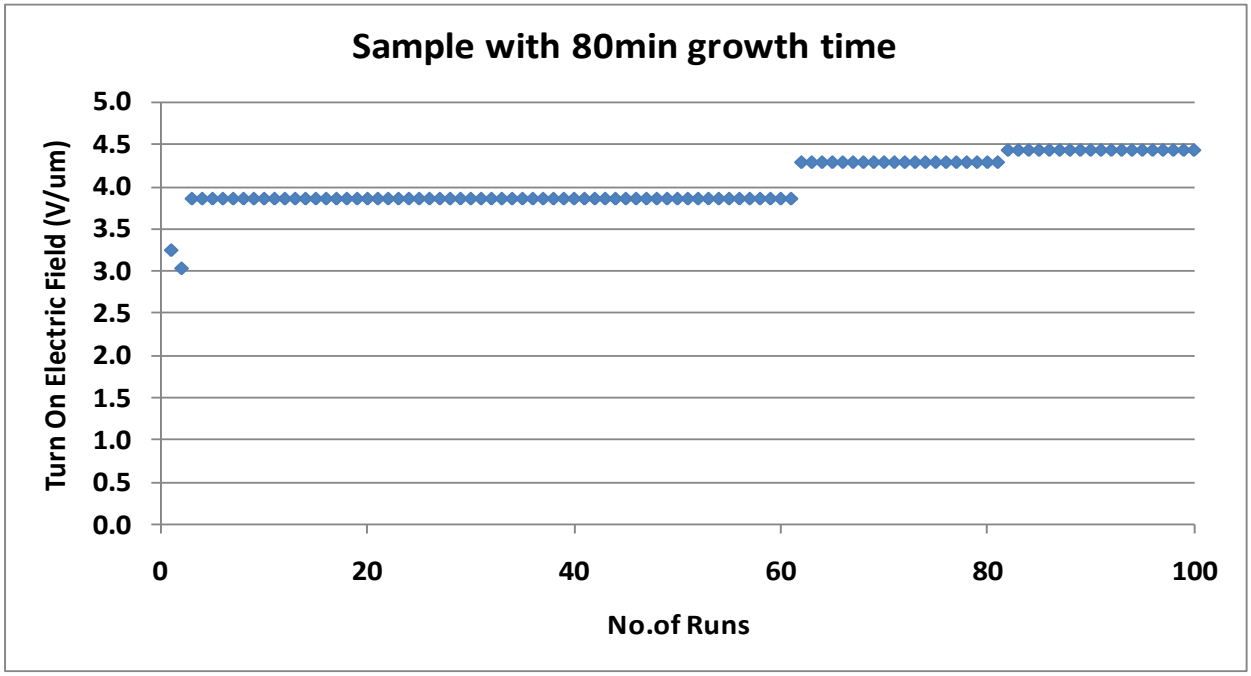
Sample with 80min growth time
Turn On Electric Field (V/um)
5.0
4.5
4.0
3.5
3.0
2.5
2.0
1.5
1.0
0.5
0.0
0
20
40
60
80
100
No.of Runs

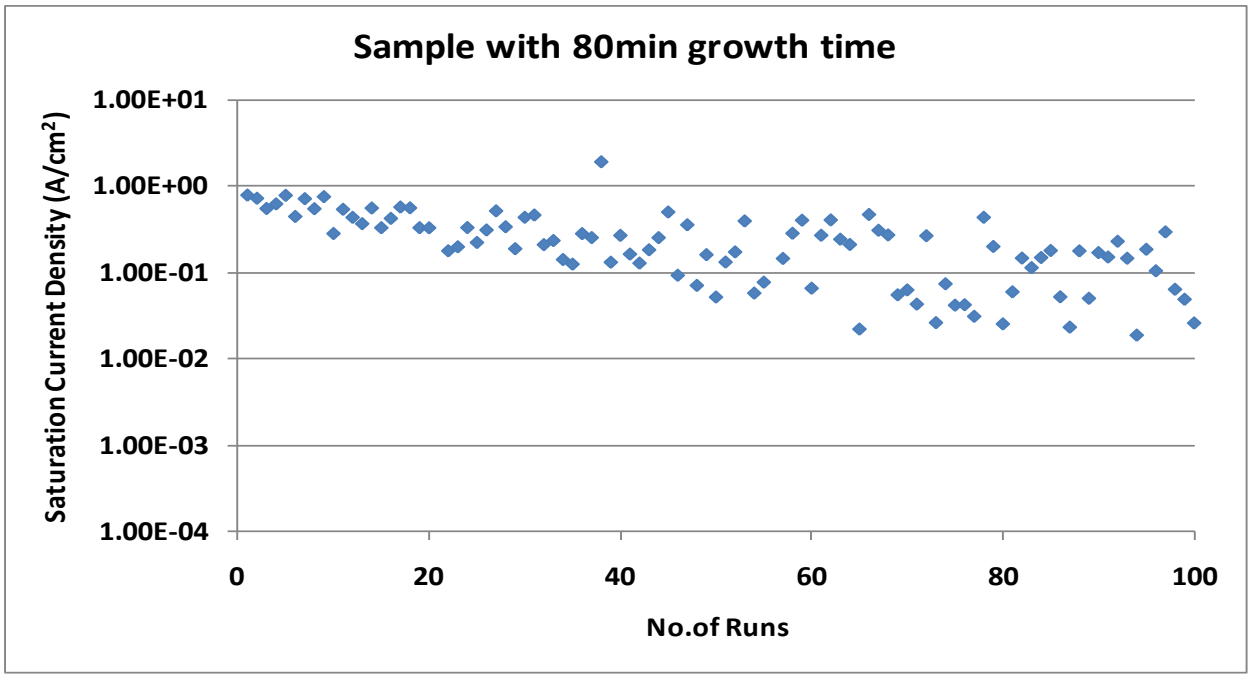
Sample with 80min growth time
Saturation Current Density (A/cm²)
1.00E+01
1.00E+00
1.00E-01
1.00E-02
1.00E-03
1.00E-04
0
20
40
60
80
100
No.of Runs

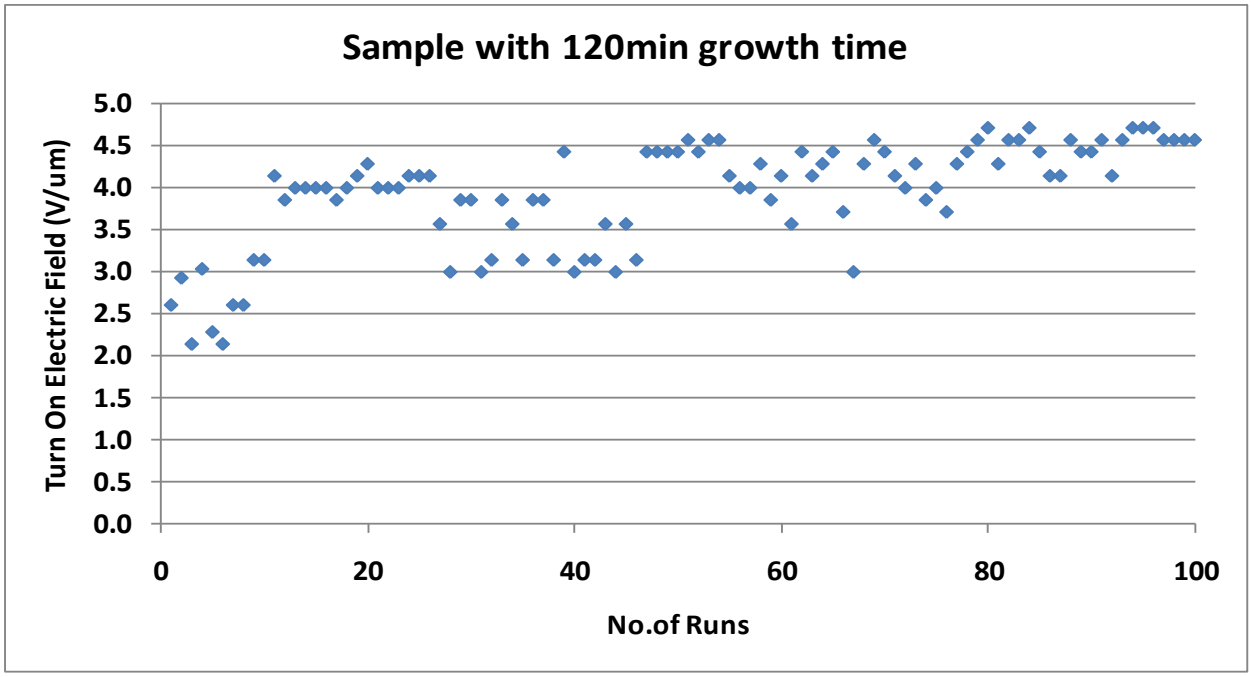
Sample with 120min growth time
Turn On Electric Field (V/um)
5.0
4.5
4.0
3.5
3.0
2.5
2.0
1.5
1.0
0.5
0.0
0
20
40
60
80
100
No.of Runs

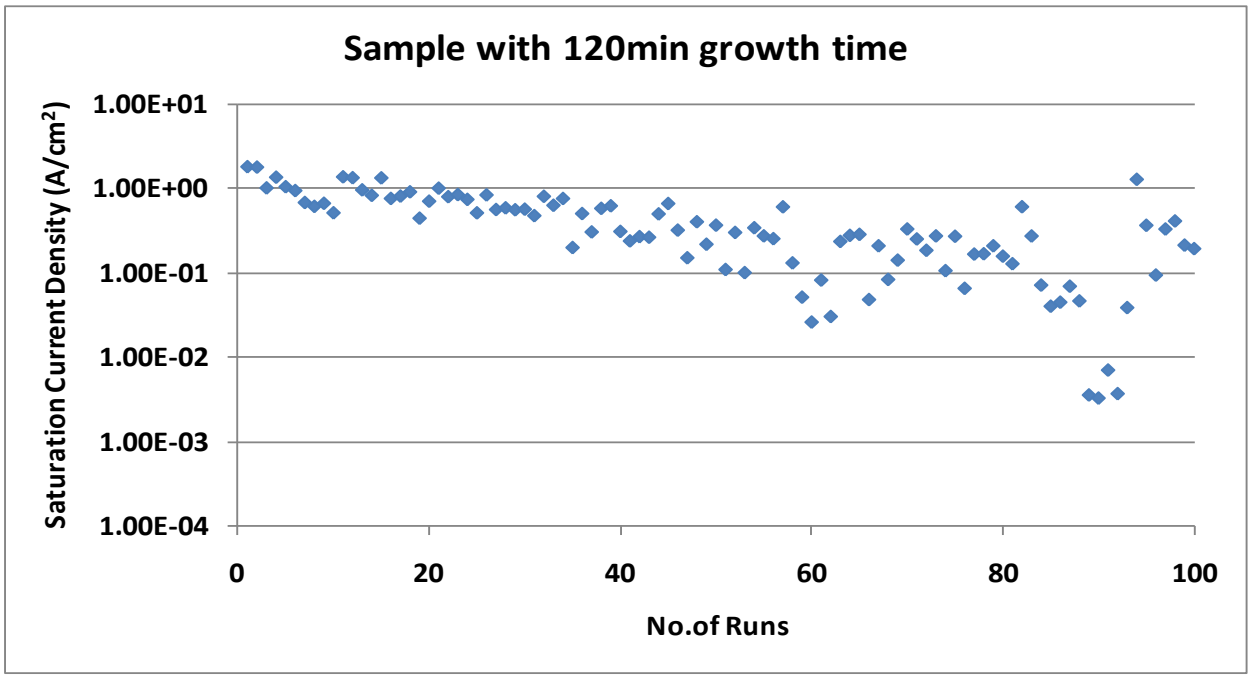
Sample with 120min growth time
Saturation Current Density (A/cm²)
1.00E+01
1.00E+00
1.00E-01
1.00E-02
1.00E-03
1.00E-04
0
20
40
60
80
100
No.of Runs

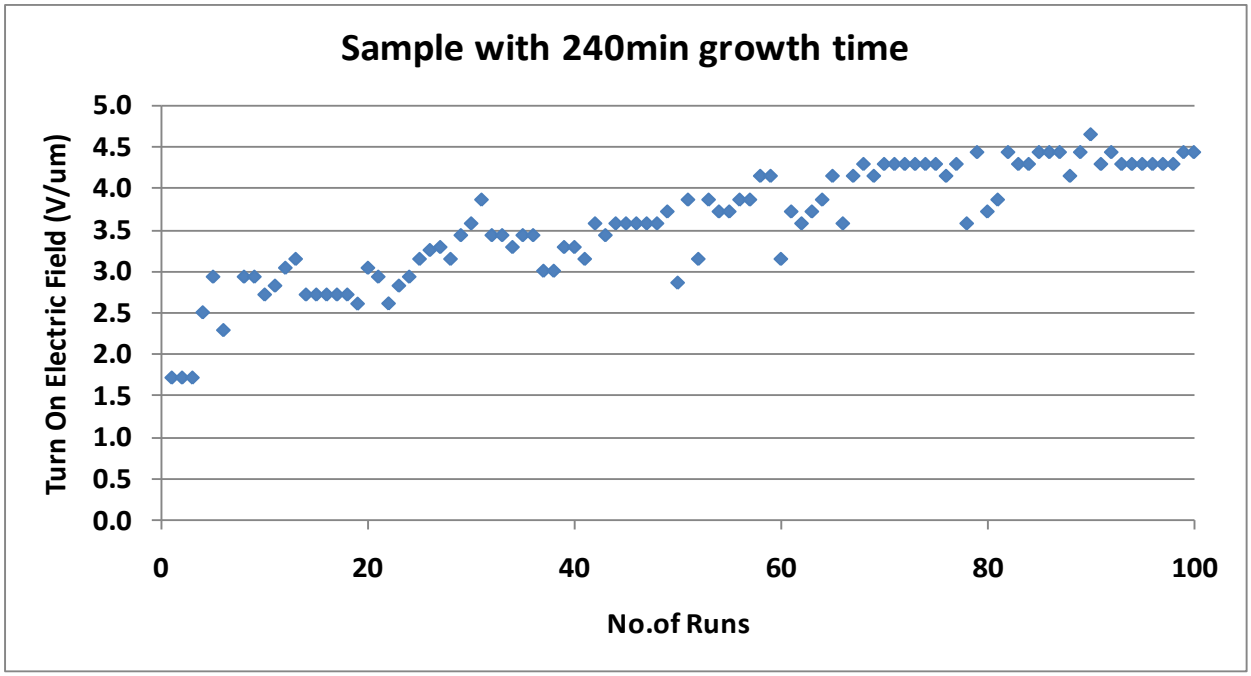
Sample with 240min growth time
Turn On Electric Field (V/um)
5.0
4.5
4.0
3.5
3.0
2.5
2.0
1.5
1.0
0.5
0.0
0
20
40
60
80
100
No.of Runs

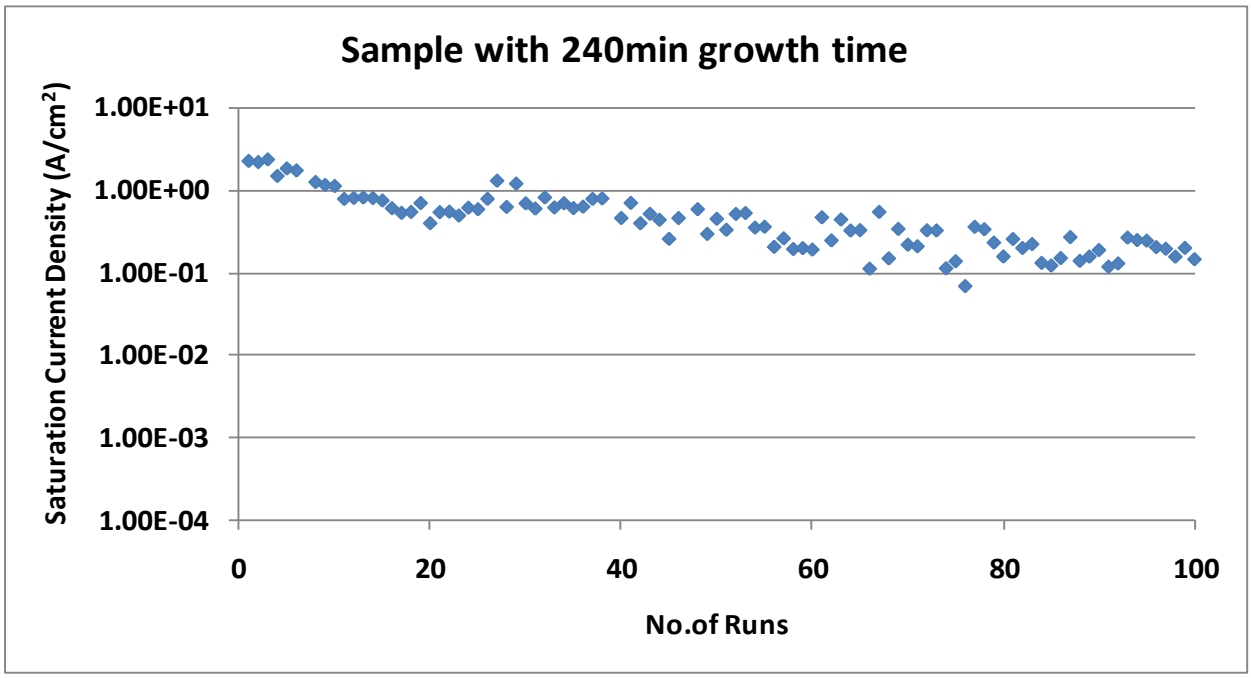
Sample with 240min growth time
Saturation Current Density (A/cm2)
1.00E+01
1.00E+00
1.00E-01
1.00E-02
1.00E-03
1.00E-04
0
20
40
60
80
100
No.of Runs

4.7.2 Samples with 10 min Sputtering

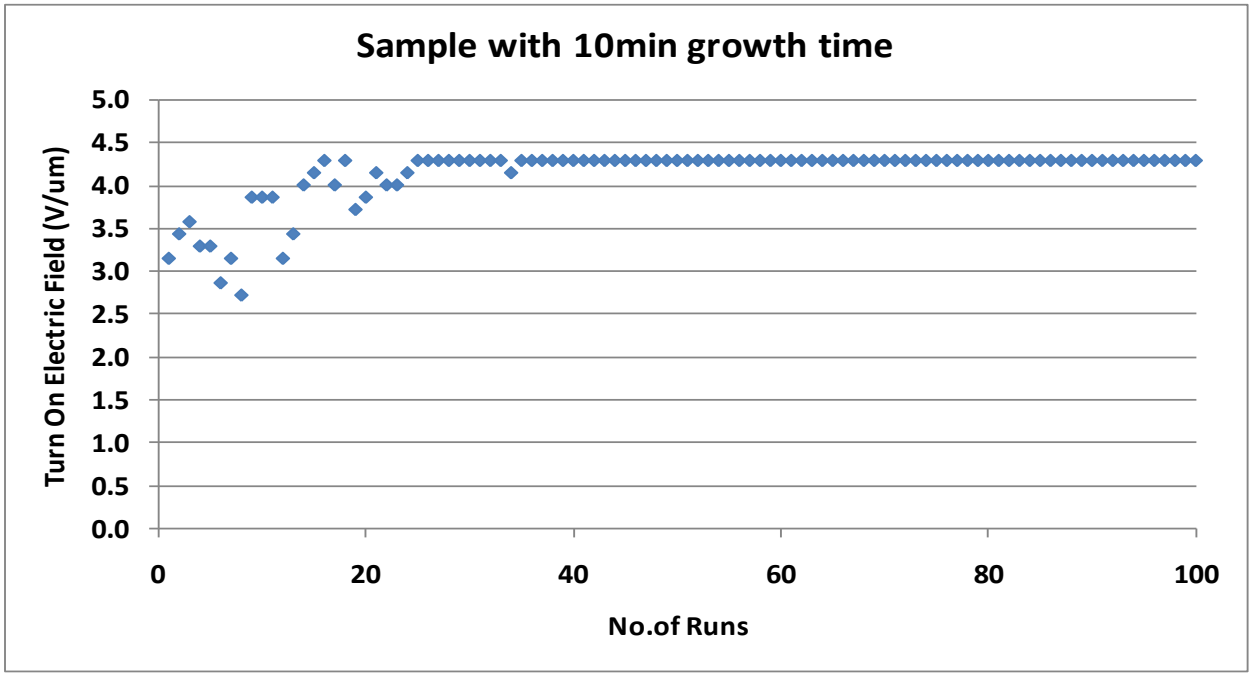

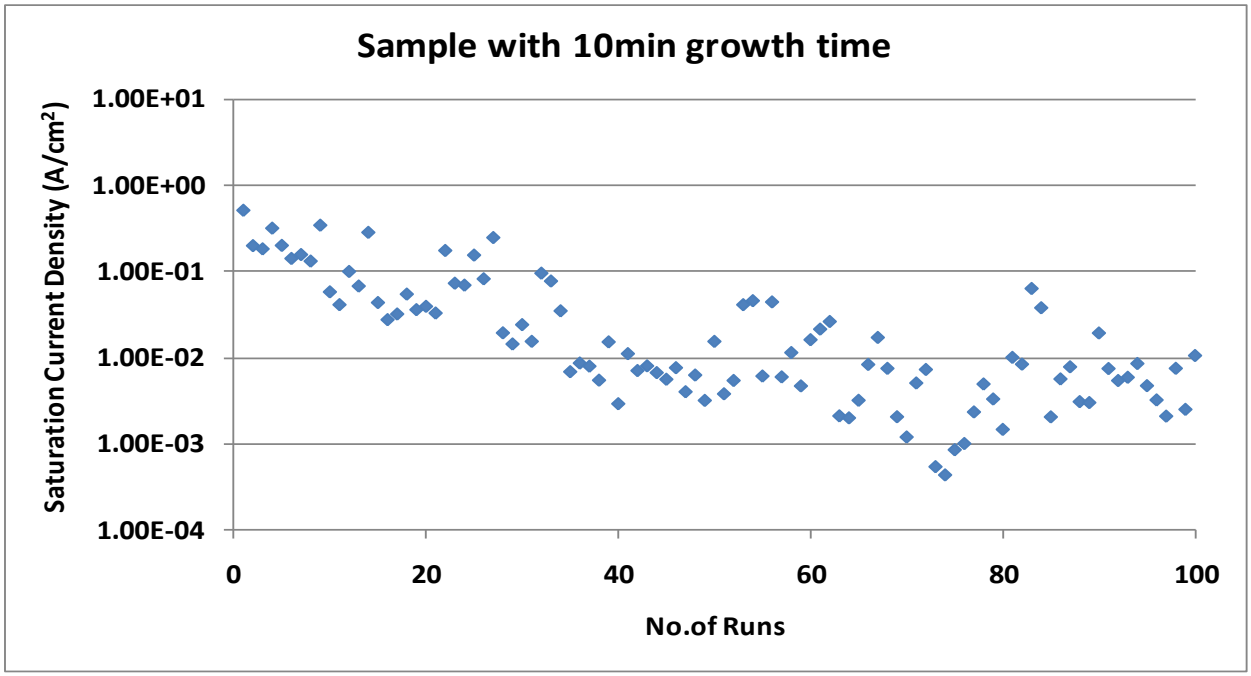

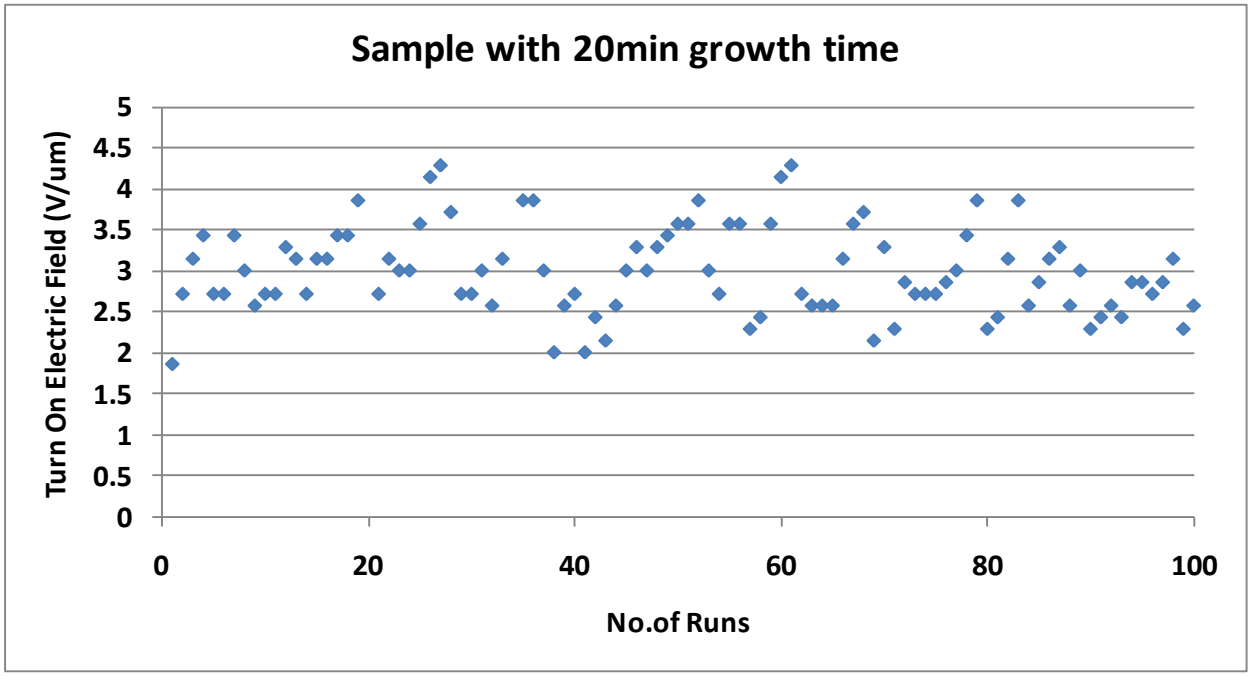
Sample with 20min growth time
Turn On Electric Field (V/um)
5
4.5
4
3.5
3
2.5
2
1.5
1
0.5
0
0
20
40
60
80
100
No.of Runs

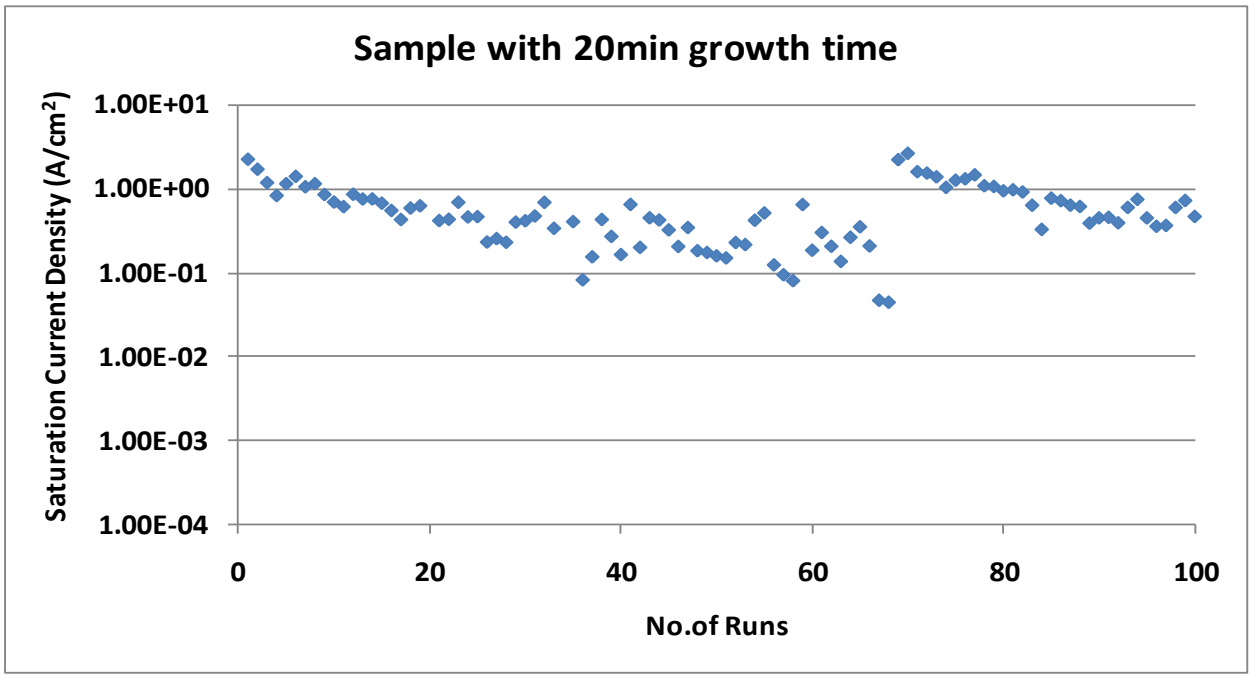
Sample with 20min growth time
Saturation Current Density (A/cm²)
1.00E+01
1.00E+00
1.00E-01
1.00E-02
1.00E-03
1.00E-04
0
20
40
60
80
100
No.of Runs

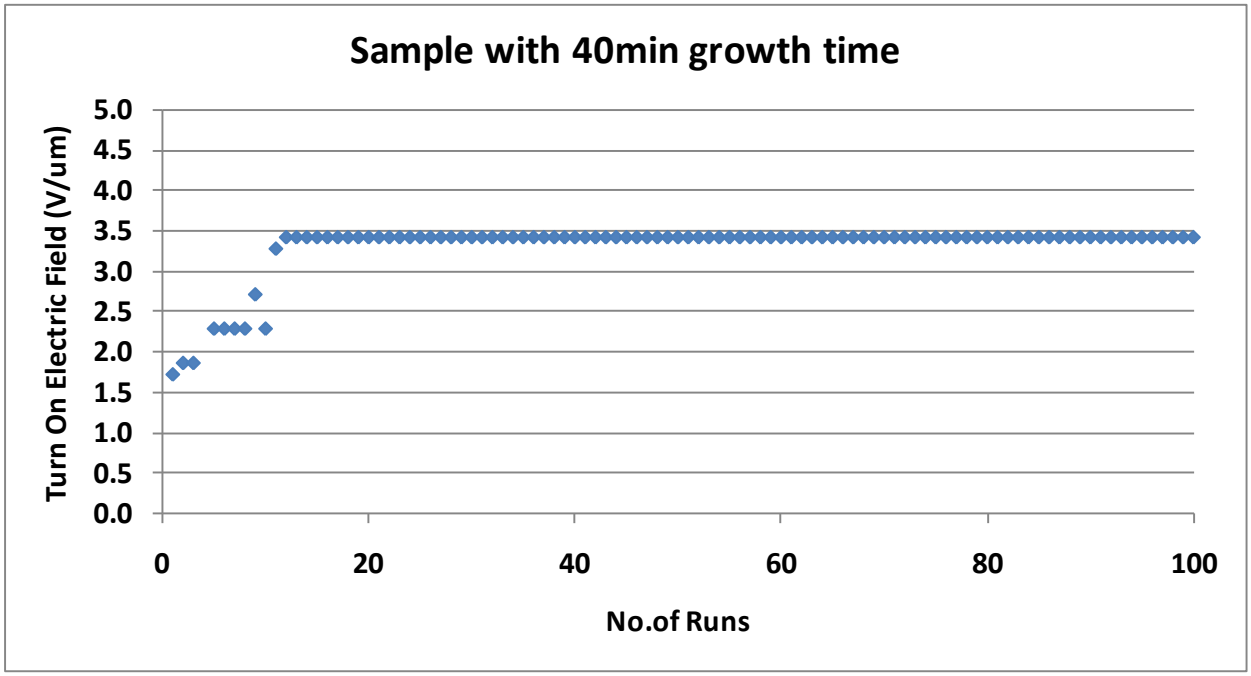
Sample with 40min growth time
Turn On Electric Field (V/um)
5.0
4.5
4.0
3.5
3.0
2.5
2.0
1.5
1.0
0.5
0.0
0
20
40
60
80
100
No.of Runs

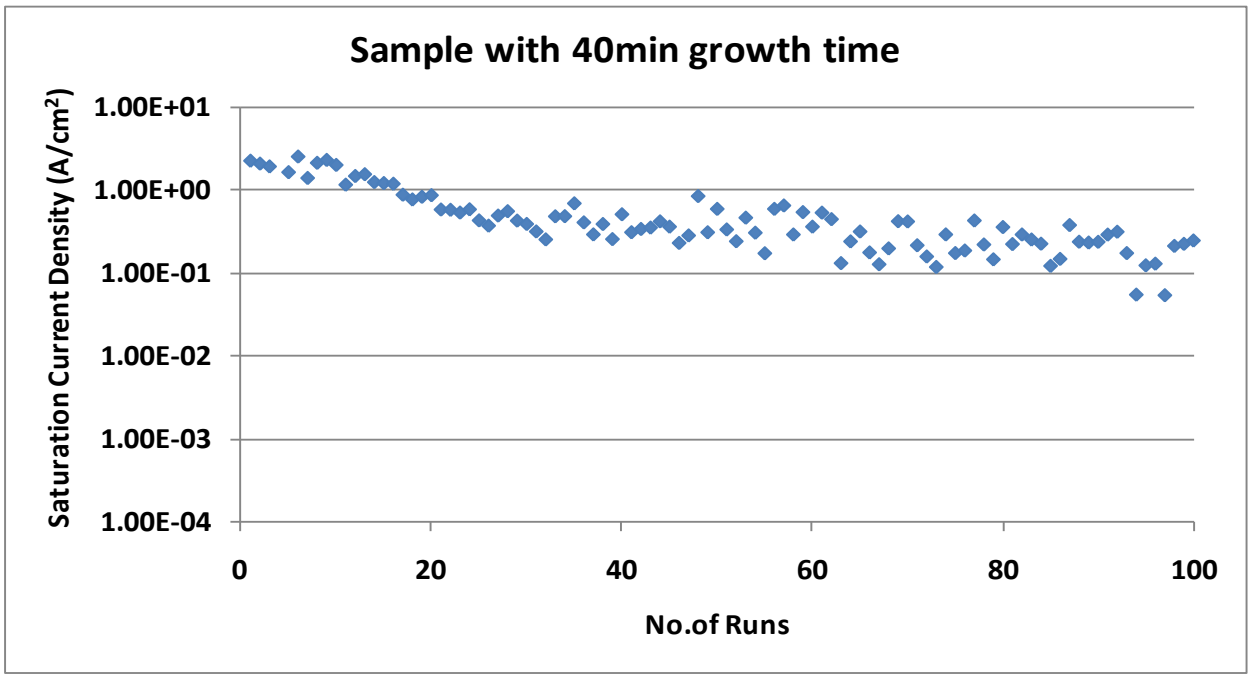
Sample with 40min growth time
Saturation Current Density (A/cm²)
1.00E+01
1.00E+00
1.00E-01
1.00E-02
1.00E-03
1.00E-04
0
20
40
60
80
100
No.of Runs

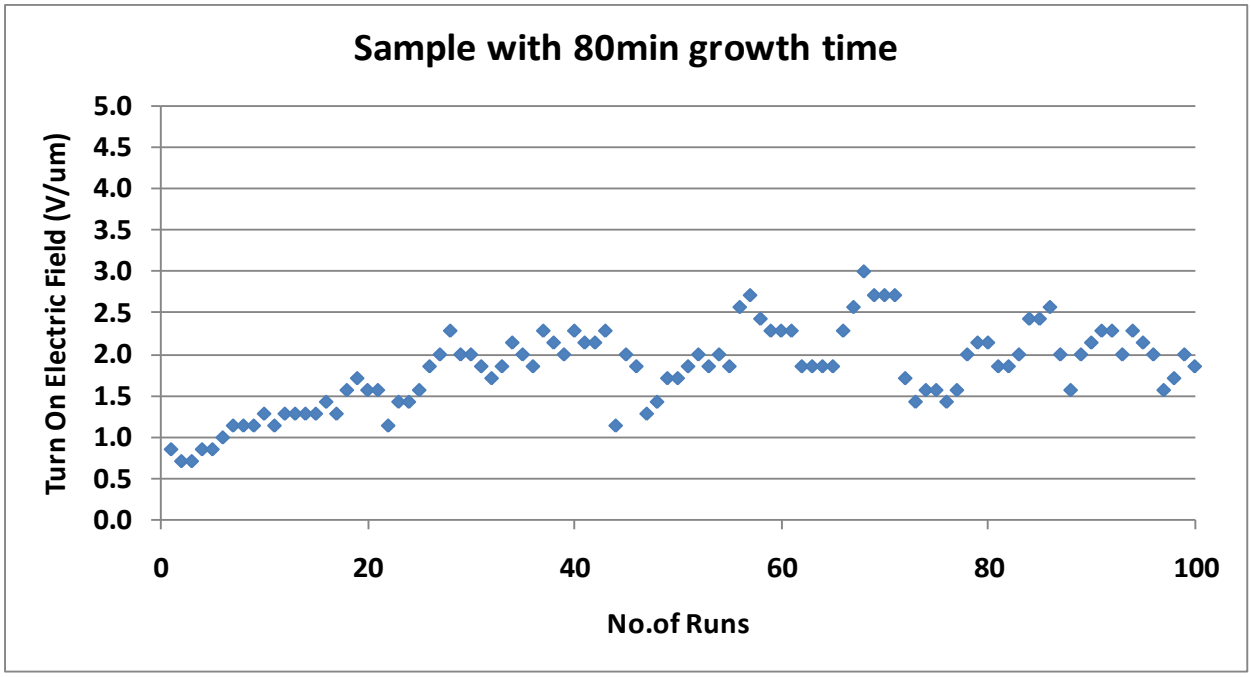
Sample with 80min growth time
Turn On Electric Field (V/um)
5.0
4.5
4.0
3.5
3.0
2.5
2.0
1.5
1.0
0.5
0.0
0
20
40
60
80
100
No.of Runs

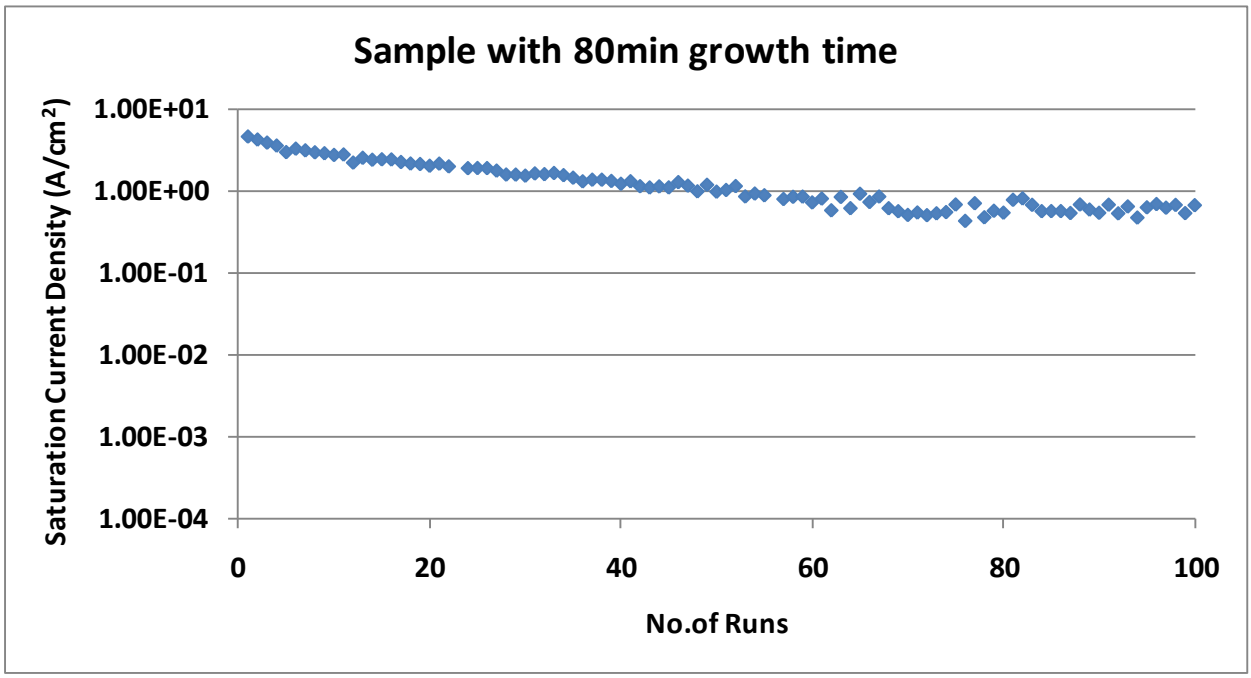
Sample with 80min growth time
Saturation Current Density (A/cm²)
1.00E+01
1.00E+00
1.00E-01
1.00E-02
1.00E-03
1.00E-04
0
20
40
60
80
100
No.of Runs

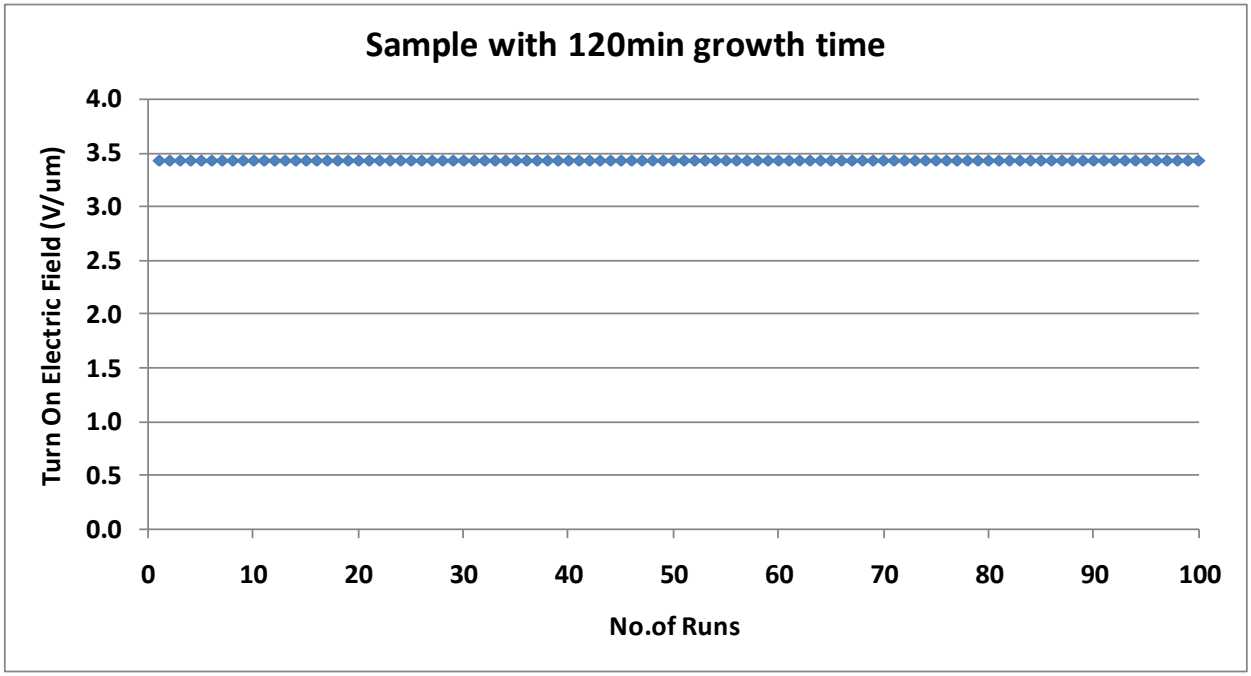
Sample with 120min growth time
Turn On Electric Field (V/um)
4.0
3.5
3.0
2.5
2.0
1.5
1.0
0.5
0.0
0
10
20
30
40
50
60
70
80
90
100
No.of Runs

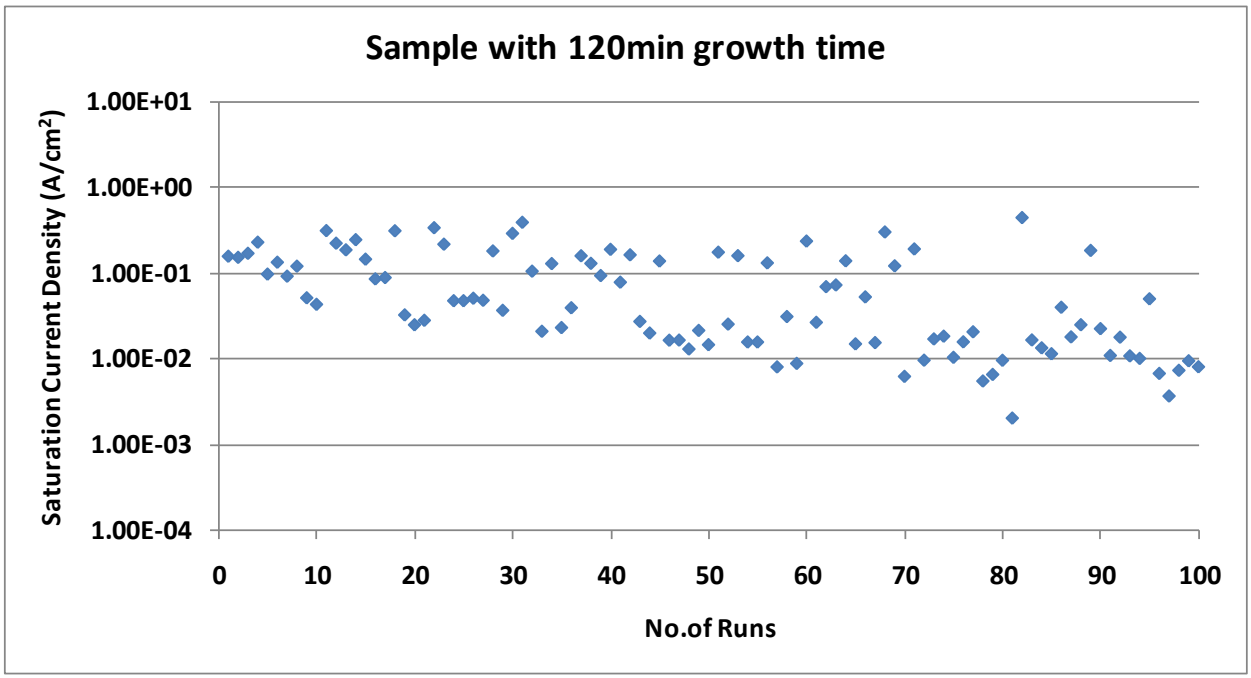
Sample with 120min growth time
Saturation Current Density (A/cm²)
1.00E+01
1.00E+00
1.00E-01
1.00E-02
1.00E-03
1.00E-04
0
10
20
30
40
50
60
70
80
90
100
No.of Runs

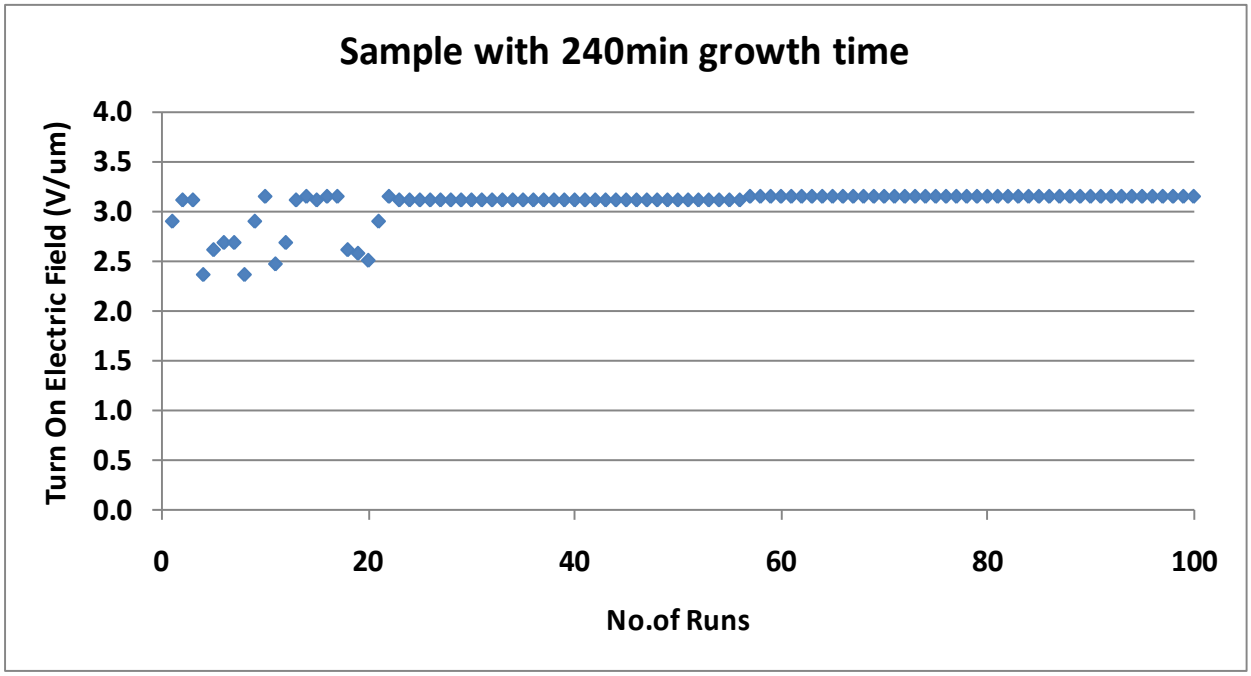

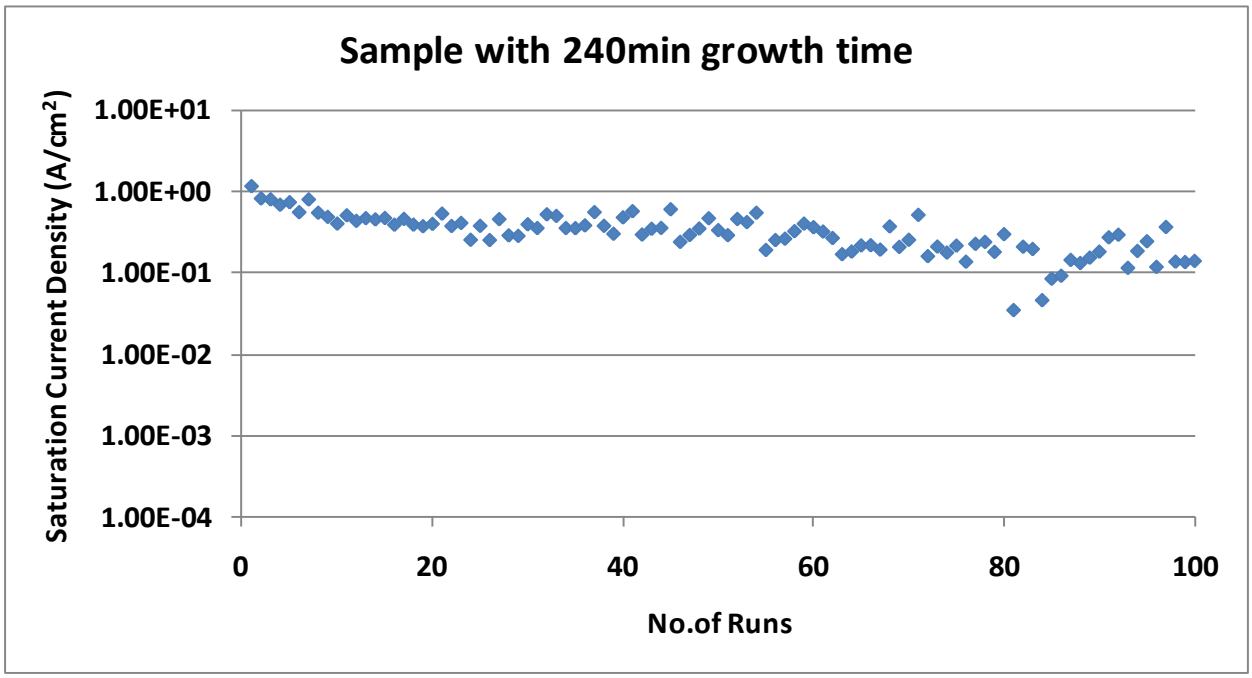

Figure 4.6: Lifetime test at 20 mTorr for samples with different growth time (a) 5 min sputtering (b) 10 min sputtering

4.8 Life Time Test for the Impurity Clustered Samples

It has been already said that the samples grown with sputtering time 20 min have impurity clusters such as polyhedral compounds in the CNTs. Samples with growth times 20, 30 and 40 min were grown for this case. Field emission experiments were carried out to see if the clusters also contribute to the field emission. Voltages are scanned through 0 to 1200 V with a step voltage of 40 V for more than 100 runs. All the experiments were performed at high vacuum conditions. Turn-on electric field and saturation current density are plotted with respect to the number of runs.

Figure 4.7 (a), (b) and (c) show the same field emission data and turn-on voltage and saturation current data resulted from the field emission characteristics of all the samples. The sample with 20 min growth time has almost no CNTs with high density of cluster impurities. The turn-on and current densities are observed to be 2.1 V/μm and 0.983 mA/cm^2 respectively. The sample with 30 min growth time consists of low density of CNTs with some thick tubes and higher density of impurity clusters. The turn-on and current densities are observed to be 1.8 V/μm and 1.3 mA/cm^2 respectively. Finally the sample with 40 min growth time has moderate density of CNTs with high density of impurity clusters and the turn-on and current densities are observed to be 1.8 V/μm and 1.33 mA/cm^2 respectively. The densities of CNTs are proportional to the growth times in all above cases. Sample with 20 min growth time, which has almost no CNTs but only clusters has the turn-on electric field ranging from 1.85-2.1 V/cm^2 clearly suggesting that even the clusters contribute for the field emission characteristics. Turn-on electric field was very much uncertain with abrupt increase and decrease and many highs and lows were observed in these characteristics during long runs as in the case of high pressure emission curves for 5 and 10 min sputtering cases. The current density obtained with the clusters was very low

0.98-0.77 mA/cm^2, where there were no tubes. In the case of Samples with growth time 30 and 40 min better current density was observed and is around 1.3-1.11 mA/cm^2, but not as good as the samples with tubes and no clusters.

(a)

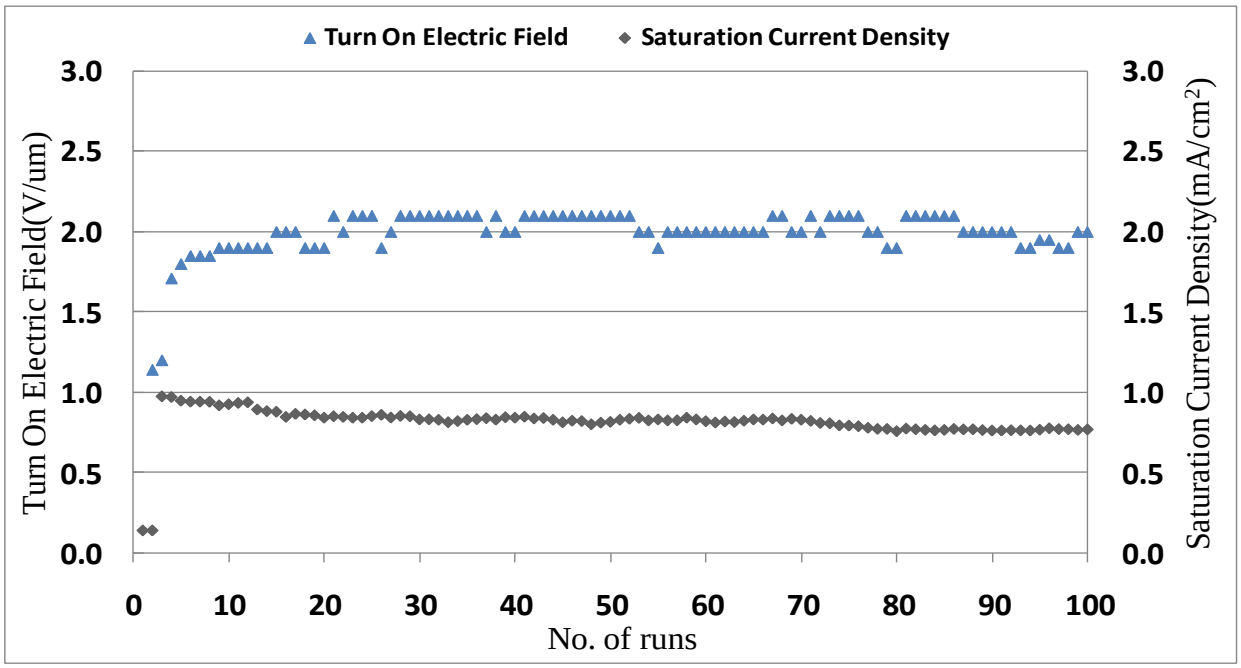

(b)

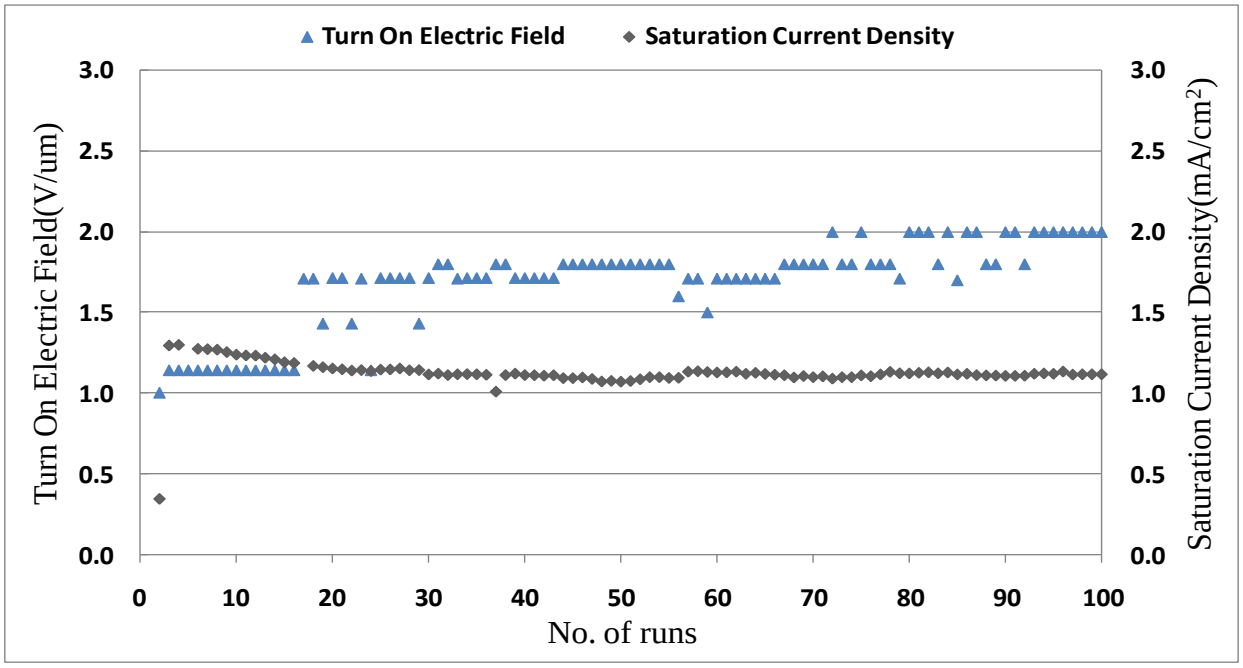

(c)

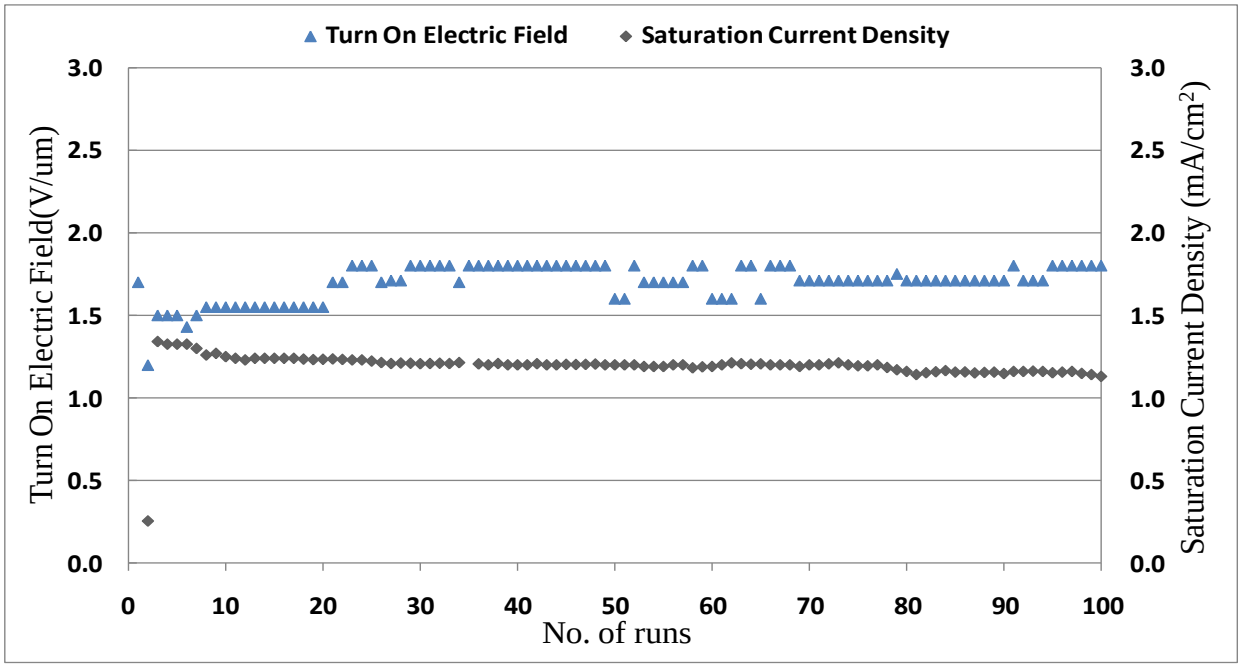

Figure 4.7: Lifetime test for samples with impurity clusters with growth times (a) 20 min (a) 30 min (c) 40 min.

CHAPTER 5

SUMMARY AND CONCLUSIONS

Phenomenal progress has been made in the science of CNTs since their discovery. Different types of CNTs such as SWNTs, MWNTs with different alignments can now be manufactured in small quantities and purified. However the exact mechanism and control methods for the synthesis of CNTs are still not clear and need to have future investigations. Carbon nanotubes are extraordinary material used in various nano electronics applications such as nano-sized tweezers, sensors, field emission display, single electron devices, hydrogen storage and interconnection for VLSI circuits etc. However the integration of nanotubes in fabrication and large scale production is still a challenge. Many of the theoretical predictions and explanations regarding the predominant electrical, mechanical behavior of CNTs have been confirmed experimentally.

Recent developments in the research of CNTs encourage using them as the cold cathode material. The seed electrons needed to initiate the breakdown for the triggering mechanism of pseudospark switch are provided by the CNTs. Since the triggering mechanism is crucial for the performance of the switch, the field emission characteristics of the CNTs becomes more important. The operating characteristics of switch such as delay jitter and repetition of the switch, which defines how well the switch can open and close and it depends on the characteristics of CNTs.

This work can be summarized as the study of thermal chemical vapor deposited carbon nanotubes with a perspective of cold cathode applications, which exhibit efficient electron field emission behaviors. Applications such as the Pseudospark switch mostly operated in high pressure conditions at mTorr range. Hence it is more important to see how the field emission of CNTs at these high pressures. The turn-on and saturation current density of all the samples at 20 mTorr is determined and presented.

The lowest turn on with highest current density was observed for the sample with 10 min sputtering and 240 min growth when they are tested in vacuum. The turn-on for samples with 40 min or longer growth period is very good with high current densities. With increase in the pressure the field emission characteristics seem to be deteriorated with highest turn-on and low current density observed at 20 mTorr range. Even at high pressures, the CNTs exhibited reasonable good field emission characteristics which can be applied for high pressure applications. The poor values observed in case of 10 min growth time and; it improved with the samples with increasing growth periods. This clearly suggests that the samples with higher growth time have edge over the samples with lower growth time.

When the field emissions are compared with different background gases, CNTs exhibit best characteristics in vacuum followed by the helium and dryair. The turn on was observed to be increasing gradually where as the current density decreased from vacuum to dry air conditions. The sputtering time of 10 min with Fe on the substrate looks ideal for the growth of CNTs in this research. The best turn-on and current densities were observed in this case than the 5 min sputtering case which are good too. But the samples with 20 min sputtering have impurity clusters which are present along with the CNTs on the substrate. From the experiments it was observed that even, the samples with impurity clusters within the CNTs exhibited the field

emission characteristics. Few clustered samples with longer growth periods are tested, showed reasonable turn-on field with current densities as good as the samples without impurity clusters.

The technological aspects of field emission characteristics such as the life time and emission degradation and its long-term emission stability became more important. In many applications of CNTs such as flat panel displays, pseudospark switches, emitters lifetime and degradation will be key aspects that are to be looked into. In this research experiments were conducted to test the stability of field emission from all the samples with different sputtering and growth time. These experiments were conducted at 20 mTorr where the voltage is applied from 0-1200 V with step voltage for at least 100 runs. Each time the turn-on and saturation current density is determined from the plots and a relation is established for both the parameters with respect to the number of runs. The turn-on electric field was not consistent but there was clear increase in it with increase in number of runs. Similarly there was clear degradation in the saturation current densities at high vacuum and high pressure conditions. But the degradation was higher while the experiments were run under high pressure. Lifetime tests were also conducted to test the current stability for all the samples at high vacuum with a constant voltage of 600 V applied at least for 5 hours. There was little decay in current density observed for all the samples and plots are presented with respect to time.

The effect on the field emission characteristics due to the presence of polydedral impurity clusters in the CNTs is also tested along with degradation and lifetime test. From the field emission curves it was observed that even the clusters contribute to the field emission and exhibits similar characteristics.

In this research work the CNTs are tested for their field emission properties in the diverse pressures and background gases. Several issues still to be investigated to find ways, where the

alignment, growth, direction and uniformity of CNTs are controlled and defined. As a part of future work these CNTs are used as cold cathode material for triggering mechanism of pseudospark switch.

BIBLIOGRAPHY

[1] S. Iijima, *Nature*, 354, 56 (1991)

[2] C Brown, J Copley and Y Qiu, "The orientational order/disorder transition in buckminsterfullerene (C60): an experiment using the NCNR Disk Chopper Spectrometer", NIST Center for Neutron Research, (2005)

[3] P M Ajayan and T W Ebbesenz, " Nanometre-size tubes of carbon", *Rep. Prog. Phys*. 60 pp. 1025-1062, (1997)

[4] M. Endo, T Hayashi, and Y A Kim, "Large-scale production of carbon nanotubes and their applications", *Pure Appl. Chem*., Vol. 78, No. 9, pp. 1703–1713, (2006)

[5] M. Meyyappan, editor, "Carbon nanotubes science and applications", CRC Press (2004)

[6] C. J. Lee and J. Park, *Appl. Phys. Lett*., 77, 3397 (2000)

[7] T.W. Ebbesen, H. Hiura, J. Fujita, Y. Ochiai, S. Matsui, and K. Tanigaki, *Chem. Phys. Lett.*, 209, 83(1993)

[8] A. Thess, R. Lee, P. Nikolaev, H. Dai, P. Petit, J. Robert, C. Xu, Y.H. Lee, S.G. Kim, A.G. Rinzler, D.T. Colbert, G.E. Scuseria, D. Tomanek, J.E. Fischer, and R.E. Smalley, *Science*, 273, 483 (1996)

[9] N. Hatta, and K. Murata, *Chem. Phys. Lett.*, 217, 398 (1994)

[10] L. Christiansen, and C. Schultcheiss, *Z. Phys. A*, 290, 35 (1979)

[11] K. Frank, O. Almen, P. Bickel, J. Christiansen, A. Gortler, W.Hartmann, C. Kozlik, A. Linsenmeyer, H. Loscher, F. Peter, A. Schwandner, and R. Stark, *Proceedings of the IEEE*, 80, 958 (1992)

[12] B. V. Oliver, P. F. Ottinger, D. V. Rose, D. D. Hinshelwood, J. M. Neri, and F. C. Young, *Physics of Plasmas*, 6, 582 (1999)

[13] K. Frank, and J. Christiansen, IEEE *Trans. Plasma Sci*., 17, 748 (1989)

[14] R. Saito, G. Dresselhaus, and M. S. Dresselhaus, editors, "Physical Properties of Carbon

Nanotubes", *Imperial College Press*, (1998)

[15] M Terrones, "science and technology of the twenty-first century: Synthesis, Properties and Applications of Carbon Nanotubes", *Annu. Rev. Mater.Res*. 33: 419–501, (2003)

[16] T. W. Ebbesen, editor, "Carbon nanotubes: preparation and properties", *CRC Press*, (1997)

[17] R.C. Batra , A. Sears, "Continuum models of multi-walled carbon nanotubes", *International Journal of Solids and Structures* 44, 7577–7596 (2007)

[18] L. Manna, E.C. Scher, A.P. Alivisatos, *J. Am. Chem. Soc.*, 122, 12 700 (2000) [37] Z.W. Pan, Z.R. Dai, Z.L. Wang, *Science*, 291, 1947 (2001)

[19] A. J. Cheng, "Cold Cathodes for Applications in Poor Vacuum and Low Pressure Gas Environments: Carbon nanotubes versus zinc oxide nanoneedles", *Thesis*, (2006)

[20] T. W. Ebbesen, H. Lezec, H. Hiura, J. W. Bennett, H. F. Ghaemi, and T. Thio, *Nature*, 382, 54 (1996)

[21] R. Saito, G. dresselhaus, and M. S. Dresselhaus, *J. Appl. Phys*., 73, 494 (1993)

[22] H. S. Nalwa, editor, " Handbook of nanostructured materials and nanotechnology", Vol. 5, Academic Press, (2000)

[23] J. Nishii, F.M. Hossain, S. Takagi, T. Aita, K. Saikusa, Y. Ohmaki, I. Ohkubo, S. Kishimoto, A. Ohtomo, T. Fukumura, F. Matsukura, Y. Ohno, H. Koinuma, H. Ohno, and M.Kawasaki, *Jpn. J. Appl. Phys.* 42, L347 (2003)**.**

[24] S. Frank, P. Poncharal, Z. L. Wang, and W. de Heer, *Science*, 280, 1744 (1998)

[25] P. M Ajayan, T. W. Ebbesen, T. Ichihashi, , S. Iijima., K. Tanigaki, and H. Hiura, *Nature*, 362, 522, (1993)

[26] H. Hiura, T. W. Ebbesen, K. Tanigaki, *Adv. Mater*. 7, 275 (1995)

[27] O. Zhou, R. M. Murphy, D. W. Chen, C. H. R. C. Haddon, A. P. Ramirez, S. H. Glarum, *Science*, 263, 1744 (1994)

[28] Z. L .Wang, X. Y. Kong, Y. Ding, P. Gao, W. L. Hughes, R. Yang, and Y. Zhang, *Adv. Funct. Mater.*, 14, 943 (2004)

[29] J Zhao, A Buldum, J Han and J. P. Lu, "Gas molecule adsorption in carbon nanotubes and nanotube bundles, *Nanotechnology* 13, 195–200 (2002)

[30] G. Overney, W. Zhou, and D. Tomanek, *Z. Phys. D*, 27, 93 (1993)

[31] J. F. Despres, E. Daguerre, and K. Lafdi, *Carbon*, 33, 87 (1995)

[32] M.Bockrath et. al. *Science*, 275, 1922 (1997)

[33] J. Lu, and J. Han, *Int. J. High Speed Elec.Sys*. , 9, 101, (1998)

[34] P. S. Davids, L. Wang, A. Saxena, A. R. Bishop, *Phys. Rev.* B 48, 17545, (1993)

[35] G. Baumgartner et. al., *Phys. Rev.* B 55, 6704 (1997)

[36] H. Ajiki and T. Ando, *J. Phys. Soc. Jpn*., 62, 1255, (1993)

[37] H. Ajiki and T. Ando, *J. Phys. Soc. Jpn*., 62, 2479, (1993)

[38] J. P. Lu, *Phys. Rev. Lett.*, 74, 1123 (1995)

[39] C. Schonenberger et. al. *Appl. Phys.* A., 69, 283, (1999)

[40] P. M. Ajayan, T. W. Ebbesen, T. Ichihashi, , S. Iijima., K. Tanigaki, and H. Hiura, *Nature*, 362, 522, (1993)

[41] C. Berger, Y. Yi, Z. L. Wang, W.A. de Heer, "Multiwalled carbon nanotubes are ballistic conductors at room temperature", *Appl. Phys. A* 74, 363–365 (2002)

[42] R. Bacon, *J. Appl. Phys*. 31, 283 (1960)

[43] W. Kratschmer, L. D. Lamb, K. Fostiropoulos, D. R. Huffman, *Nature*, 37, 354 (1990)

[44] T. W. Ebbesen, and P. M. Ajayan, *Nature*, 358, 220 (1992)

[45] S. Seraphin, D. Zhou, J. Jiao, J. C. Withers, R. Loufty, *Carbon*, 31, 685 (1993)

[46] S. Iijima and T. Ichihashi, *Nature*, 363, 603 (1993)

[47] D. S. Bethune et. al., *Nature*, 363, 605 (1993)

[48] P. M. Ajayan et. al., *Chem Phys. Lett*., 215, 509 (1993)

[49] S. Serapin et. al., *Chem. Phys. Lett.*, 217, 191 (1994)

[50] C. H. Kiang et. al., *Carbon* 33, 903 (1995)

[51] Y. Saito, K. Kawabata, and M. Okuda, *J. Phys. Chem.*, 99, 16076 (1995)

[52] D. S. Bethune, C. H. Kiang, M. S. de Vires, G. Gorman, R. Savoy, J. Vazquez, R. Beyers, *Nature*, 363, 605 (1993)

[53] K. Tanaka, T. Yamabe, and K. Fukui, "The Science and Technology of Carbon Nanotubes", Elsevier, (1999)

[54] L. Manna, E.C. Scher, A.P. Alivisatos, *J. Am. Chem. Soc.*, 122, 12 700 (2000)

[55] T. Guo et. al. *J. Phys. Chem.* 99, 10694 (1995)

[56] B. Bhushan editor, "Handbook of Nanotechnology", Springer *3rd revised edition* (2010)

[57] M. Daenen , R.D. de Fouw , B. Hamers , P.G.A. Janssen , K. Schouteden , M.A.J. Veld, "The Wondrous World of Carbon Nanotubes", *project*, (2003)

[58] Bhushan editor, "Handbook of Nanotechnology", Springer (2004)

[59] F. Krumeich, H.J. Muhr, M. Niederberger, F. Bieri, B. Schnyder, R. Nesper, *J. Am. Chem. Soc.*, 121, 8324 (1999)

[60] R. E. Smalley, *Acc. Chem. Research*, 25, 98 (1992)

[61] O. A. Louchev, *Phys. Stat. Sol*, 193, 585 (2002)

[62] R. T. K. Baker, and P. S. Harris, *Chemistry and Physics of Carbon*, 83 (1978)

[63] L. Manna, E. C. Scher, A. P. Alivisatos, *J. Am. Chem. Soc.*, 122, 12 700 (2000)

[64] B. J. Norris, J. Anderson, J. F. Wager, D. A. Kszler, *J. Phys. D: Appl. Phys.* 36, L105 (2003).

[65] E. Dujardin, T. W. Ebbesen, A. Krishnan, and M. M. J. Treacy, adv. Mater, 10, 611 (1998)

[66] A. G. Rinzler, J. H. Hafner, P. Nikolaev, L. Lou , S. G. Kim, D. Tomanek, P. Nordlander, D. T. Colbert and R.E. Smally, *Science*, 269, 1550 (1995)

[67] J. M. Bonard, T. Stora, J. P. Salvetat, F. Maier, T. Stockli, C. Duschl, L. Forro, W. A. De Heer, and A. Chatelain, *Adv. Mater*, 9, 827 (1997)

[68] J. Bonard, J. Salvetat, T. Stockli, W. de Heer, L. Forro, and A. Chatelain, *Appl. Phys. Lett.*, 73, 918 (1998)

[69] C. Bower, W. Zhu, S. Jin, and O. Zhou, *Appl. Phys. Lett*., 77, 830 (2000)

[70] R. T. K. Baker, and P. S. Harris, *Chemistry and Physics of carbon*, 83 (1978)

[71] T. Bair, and J. R. Fryer, Carbon, 12, 591 (1974)

[72] A. Oberlin, M. Endo, and T. Koyama, J. Cryst. Growth, 32, 335 (1976)

[73] R. T. K. Baker, and P. S. Harris, R. B. Thomas, and R. J. Waite, J. Catal., 30, 86 (1973)

[74] C. Bower, O. Zhou, W. Zhu, D. J. Werder, and S. Jin, *Appl. Phys. Lett*., 77, 2767 (2000)

[75] O. A. Louchev, *Phys. Stat. Sol*, 193, 585 (2002)

[76] A. Modinos, "Field, Thermionic, and Secondary Electron Emission Spectroscopy", *Plenum Press*, (1984)

[77] L. N. Dobretsov, and M. V. Gomoyunova, "Emission Electronics", Israel Program for Scientific Translations, (1971)

[78] L. Marton, editor, "Advanced in Electronics and Electron Physics", Vol. VIII, Academic Press INC., (1956)

[79] M. Shiraishi, and M. Ata, Carbon, 39, 1913 (2001)

[80] W. Zhu, C. Bower, O. Zhou, G. Kochanski, and S. Jin, *Appl. Phys. Lett.*, 75, 873 (1999)

[81] J. Bonard, F. Maier, T. Stockli, A. Chatelain, W. de Heer, J. Salvetat, and L. Forro, *Ultramicroscopy*, 73, 7 (1998)

[82] W. de Heer, A. Charelain, and D. Ugart, *Science*, 270 1179 (1995)

[83] W. B. Choi, D. S. Chung, J. H. Kang, Y. W. Jin, and I. T. Han, *Appl. Phys. Lett*., 75, 3129 (1999)

[84] S. J. Sanders, R. M. Verschueren, and C. Dekker, *Nature*, 393, 49 (1998)

[85] B.C. Satishkumar, A. Govindaraj, M. Nath, and, C. N. R. Rao, *J. Mater. Chem*., 10, 2115 (1997)

[86] C. Liu, "Cold electron emitters using chemical vapor deposited carbon nanotubes", *Thesis*, (2000)

[87] P. Kim, and C. M. Leiber, Science, 286, 2148 (1999)

[88] K. Tanaka, T. Yamabe, and K. Fukui, "The Science and Technology of Carbon Nanotubes", Elsevier, (1999)

[89] P. M Ajayan, T. W. Ebbesen, T. Ichihashi, , S. Iijima., K. Tanigaki, and H. Hiura, *Nature*, 362, 522, (1993)

[90] R. H. Baughman, C. X. Cui, A. A. Zakhidov, Z. Iqbal, and J. N. Barisci, *Science*, 284, 1340 (1999)

[91] C. Liu, "Diamond and Carbon Nanotubes Coated Cold Cathodes for Vacuum Electronic Applications, D*issertation*, Auburn University (2004)

[92] W. Zhu et. al., *Apply. Phys*., 75, 6, 873 (1999)

[93] H. Kirkici and D. Bruno, "Operating characteristics of a segmented hollow cathode over a wide pressure range," *IEEE Trans. on Plasma Science*, Vol. 23, pp: 229 - 234, (1995)

[94] S. T. Pai, Qi Zhang, "Introduction to high power pulse technology", (2005)

[95] A. Modinos, "Field, Thermionic, and Secondary Electron Emission Spectroscopy", Plenum Press, (1984)

[96] Satio Y, Hamaguchi K. Nishino T. Uuchida K. and Nishina Y., *Nature* 389, 918 (1997)

[97] Do-Hyung Kim, Hoon-Sik Jang, Sung-Youp Lee, and Hyeong-Rag Lee, *Nanotechnology*, 15, 1433 (2004).

[98] G. F. Zhong, T. Iwasaki, H. Kawarada, and I. Ohdomari, *thin solid films* 464, 315 (2004)

[99] A. Wadhawan, R.E. Stallcup II, K. F. Stephen II, J. Perez, I. A. Akwani, *Appl. Phys. Lett.*,79, 1867 (2001)

[100] Z. Yao, H. W. C. Postma, L. Balents, C. Dekkar, *Nature*, 402, 273 (1999)

[101] P. Chen, X. Wu, J. Lin, and K. L. Tan, *Science*, 285, 91 (1999)

[102] P. J. Britto, K. S. V. Santhanam, A. Rubio, J. A. Alonso, and P. M. Ajayan, *Adv. Matter*, 11, 154 (1999)

[103] N. M. Rodriguez, M. S. Kim, and R. T. K. Baker, *J. Phys. Chem*., 98, 108 (1994)

[104] H. D. Wagner, O. Lourie, Y. Feldman, and R. Tenne, *Appl. Phys. Lett*., 72, 188 (1998)

[105] O. Inganas, and I. Lundstrum, *Science*, 284, 1281 (1999)